The 4th Annual Cardiovascular Retreat
Sponsored by

Lillihei Heart Institute

Department of Integrated Biology and Physiology

UNIVERSITY OF MINNESOTA

Medical School

Driven to Discover℠

UNIVERSITY OF MINNESOTA

Celebration of Discovery in Cardiovascular Science and Medicine

August 1, 2012 ♥ 2 - 7 pm

McNamara Alumni Center
Memorial Hall

4th Annual Cardiovascular Retreat

August 1, 2012

Agenda

1:00-1:45pm Registration & Set up

Hospitality & Refreshments - 2:00-5:00pm

Poster Judging

2:00-3:00pm Summer Scholars/Undergraduates

3:00-4:00pm Graduate Students

4:00-5:00pm Postdocs/Scientists/Research Associates

5:00-6:00pm Clinical Fellows

Buffet Dinner - 5:00-6:15pm

Oral Presentations

6:15pm Summer Scholar/Undergraduate Awardee

6:30pm Graduate Student Awardee

6:45pm Postdoc Fellow Awardee

7:00pm Clinical Fellow Awardee

UNIVERSITY OF MINNESOTA

Medical School

Driven to Discover℠

CV Poster Judging Teams
Organizer- Joe Metzger

Summer Scholars/Undergrad Researchers
Mary Garry – lead
Lena Talkachova, Paul Iaizzo, Vince Barnett, Steve Katz, Scott O'Grady, Xiaozhong Shi, Radbod Darabi, Osha Roopnarine, Michael Kyba, Jamie Lohr

Graduate Students
John Osborn –lead
DeWayne Townsend, Alessandro Bartolomucci, Rita Perlingeiro, Jen Hall, Bob Tranquillo, Cindy Martin, Dawn Lowe, LaDora Thompson, Dick Bianco, Kevin Wickman, Naoko Koyano-Nakagawa, Dave Thomas

Postdocs
Cliff Steer –lead
Dan Garry, Jim Ervasti, Jay Zhang, Gianluigi Veglia, Bin He, Peter Bitterman, Jonathon Slack, Angela Mortari, Yingjie Chen, Yuquig Huo

Clinical Fellows
Ganesh Raveendran – lead
Gary Francis, Daniel Duprez, Demetris Yannopoulos, Liz Braunlin, Carolina Masri, Bob Bache, Peter Eckman, Bob Wilson, Jay Cohn, Marc Pritzker, Monica Colvin –Adams, Alan Hirsch, Uma Valeti, Scott Sakaguchi, Alan Berger

Celebration of Discovery in Cardiovascular Science and Medicine
The 4th Annual Cardiovascular Retreat, August 1, 2012
Lillehi Heart Institute and Integrative Biology and Physiology

Poster Presentations

Summer Scholars

100. Mesp1-mediated skeletal muscle differentiation.
Hannah Hagen, Sunny Chan, and Michael Kyba

101. Use of Sca*l*e clearing method on visualization of TRPv1 positive neurons in normal and cardiomyopathic rats.
Andrew Donaldson, Lawrence Stout, Cyprian Weaver, PhD, and Mary G. Garry, PhD

102. Effects of medium conditions and hypoxic environment on the formation of tunneling nanotubes in colon cancer.
Wen Zhang, Zhilian Xia, Clifford Steer, Emil Lou

103. Reprogramming of Fibroblasts from Duchenne Muscular Dystrophy Patients into Induced Pluripotent Stem (iPS) Cells.
Alexandra Peterson[1], Radbod Darabi[1], Peter Karachunski[2], Jakub Tolar[3], and Rita Perlingeiro[1]

104. Fluorescence quenching measurements to study the structural defects caused by a myosin essential light chain cardiomyopathy mutation.
Ryan Price and Osha Roopnarine.

105. Effect of Endoglin Overexpression in Cardiac Development.
Jeff Zhang, Luciene Borges, Jacquelyn Catanese, and Rita Perlingeiro
Stefani Prigozhina, Dr. Bob Tranquillo

106. Effects of Voluntary Exercise on Dystrophic Cardiac Muscle.
Zach Stevens, Susan Novotny, Michael Eckhoff, Tara Mader, Angela Greising, Shaojuan Lai, Dawn Lowe

107. Etv2 expressing cells contribute to definitive hematopoiesis and adult vasculature.
Matthew D. Schreier, Tara L. Rasmussen, Michelle J. Doyle, Kathy Bowlin, Daniel J. Garry

108. Expression and Purification of Spin-Labeled PLB for EPR Analysis of the SERCA-PLB Complex.
Monica Knaack, Zach James, Jesse McCaffrey, and David D. Thomas

109. Analysis of the Phosphorylation States of TRPv1 in Dorsal Root Ganglia from Normal and Heart Failure Rats.
Tom Mulvey, Rose Hartnett, Lawrence Stout, Minh Nguyen PhD, Mary Garry

110. Calcium Imaging: Study of Group III and Group IV Afferent Neurons in Normal and Heart Failure Rats.
Will Barth1, Minh Nguyen PhD1, Larry Stout1, Iryna Khasabova PhD2, Virginia Seybold PhD2, Mary Garry PhD1

111. Protein-based sarcomeric therapeutics for the diseased heart.
Gabriela Ruiz-Colón, Anthony Vetter and Joseph M. Metzger

112. Genetic and environmental models of obesity: role of β-adrenergic receptors.

Jacob T. McCallum, Maria Razzoli, Cheryl Cero, Ivana Ninkovic, Bradford Lowell1, Alessandro Bartolomucci.

113. **Chronic stress shifts the phase of adrenal clock gene rhythms.**
Carley Karsten, Maria Razzoli, J. Marina Yoder, Alessandro Bartolomucci, and William Engeland
114. **Cellular reprogramming to blood using a transcription factor cocktail.**
Thomas Knoedler, Jai Prakesh Richard, and Michael Kyba
115. **Regulation of actin dynamics by cofactors within striated muscle.**
Praveena Narayanan1, Benjamin J. Perrin2, James M. Ervasti2
116. **α-Dystrobrevin functions to reinforce the interaction between dystrophin and the membrane, loss of α-dystrobrevin results in significant loss of cardiac reserve.**
Jon Dean, Katharine Sharpe, and DeWayne Townsend
117. **Coronary regulation in dystrophic cardiomyopathy.**
Zachary Stelter and DeWayne Townsend
118. **Green Fluorescent Protein membrane localization via N-terminal myristylation: proof-of-concept study for the design of a calcium buffering system at the plasma membrane.**
Jenny Seong, Michelle L. Asp, Joshua J. Martindale and Joseph M. Metzger
119. **Characterization of myocytes derived from human inducible pluripotent stem cells.**
Sophie Zhang
120. **Identification of regulatory region(s) for MyoD gene transcription in muscle stem cells.**
Wilsen Hadiwikarsa, Atsushi Asakura
121. **The effects of cyclic stretching on cell and fiber alignment and ERK pathway activation of human dermal fibroblasts entrapped in fibrin gels.**
Stefani Prigozhina

Graduate Students

200. Effect of ENDOGLIN Induction on the Generation of Hematopoeitic Progenitors from Human Embryonic Stem Cells.
Kerem Fidan, Radbod Darabi, Rita CR Perlingeiro

201. Molecular Dynamics of a pH responsive histidine-modified cardiac troponin I.
Evelyne M. Houang[a,b] ,Nathan J. Palpant[a], Yuk Y. Sham[b], Joseph M. Metzger[a]

202. Tools to Evaluate SERCA and Phospholamban Function in HEK Cells.
Vaibhav Sharma, Simon J. Gruber, David D. Thomas

203. The Atlas of Human Cardiac Anatomy. A Free-Access Educational Website.
Paul A. Iaizzo1,2,3, Michael G. Bateman1,2,4, Jason L. Quill4, Christopher D. Rolfes1,2,4, Stephen Howard1,2,4, Julianne Eggum1,2, Ryan Goff1,2, Michael D. Eggen4, Gary Williams3, Alexander J. Hill4

204. Digital Reconstructions of the Human Coronary Arteries and Cardiac Veins using Contrast-Computed Tomography.
Julianne H Eggum, Matt Venegoni

205. 3D Reconstructions of the Human Cardiac Venous System using Contrast Computed Tomography for Anatomical Evaluation.
Julianne Eggum, Allison Larson, Emily Fitch, Paul Iaizzo

206. Structural Dynamics of Calcium Transport Proteins Detected by Saturation Transfer Electron Paramagnetic Resonance.
Jesse E. McCaffrey, Zachary M. James, Kurt D. Torgersen, Christine B. Karim, Edmund Howard, and David D. Thomas

207. Comparable Analysis of Vasculature Functions in Mesenchymal Stem/Stromal Cells Derived from Bone Marrow, Human Embryonic Stem Cells and iPS cells.
Li, Li (MS)

208. Local onset of Calcium Alternans precedes voltage alternans in Langendorff perfused rabbit hearts.
Ramjay Visweswaran, Stephen McIntyre, Elena Tolkacheva

209. Intermittent Vagus Nerve Stimulation Reflexively Modulates Heart Rate Variability in Rats with Chronic Ischemic Heart Failure
Joseph Ippolito, Thomas Xie, Iryna Talkachova, Bruce H. KenKnight, Elena G. Tolkacheva

210. Towards development of a pacing protocol to mimic physiological heart rate.
Virendra Kakade, Stephen McIntyre, Elena G. Tolkachveva

211. The Effect of Stretch Parameters on the Contractility of Fibrin-based Myocardial Tissue Equivalents.
Jacqueline Wendel

212. Epigenetic memory and BMP4-mediated lineage specific differentiation of myoblast-derived induced pluripotent stem cells.
Jesse Mull, Yoko Asakura, and Atsushi Asakura

213. Conditional Serca2 ablation impairs systolic and diastolic performance of isolated perfused hearts.
Frazer I. Heinis1, Kristin B. Andersson3, Geir Christensen3, and Joseph M. Metzger1,2

214. Functional β –adrenergic receptors are required for the pro-lipolytic effects of the VGF-derived peptide TLQP-21.
Cheryl Cero1, Maria Razzoli1, Ivana Ninkovic1, Rana Mohammed1, Jake McCallum1, Bradford Lowell2, Alessandro Bartolomucci1

215. Dystrophin and Utrophin: Interaction with Microtubules.
Joseph J. Belanto1,2, Davin M. Henderson1, Michele A. Jaeger1, and James M. Ervasti1,2

216. Effect of Selective Afferent Renal Denervation by Periaxonal Application of Capsaicin on Salt Sensitivity of Arterial Pressure.
Jason D. Foss, W. E. Engeland and John W. Osborn

217. Interstitial Flow Improves Lumen Formation in Aligned Engineered Microvasculature.
Kristen T. Morin and Robert T. Tranquillo

218. The Effect of Continuous Flow Left Ventricular Assist Device (CF-LVAD) Implantation on Serum Uric Acid Levels.
Andrew N Rosenbaum1, Sue Duval2, Muhammad Bilal Salman Khan1, Marc Pritzker1, Ranjit John3, and Peter M Eckman1.

219. Noninvasive Imaging of the Three-dimensional Ventricular Activation Sequence of Paced Rhythm and Ventricular Tachycardia in the Canine Heart.
Chengzong Han1, Steven Pogwizd2, Cheryl Killingsworth2, Bin He1

220. Noninvasive imaging of atrial arrhythmias in humans.
Zhaoye Zhou1, Jorge Pedrón Torrecilla1, Jian Sun2, Dakun Lai1, Yigang Li2, Bin He1

221. Noninvasive Imaging of Global Ventricular Activation in a Swine Model during Pacing
Zhaoye Zhou1, Chenguang Liu1, Michael G. Bateman2, Chengzong Han1, Cory Swingen3, Paul A. Iaizzo2, Bin He1

222. Stability of human dystrophin constructs skipped around exon 45.
Jackie McCourt, Michele A. Jaeger, Joseph J. Belanto, Dana Strandjord, Davin M. Henderson and James M. Ervasti

223. Single amino acid changes in distinct domains of dystrophin can affect protein folding and cause disease, but not always.
Dana M. Strandjord, Davin M. Henderson, Bin Li, James M. Ervasti

224. Spectroscopic Design of SERCA Activators for Drug or Gene Therapy.
Simon J Gruber1, Suzanne Haydon1, Razvan L Cornea1, Bengt Svensson1, Dongzhu Jin2,
Jiqui Chen2, Joseph M Muretta1, Gregory D Gillispie1,3, and David D Thomas1

225. Guanylyl Cyclase A and B Are Asymmetric Dimers That Are Allosterically Regulated by ATP Binding to the Catalytic Domain

Jerid W. Robinson, Dr. Lincoln R. Potter

226. Title: In Vitro Modeling of Duchenne Muscular Dystrophy Cardiomyopathy Using Human Induced Pluripotent Stem Cells.
Forum D.K. Kamdar, Michelle J Doyle, Christopher S Chapman, Jaime Lohr, Daniel J Garry

227. Effect of Endoglin overexpression during embryonic body development
June Baik

228. Platform for small molecular discovery in "titratable" cardiac inotropic therapy.
Anthony Vetter, Brian Thompson, Joe Muretta, Yuk Sham, David D. Thomas, Joseph M. Metzger

229. Structure of the Phospholamban/Ca2+-ATPase membrane protein complex in lipids by hybrid solid-state NMR methods.
Martin Gustavsson1, Raffaello Verardi1, Nathaniel J. Traaseth1, and Gianluigi Veglia1

230. Oriented Solid State NMR Reveals the Molecular Mechanism by which Sarcolipin Inhibits SERCA.
Kaustubh R. Mote1 and Gianluigi Veglia1,2

Postdocs/Research Associate/Scientist

300. Characterization of Pseudotyped and Inducible Adeno Associated Virus Vectors in Cardiac Gene Transfer
Erik Arden, Qingli Lu, Martina Maerz Mary Garry and Joseph Metzger

301. The C-terminal fragment of dystrophin cleavage by enteroviral protease 2A causes dystrophic cardiomyopathy.
Matthew S. Barnabei and Joseph M. Metzger

302. MIR-208A Targeted suppression of PDE4D directly enhances myocyte concentration function via PKA-mediated phosphorylation of CTNI and PLN.
Fikru Belema-Bedada and Joseph M. Metzger

303. MyEIF.org a Hybrid Personal and Medical Health Record with an Emergency Focus.
Pouya Hematti, MSII, Lee Pyles, MD

304. Etv2-regulated microRNAs are essential for endothelial development.
Bhairab N. Singh, Xiaozhong Shi, Tara L. Rasmussen, Alicia Wallis, Kathy Bowlin, Naoko Koyano-Nakagawa and Daniel J. Garry*

305. An ex vivo Gene Therapy Approach to Treat Muscular Dystrophy Using iPS cells.
Antonio Filareto1, Sarah Parker1, Radbod Darabi1, Luciene Borges1, Michelina Iacovino2, Tory Schaaf1, Timothy Mayerhofer1, Jeffrey S Chamberlain3, James M. Ervasti4, R. Scott McIvor5, Michael Kyba2 and Rita C.R. Perlingeiro1

306. Endoplasmic reticulum stress sensor PERK protects against pressure overload induced heart failure.
Xiaoyu Liu, Xin Xu, Huan Wang, Dongmin Kwak, Xinli Hu, John Fassett, Ping Zhang, Robert J. Bache, Yingjie Chen

307. A novel role for Pax3 as regulator of the skeletal versus cardiac myogenic program during mesoderm formation.
Alessandro Magli, Erin Schnettler and Rita Perlingeiro

308. Nucleotide activation of the Ca-ATPase.
J. Michael Autry, John E. Rubin, Bengt Svensson, Ji Li, and David D. Thomas

309. Double-strand RNA–dependent Protein kinase deficiency protects the heart From systolic overload-induced congestive heart failure.
Huan Wang; Xin Xu, Dongmin Kwak, John Fassett, Xinli Hu, Ping Zhang, Haipeng Guo, Jennifer Hall, Robert J. Bache, and Yingjie Chen

310. Multiple DDAH1 knockout strains reveal abnormal vascular endothelial DDAH1 function as the major contributor for exacerbated hypoxia-induced pulmonary artery hypertension in mice.
Dongmin Kwak, Xin Xu, Dachun Xu, Haipeng Guo, Xinli Hu, Ping Zhang, Zhongbing Lu, E. Kenneth Weir, Yingjie Chen

311. Microtubule Actin Cross linking Factor(MACF1/ACF7) gene disruption causes cardiomyocyte microtubule disorganization and exacerbates pathological hypertrophy.
John Fassett

312. Reduced translocation of the TRPv1 receptor in afferent neurons of cardiomyopathic rats.
Minh M. Nguyen, Laurence E. Stout, Qinglu Li, and Mary G. Garry

313. Validation of systemic cell delivery and generation of integration free human ES/iPS derived myogenic precursors.
Radbod Darabi and Rita C.R. Perlingeiro

314. DDAH1 protects the heart from systolic overload-induced ventricular hypertrophy and heart failure.
Ping Zhang, Xin Xu, Xinli Hu, Dorothee Atzler, Dongming Kwak, Haipeng Guo, Dachun Xu, Zhongbing Lu, Edzard Schwedhelm, Rainer H. Böger, Yingjie Chen, Robert J. Bache

315. The Chemical Membrane Sealant Poloxamer 188 Ameliorates Myocardial Ischemia/Reperfusion-induced Injury by Preventing Sarcolemmal Permeability.
Joshua J. Martindale, Martina Maerz, Joseph M. Metzger

316. Dominant effect of histidine modified troponin to normalize SR Ca2+ load and rescue ischemia/reperfusion deficits in phosholamban deficient hearts.
Joshua J. Martindale, Todd J. Herron, Sharlene M. Day, Joseph M. Metzger

317. Loss of the eIF2 kinase GCN2 protects mice from pressure overload induced congestive heart failure.
Xin Xu, Zhongbing Lu, John Fassett, Ping Zhang, Xinli Hu, Dongmin Kwak, Huang Wang, Robert J. Bache, Yingjie Chen

318. Transcriptional regulation of Etv2 gene expression governs vasculogenesis;
Tara L. Rasmussen, Naoko Koyano-Nakagawa, Alicia Wallis, Xiaozhong Shi, Christine Wasylyk, Bohdan Wasylyk, and Daniel J. Garry

319. Tamoxifen has acute inhibitory effects on contractility in isolated adult rat cardiac myocytes.
Michelle L. Asp, Joshua J. Martindale, and Joseph M. Metzger

320. Heart function following exposure to bile acids during cold storage.
Karen Porter PhD1, Tyler Mingo1, Glynnis Garry1, Peter I. Dosa PhD2, and Mary G. Garry PhD1

321. Circadian and infradian rhythms of some parameters of the ECG on days with or without examination.
Lyazzat Gumarova

322. Combating Adaptation to Stretch Conditioning Through Prolonged Activation of Extracellular Signal-Regulated Kinase.
Justin Weinbaum, Jill Schmidt, Robert Tranquillo

323. Maternal stress, NPY system and adult metabolic syndrome.

Ruijun Han, Xinying Wang, Joanna Kitlinska1, Aiyun Li1, G Ian Gallicano1 and Zofia Zukowska.

324. Modeling Cardiac Differentiation in Human Induced Pluripotent Stem Cells (hiPSC).
Michelle J Doyle, Jamie L Lohr, Christopher Chapman, Forum D Kamdar, Naoko Koyano-Nakagawa, Daniel J Garry

325. A novel automated method for the morphological analysis of adipocytes: preliminary evidence.
Ivana Ninkovic, Rana Mohammed, Cheryl Cero, Alessandro Bartolomucci

326. Molecular Mechanisms of A164H cTnI.
Brian Thompson1, Evelyne Houang1,2, Yuk Sham2, Joseph Metzger1

327. A focused region of D4Z4 demethylation in FSHD2.
LM Hartweck1, LJ Anderson1, RJ Lemmers2, A Dandapat1, S Grindle1, EA Toso1, JC Dalton3, R Tawil4, JW Day5, SM van der Maarel2, M Kyba1

328. In vitro characterization of DUX4c, a gene involved in FSHD.
Megan Roth, Robert W. Arpke, Darko Bosnakovski, Megan M. Multhaup, Michael Kyba

329. Functional improvement after satellite cell transplantation into NSG-mdx4Cv mice.
Robert W. Arpke1,2, Radbod Darabi1,3, Tara Mader4,5, Kerri T. Haider1,2, Akira Toyama1,2, Cara-lin Lonetree1,2, Nardina Nash1,2, Dawn Lowe4,5, Rita Perlingeiro1,3 and Michael Kyba1,2

330. Cardiac Myosin Binding Protein-C Restricts Intrafilament Torsional Dynamics of Actin in a Phosphorylation-Dependent Manner
Colson, Brett A., Inna N. Rybakova, Ewa Prochniewicz, Richard L. Moss, and David D. Thomas

331. Context-dependent lineage determination by Mesp1.
Sunny Sun-Kin Chan,1,2 Akira Toyama,1,3 Robert W. Arpke,1,3 Abhijit Dandapat,1,2 Michelina Iacovino,1,3 Jin-Joo Kang,1,2 Gengyun Le,1,2 Hannah R. Hagen,1 Daniel J. Garry,1,3 and Michael Kyba1,2,*

332. Heterogeneity of ATP turnover rates in the LV of swine hearts with post-infarction remodeling.
Qiang Xiong, Pengyuan Zhang, Lei Ye, Albert Jang, Jianyi Zhang

333. Genetic down-regulation or pharmacological inhibition of Flt-1 ameliorates the muscular dystrophy phenotype by increasing the vasculature in DMD model mice.
James Ennen, Mayank Verma, Yoko Asakura, Hiroyuki Hirai, Shuichi Watanabe, Jarrod A Call, DeWayne Townsend, Dawn A Lowe, Atsushi Asakura

334. Cellular reprogramming to blood using a transcription factor cocktail.
Jai Richard1, Ismail Ismailoglu1, Michelina Iacovino1 & Michael Kyba1

335. Identification of a Novel microRNA-Protease Signaling Pathway in Symptomatic Carotid Plaques
Neeta Adhikari1, Marjorie Carlson1, Darrell Loeffler2, Dinesha Walek3, Jerry Daniel3, Mark J Lawson4 Aaron J Mackey4, Amir Lerman2 and Jennifer L. Hall1

336. Mouse model to understand the role of Dux4 in Facioscapulohumeral muscular dystrophy
Abhijit Dandapat, Darko Bosnakovski, Kristen A. Baltgalvis, Lynn Hartweck, Cara-lin Lonetree, Nardina Nash, Dawn A. Lowe, and Michael Kyba,

337. Smooth Muscle Specific Deletion of N-deacetylase-sulfotransferase1 (Ndst1) Results In Altered Arterial Elasticity.
Kim Ramil C Montaniel1, Neeta Adhikari1, Spencer P Lake2, Marie Billaud3 Marjorie Carlson1, Brant E Isakson3, Victor H Barocas2, Jennifer L Hall1

338. An evidence-based score to detect prevalent peripheral artery disease (PAD).
Sue Duval1, Joseph M Massaro2, Michael R Jaff3, William E Boden4, Mark J Alberts5, Robert M Califf6, Kim A Eagle7, Ralph B D'Agostino Sr8, Alison Pedley2, Gregg C Fonarow9, Joanne M Murabito10, P Gabriel Steg11, Deepak L Bhatt12 and Alan T Hirsch13

339. Trends in Utilization of the Ankle-Brachial Index (ABI) in the US Medicare Population: 1998 to 2008.
Sue Duval, PhD, Stephen T. Parente, PhD, MPH, MS, Niki C. Oldenburg, DrPH, and Alan T. Hirsch, MD.

340. NF-κB-mediated degradation of the coactivator RIP140 regulates inflammatory responses and contributes to endotoxin tolerance.
Ping-Chih Ho, Yao-Chen Tsui, Xudong Feng, David R Greaves & Li-Na Wei

341. Rational Structure-Based Design of PLN Mutants to Tune SERCA Function.
Kim N. Ha1, Martin Gustavsson1, Raffaello Verardi1, Gianluigi Veglia1,2

Clinical Fellows

400. Dexmedetomidine may unmask atrioventricular node disease.
Kalpana Thammineni, Arif Somani, Parvin Dorostkar

401. Risk of Acute Kidney Injury is Not Higher in Patients Who Undergo Coronary Angiography and Cardiac Surgery in Close Succession.
Byungsoo Ko, MD, Salima Mithani, MD, Santiago Garcia, MD, Venkat Tholakanahalli, MD, and Selcuk Adabag, MD, MS

402. Utility of Claims Based Data to Identify Critical Limb Ischemia Patients.
Wobo Bekwelem, Lindsay G. Smith, Niki C. Oldenburg, Tamara J. Winden, Hong H. Keo, Alan T. Hirsch, Sue Duval

403. Incidence of Appropriate Shock in Implantable Cardioverter-Defibrillator Patients with Improved Ejection Fraction.
Niyada Naksuk, MD, Ali Saab, DO, Jian-Ming Li, MD, PhD, FHRS, Viorel Florea, MD, PhD, Inder S. Anand, MD, DPhil, David G. Benditt, MD, FHRS, and Selcuk Adabag, MD, MS

404. Resource Utilization in HeartMate II Left Ventricular Assist Device Patients with Gastrointestinal Bleeding.
Niyada Naksuk, MD, Prangthip Chareonpong, MD, Eva Tone, MBA, Andrew Rosenbaum, Brian S Milavitzl, Ranjit John, MD, and Peter M Eckman, MD

405. Ultrafiltration Therapy for Heart Failure Patients with Preserved and Reduced Ejection Fraction Results in Similar Morbidity and Mortality.
Niyada Naksuk, MD, Monica Colvin-Adams, MD, MS, Prangthip Charoenpong, MD, Michael Petty, PhD, RN, Marc Priztker, MD and Sofia Carolina Masri, MD.

406. Novel transcripts and pathways identified in blood one week following implant of continuous-flow left ventricular assist device (CF-LVAD).
Adam Mitchell, Rodney Staggs, Weihua Guan, Suzanne Grindle, Neeta Adhikari, Sameh Hozayen, Peter Eckman and Jennifer L. Hall

407. Survey of Treatment Choices in Acute Decompensated Heart Failure Suggests Vasodilators Underused Compared to Guideline Recommendations.
Michelle D Carlson, MD1,† and Peter M Eckman, MD1

408. Lack of Association between Operative Technique and Early Atrial Arrhythmias after Orthotopic Heart Transplantation
Srinivasan Sattiraju MD, Balaji Krishnan MD MS, David Benditt MD, Kenneth Liao MD PhD, Ilknur Can MD, Venkatakrishna Tholakanahalli MD, Mariana Canoniero MD, Lauren Benditt MA, Philippe Gaillard PhD, Wayne Adkisson MD, Lin Y Chen MD

409. Association of Common Variations on Chromosome 4q25 and Left Atrial Volume in Patients with Atrial Fibrillation.
Hirad Yarmohammadi, MD, MPH, Hana Hoyt, MD, Irfan M. Khurram MD, Rozann Hansford, RN, MPH, Menekhem M. Zviman, PhD, Stefan L. Zimmerman, MD, Steven J. Steinberg, PhD, Daniel P. Judge, MD, Gordon F. Tomaselli, MD, Henry R. Halperin, MD, MA, Alan Cheng, MD, David D. Spragg, MD, Charles A.

Henrikson, MD, Sunil Sinha, MD, Joseph E. Marine, MD, Ronald Berger, MD, PHD, Hugh Calkins, MD, Saman Nazarian, MD

410. Long-term Prognosis of Patients with Ventricular Arrhythmias After Cardiac Surgery.
Farzad Azimpour, MD, Henri Roukoz, MD, Selcuk Adabag MD, MS

411. Comorbidities and Physical and Cognitive Impairments in Elderly Heart Failure Patients: Impact on Total Mortality: The Cardiovascular Health Study (CHS).
Khalil Murad; Timothy M Morgan; Gregory L Burke; David C Goff, Jr.; Dalane W Kitzman

412. 3-D TTE Calculation of Stroke Volume: a Comparison to 2-D and Thermal Calculations.
Matthew Chu M.D. and Richard Madlon-Kay M.D.

413. QRS Shortening after Cardiac Resynchronization Therapy is Associated with Increased Left Ventricular Ejection Fraction in Patients with Non-Ischemic Cardiomyopathy.
William H. Sauer, MD, R. Todd Drexel, MD, Diego F. Belardi, MD, Royce L. Bargas, DO, Christopher S. Stees, DO, Joseph L. Schuller, MD, Christopher M. Lowery, MD and Michelle SC. Khoo, MBChB

414. Lung to Finger Circulation Time is Prolonged in Patients with Obstructive Sleep Apnea and Underlying Heart Failure.
Younghoon Kwon, MD 1 2 3 ; Talha Khan, MD 1 2 ; Conrad Iber, MD 1 2

415. Baroreceptors gone awry: Exaggerated Impact of Cough on Cardiovascular Dynamics.
Oana Dickinson, MD, Prabhjot S. Nijjar, MD, David G. Benditt, MD

416. High Renal Morbidity with Slow Continuous Ultrafiltration in Advanced Decompensated Heart Failure Despite Hemodynamic Improvement.
Patarroyo M, Wehbe E, Demirjian S, Hanna M, Taliercio J, Tang W.H.

417. Low Systolic Blood Pressure At Admission Identifies Patients with Decompensated Heart Failure Who are Undergoing Slow Continuous Ultrafiltration At High Risk of Short Term Mortality.
Patarroyo M, Wehbe E, Hanna M, Demirjian S, Tang W.H.

418. Discordance between Aortic Augmentation Index and Hemodynamic Measurements in Patients with Acute Decompensated Heart Failure Receiving Intensive Medical Therapy.
Maria Patarroyo, MD, Yi Lu, RN, Mohammad Rafey, MD, W. H. Wilson Tang, MD.

419. Multiple Systemic Emboli Originating from the Aorta and Left Atrium in a Patient with Reduced Left Ventricular Ejection Fraction.
Ann Coumbe MD, Emil Missov MD, PhD

420. Long-term Follow-up of Elderly Patients with Mobitz Type I, Second Degree Atrioventricular Block.
Ann Coumbe, MD, Niyada Naksuk, MD, Marc Newell, MD, Porur Somasundaram, MD, Jian-Ming Li, MD, PhD, David Benditt, MD, Selcuk Adabag, MD, MS

421. Lack of Association between Operative Technique and Early Atrial Arrhythmias after Orthotopic Heart Transplantation.
Srinivasan Sattiraju MD, David Benditt MD, Kenneth Liao MD PhD, Ilknur Can MD, Balaji Krishnan MD MS, Venkatakrishna Tholakanahalli MD, Mariana Canoniero MD, Lauren Benditt MA, Philippe Gaillard PhD, Wayne Adkisson MD, Lin Y Chen MD

422. Hospital Readmissions Are A Common Occurrence in the Current Era with Continuous Flow (CF) LVADs.
Forum Kamdar, MD1, Jason Rasmussen, MD1, Peter Eckman, MD1, Kenneth Liao, MD1, Brian Milavitz2, Monica Colvin-Adams, MD1 and Ranjit John, MD1.

423. Post-Cardiac Transplant Survival in the Current Era in Patients Receiving Continuous-Flow LVADs.
Forum D.K. Kamdar1, Kenneth K. Liao2, Peter M Eckman1, Monica Colvin-Adams1, Sara J. Shumway2, Ranjit John2

424. COPD as a Predictor of Adverse Outcomes in Heart Failure with Preserved Ejection Fraction: Data from IPRESERVE Trial.
Ashenafi Tamene, MD; Sithu Win, MD, MPH; Inder S. Anand, MD, FRCP, D Phil (Oxon.)

425. Survival of Kidney Transplantation Patients in the United States After Cardiac Valve Replacement.
Alok Sharma, MD; David T. Gilbertson, PhD; Charles A. Herzog, MD

426. Beneficial Effects of Carvedilol in Dilated Cardiomyopathy in Dialysis Patients.
Alok Sharma, Charles Herzog.
University of Minnesota Medical School, Hennepin County Medical Center.

427. Comparative Long-Term Survival of Dialysis Patients in the US after Mitral Valve Replacement and Mitral Annuloplasty.
Alok Sharma, Eric Weinhandl, Charles Herzog

Summer Scholars

100.
Mesp1-mediated skeletal muscle differentiation

Hannah Hagen, Sunny Chan, and Michael Kyba
Lillehei Heart Institute

Mesp1 is play an important role in cardiac development, and is widely considered the master regulator in cardiac development. Recent work has shown that the influence of Mesp1 may not be limited to the cardiac lineage, and that Mesp1 is also expressed in the development of facial skeletal muscles. We have generated a mouse ES cell ilne in which Mesp1 can be induced by doxycycline and find that while Mesp1 induces cardiac differentiation in the presence of serum-derived factors, in the absence of serum-derived factors it instead induces skeletal myogenic genes such as Myf5, Myod1, Myog, and Mef2c, and also produces multi-nucleated myosin heavy chain (MHC) positive myotubes. Using this protocol approximately 2% of the cells produced are skeletal myoblasts and myotubes. The current goal is to increase this low rate of skeletal myogenic differentiation. Several conditions, such as oxygen levels, small molecule inhibitors, and serum time points were screened and the skeletal muscle output measured. We found that dorsomorphin, a small molecule inhibitor of the BMP pathway, was able to increase the number of multi-nucleated myotubes formed, but only when used in concert with serum provided at specific time points. Inhibition of the TGFβ (ALK 4/5/7) pathway in concert with serum culture also caused an increase in MHC+ cells. Additionally, cultures grown in low oxygen conditions displayed overall higher levels of skeletal muscle differentiation.

101.
Use of Scale clearing method on visualization of TRPv1 positive neurons in normal and cardiomyopathic rats.

Andrew Donaldson, Lawrence Stout, Cyprian Weaver, PhD, and Mary G. Garry, PhD
Lillehei Heart Institute, University of Minnesota, Minneapolis, MN 55455

The exercise pressor reflex (EPR) controls blood pressure and heart rate in response to exercise. It has previously been demonstrated that the EPR is exaggerated in heart failure and that this abnormal response to exercise contributes to morbidity and mortality (1). We have shown that the responsiveness of group IV afferent neurons is blunted in heart failure while group III afferent neurons are hyperresponsive to exercise in heart failure (2). We have preliminary data that suggests that the spinal projections of these afferent neurons are re-organized in heart failure. Therefore, the aim of this study is to investigate the organization of the afferent neurons within the dorsal horn of the spinal cord (central projections), dorsal root ganglia (DRG; cell bodies), and skeletal muscle (peripheral projections) in normal and cardiomyopathic animals. To do this, we are using a novel method of tissue clearance (3) to enhance visualization of projections

within the spinal cord. Following transcardial perfusion with 4% paraformaldehyde (PFA), DRG, spinal cord, and brain were removed from normal and cardiomyopathic rats and postfixed overnight at 4°C in PFA. Tissue samples were washed in PBS and processed through the Scale method of clearing in which tissues were placed in Scale A2 (4M urea) and Scale B4 (8M urea) respectively for 48 hrs and subsequently stored in Scale A2 until used. Whole DRG, in addition to paraffin and frozen DRG sections, were stained for TrpV1 (1:500), a protein that is expressed exclusively in Group IV neurons and NF200 (1:2000), a marker of myelinated neurons. DAPI was used as a nuclear marker. Paraffin sections rendered superior morphology to frozen sections. We also observed that transparency of the tissue was associated with length of clearing time. This clearing technique will be applied to spinal cord and skeletal muscle to evaluate whether neural restructuring occurs in the central and peripheral neurons of afferent neurons in cardiomyopathic rats when compared to normal rats.

1. Garry MG (2011). Abnormalities of the exercise pressor reflex in heart failure. Exerc Sport Sci Rev. 39:167-76.
2. Smith SA, Mitchell JH, and Garry MG (2006) The mammalian exercise pressor reflex in health and disease. Exp Physiol. 91:89-102.
3. Hama H, Kurokawa H, Kawano H, Ando R, Shimogori T, Noda H Miyawaki A (2011). Scale: a chemical approach for fluorescence imaging and reconstruction of transparent mouse brain. Nature Neuroscience. 14: 1481-1488.

102.

Effects of medium conditions and hypoxic environment on the formation of tunneling nanotubes in colon cancer

Wen Zhang, Zhilian Xia, Clifford Steer, Emil Lou
Department of Medicine, Divisions of Hematology, Oncology, and Transplantation and Gastroenterology, University of Minnesota, Minneapolis, MN

BACKGROUND: Intercellular communication is vital for growth, survival, and differentiation of all cell types. Recently characterized Tunneling Nanotubes (TNT) are novel structures implicated in long range cell to cell communication by acting as a conduit for the transfer of molecules and organelles in cell types such as cardiomyocytes, mesenchymal stem cells, and cancer cells. The metabolic conditions by which nanotubes form remains unclear and we hypothesized that hypoxia will induce TNT formation.

METHODS: Using colon cancer cell lines as a model, we evaluated the difference in nanotube formation between cells. To test the effects of medium conditions on TNT formation, we incubated cells in high glucose (50mM), low serum (2.5% FCS) medium and in regular medium (25mM glucose, 2.5% FCS). Furthermore, the cells in both medium conditions were then incubated in oxygen concentrations of either 20% (normoxic) or 2% (hypoxic). Nanotube formation was scored under 20x objective magnification and the average of five high power fields was taken.

RESULTS: In preliminary experiments, we observed greater nanotube formation in cells incubated in high glucose, low serum medium and in 2% oxygen. Replication of the experiment is underway.
DISCUSSION: In cancer, the microenvironment affects invasiveness and metastasis. Hypoxia, in particular, is correlated with malignant tumours and nanotube formation might play a role in a tumour's transition from benign to malignant.

103.
Reprogramming of Fibroblasts from Duchenne Muscular Dystrophy Patients into Induced Pluripotent Stem (iPS) Cells

Alexandra Peterson1, Radbod Darabi1, Peter Karachunski2, Jakub Tolar3, and Rita Perlingeiro1
1Lillehei Heart Institute, Department of Medicine, 2Department of Neurology, 3Department of Pediatrics, University of Minnesota

Human induced pluripotent stem (hiPS) cells are derived from somatic cells which have been reprogrammed to a pluripotent state following genetic modification with a cocktail of reprogramming factors (Oct4, Sox2, Klf4, and c-Myc). In contrast to human embryonic stem (hES), cells hiPS cells can be derived from an adult patient rather than an embryo. Not only does the use of hiPS cells circumvent the ethical quandary of hESC use, hiPS cells hold great potential for patient-specific research and therapies. However, when using hiPS cells, it is critical to demonstrate that these cells have pluripotency equivalent to hES cells, and thus hold the capacity to differentiate into multiple lineages.
Fibroblast samples from 4 Duchenne muscular dystrophy (DMD) patients, with ages varying from 12 to 19, and encoding various distinct mutations were subjected to reprogramming using standard retroviral methods. The first iPS colonies emerged in these cultures between 3 and 4 weeks following reprogramming. One representative iPS cell clonal line for each DMD patient was chosen for further characterization.
The pluripotency of these four DMD hiPS cell lines was evaluated by quantitative RT-PCR, FACS, and immunostaining for reprogramming and pluripotency genes, including TRA-1-60, SSEA-4, OCT 3/4, NANOG, and SOX2, as well as staining for alkaline phosphatase. We also evaluated the ability of each DMD iPS cell line to differentiate into embryoid bodies. Further analysis will include the teratoma assay and karyotype analysis, whose results will not be available in time for this presentation. All experiments were carried along with the human ES cell line H1, which was our reference for pluripotency.
We found that all four cell lines expressed very high levels of TRA-1-60 and SSEA-4, with no significant difference from the hES cell control. Expression of OCT 3/4, NANOG, and SOX2 in all four cell lines was also comparable to the control. The same was the case for alkaline phosphatase staining. Although we observed some differences in terms of morphology, with some clones resembling more hES cells, while others displayed certain degrees of differentiation at different passages, morphology per se may not be the best indicator of pluripotency, as all cell lines showed very similar

expression of pluripotency markers, as well as the capacity to differentiate efficiently into embryoid bodies.
Based on these results and the upcoming data on teratoma and karyotype, we have fully characterized 4 DMD iPS cell lines, which are now available for gene correction studies, myogenic differentiation, and future transplantation experiments.

104.
Fluorescence quenching measurements to study the structural defects caused by a myosin essential light chain cardiomyopathy mutation

Ryan Price and Osha Roopnarine. Department of Biochemistry, Molecular Biology and Biophysics, University of Minnesota Medical School.

Our research focuses on the human cardiac disease, familial hypertrophic cardiomyopathy (FHC), in which the left ventricle and inter-ventricular septum of the myocardium is hypertrophied. FHC causes sudden cardiac death in young athletes. It is caused by point mutations in myosin, which is a dimer with a regulatory and an essential light chain (RLC and ELC, respectively). The specific aim is to determine the effect of the E143K-ELC mutation on the structure of myosin using time-resolved fluorescence quenching measurements. A cysteine at C187 in ELC will be labeled in the absence (wildtype) and presence of the E143K-FHC-ELC, with a fluorescent probe, called IAEDANS. The labeled ELCs will then be separately reconstituted into ELC-depleted skeletal muscle fibers. Acrylamide will be used as a “quencher” to determine whether the FHC mutation changes the environment of the probe during rigor, relaxation and contraction of the isometrically held muscle fiber bundle. The probe will be excited at 355nm and time-resolved emission lifetimes will be collected at 460nm during varying [acrylamide] for the wildtype and E143K-FHC-ELC in the muscle fibers. The fluorescence lifetime will decay faster if it is exposed to the acrylamide on the outside of the protein as compared to the more-protected protein interior. The lifetimes will be fitted to two exponential decays, which will be used to determine the quenching constant using the Stern-Volmer equation. This research is significant to understanding how myosin dysfunction is correlated with the phenotype of the FHC disease, and may allow physicians to develop therapeutic methods for managing the disease. This work is supported by funds from a NIH grant AR052360 to OR., and a Gregory Marzolf Undergraduate Research Fellowship to RJP from the Paul and Sheila Wellstone Muscular Dystrophy Center.

105.
Effect of Endoglin Overexpression in Cardiac Development

Jeff Zhang, Luciene Borges, Jacquelyn Catanese, and Rita Perlingeiro Lillehei Heart Institute, Department of Medicine, University of Minnesota

Endoglin (Eng) is an auxiliary receptor for several members of the Transforming Growth Factor (TGF)-beta superfamily, which our laboratory has shown to play a fundamental

role in hematopoiesis. The knockout of endoglin proves fatal to the mouse embryo, and endoglin knockout embryos display enlarged ventricles and an abnormally thin myocardial layer, suggesting that this receptor may also play a role in cardiac growth and development. However, the mechanism by which endoglin affects cardiogenesis is still unknown. In this study, we investigated the effect of endoglin overexpression in the context of cardiac development. We hypothesized that changes in the levels of endoglin expression may affect cardiogenesis. To test this hypothesis, we made use of a mouse embryonic stem cell line encoding an Nkx2.5-EmGFP BAC reporter that was then inserted with a doxycycline-inducible endoglin transgene tagged to IRES-mCherry for selection. We subjected these cells to embryoid body (EB) differentiation, and then assessed the frequency and differentiation ability of cardiac precursors by FACS and qPCR analyses. Our preliminary results demonstrate that endoglin overexpression significantly diminishes the frequency of Nkx2.5+ cardiac progenitors, as the frequency of GFP positive cells was reduced upon doxycycline induction. These data are supported by qPCR analyses that show reduced expression of important cardiac transcription factors, such as Nkx2.5, Mef2c, and Tbx5, as well as late markers of cardiac differentiation, including myosin light chain-2 (Myl2) and -7 (Myl7). Overall, our results indicate that appropriate levels of endoglin are critical for proper cardiac development. Lack of this receptor, as observed by others in vitro and in vivo, as well as forced expression of this receptor, observed in this study, results in reduced and/or abnormal cardiac development, thus suggesting that endoglin plays a significant role in cardiogenesis during embryonic development.

106.

Effects of Voluntary Exercise on Dystrophic Cardiac Muscle

Zach Stevens, Susan Novotny, Michael Eckhoff, Tara Mader, Angela Greising, Shaojuan Lai, Dawn Lowe

This study tests the hypothesis that voluntary, low intensity exercise does not cause additional damage (such as fibrosis, deleterious hypertrophy, or other signs of cardiomyopathy) to dystrophin-deficient cardiac muscle. Previous research has shown that such exercise can benefit dystrophic skeletal muscle but less is known about the heart's response. To investigate this, 4 week old dystrophic mice (mdx) were assigned cages with (n=9) or without (n=5) a running wheel for 8 weeks. Mice with access to running wheels ran 2.6 to 9.0 km/24 hours. At the end of the study mice were sacrificed and hearts are being examined histologically, biochemically for collagen content, and through RT-PCR for changes in gene expression related to fibrosis and heart failure. Preliminary data on hearts from a previous study in which mdx mice wheel ran for 12 weeks indicates no significant difference between exercised and non-exercised hearts in terms of fibrosis.

107.
Etv2 expressing cells contribute to definitive hematopoiesis and adult vasculature

Matthew D. Schreier, Tara L. Rasmussen, Michelle J. Doyle, Kathy Bowlin, Daniel J. Garry
Lillehei Heart Institute, University of Minnesota, Minneapolis, MN 55378

The transcription factor Etv2/ER71 has been shown to be essential in hematopoietic and endothelial cell development. Etv2 is expressed in a short temporal window between embryonic day (E)7.5 and E9.5 and it is unclear whether the early endothelial or primitive hematopoietic cells found during this timeframe contribute to the adult vasculature or to definitive hematopoiesis, respectively. We utilized a transgenic Etv2-Cre in which the 3.9kb regulatory region of Etv2 is used to drive expression of Cre recombinase. Transgenic Etv2-Cre mice were crossed to the Rosa-CAG-ZsGreen Cre reporter, and the brain, testes, liver, spleen, thymus, bone marrow, skeletal muscle, and heart from adult mice, and whole E11 embryos from two hree independent transgenic lines were analyzed using FACS analysis. We found that the majority of cells from the thymus, spleen, and bone marrow expressed ZsGreen, suggesting that these tissues were derivatives of Etv2 expressing progenitors. We further observed that a subset of cells from the liver, skeletal muscle, and heart expressed ZsGreen, and very few cells from the brain and testes expressed ZsGreen. In all tissues the ZsGreen expressing cells were predominantly endothelial or hematopoietic. We confirmed these results using immunohistochemistry. Therefore, we conclude that the Etv2 expressing cells contribute strongly to both definitive hematopoiesis and adult vasculature.

108.
Expression and Purification of Spin-Labeled PLB for EPR Analysis of the SERCA-PLB Complex

Monica Knaack, Zach James, Jesse McCaffrey, and David D. Thomas
Department of Biochemistry, Molecular Biology, and Biophysics, University of Minnesota

We have studied the structure of phospholamban (PLB), a small membrane protein in the sarcoplasmic reticulum (SR) that can inhibit cardiac Ca-ATPase (SERCA), a protein that pumps calcium into the SR after muscle contraction to facilitate relaxation. When PLB inhibits SERCA, the calcium flow is reduced unless PLB is phosphorylated at Ser16. We are interested in studying the structure and dynamics of PLB and the SERCA-PLB complex before and after phosphorylation to determine how phosphorylation relieves PLB's inhibition on SERCA. In order to obtain a better picture of PLB, we have used site-directed mutagenesis to introduce a cysteine residue in place of the native amino acid at specific points along PLB's sequence. This cysteine is later used for spin labeling and electron paramagnetic resonance (EPR) to measure the accessibility and dynamics of PLB at that specific location. We have used a mutant PLB that exists exclusively as a monomer (AFA-PLB) and includes only the cysteine

introduced during mutagenesis to ensure that the spin label will attach to the correct site.

109.

Analysis of the Phosphorylation States of TRPv1 in Dorsal Root Ganglia from Normal and Heart Failure Rats.

Tom Mulvey, Rose Hartnett, Lawrence Stout, Minh Nguyen PhD, Mary Garry PhD, Lillehei Heart Institute, University of Minnesota.

The exercise pressor reflex (EPR) is a mechanism where signals from the contracting muscle, propagated via group III (predominately mechanically-sensitive) and group IV (predominately metabolically-sensitive) skeletal muscle afferent fibers (Kaufman et al., 1984, McCloskey and Mitchell, 1972), elevate mean arterial pressure (MAP) and heart rate (HR).This reflex is abnormal in humans and rats in heart failure and contributes significantly to the morbidity and mortality of this disease. We have attempted to determine the mechanisms that underlie this abnormal reflex in heart failure. Nerve growth factor (NGF) is a target derived trophic factor and its gene is a highly conserved molecule with a high interspecies homology. The biological activity of NGF is regulated by two structurally unrelated receptors: a low-affinity receptor (p75) and a high affinity tyrosine kinase receptor known as trkA. Approximately two-thirds of small diameter (<30 micron), capsaicin sensitive primary afferent neurons express a functional trkA receptor (Shu and Mendell, 2001) and approximately 50-65% of neurons expressing TRPv1 mRNA also expressed trkA mRNA in rat dorsal root ganglia (DRG; Michael and Priestley, 1999; Kobayashi et al., 2005). Nerve growth factor is taken up by TrkA expressing DRG neurons and transported to the cell bodies. Consistent with these observations, NGF positively regulates TRPv1 expression (Winston et al., 2001; Xue et al., 2007), and promotes TRPv1 sensitization by enhanced cell surface expression via phosphorylation of TRPV1 at a single tyrosine residue, Y200 (Zhang et al., 2005; Stein et al., 2005). We have observed significant decreases in the levels of NGF in fast and slow twitch skeletal muscle and dorsal root ganglia of rats with heart failure as well as a reduction of TRPv1 on the surface of cells from animals in heart failure. In these studies, we will determine the phosphorylation state using immunoprecipitation of the TRPv1 receptor in DRG from rats in heart failure compared to control animals.

110.

Calcium Imaging: Study of Group III and Group IV Afferent Neurons in Normal and Heart Failure Rats

Will Barth1, Minh Nguyen PhD1, Larry Stout1, Iryna Khasabova PhD2, Virginia Seybold PhD2, Mary Garry PhD1
1Lillehei Heart Institute, University of Minnesota, Minneapolis, Minnesota
2Department of Neuroscience, University of Minnesota, Minneapolis, Minnesota

The exercise pressor reflex (EPR) is a cardiovascular reflex that controls blood pressure and heart rate in response to exercise. We, and others, have determined that the EPR is exaggerated in heart failure. We have also determined that this abnormality is mediated by a reduced responsiveness of group IV (metabolically sensitive) afferent neurons together with an increased responsiveness of group III (mechanically sensitive) afferent neurons. While group IV neurons are marked by TRPv1 cation channels, known to be selectively activated by capsaicin, there is no known marker for group III neurons. The purpose of this experiment is to discover a marker for group III neurons as this could be a potential therapeutic target for the normalization of the EPR in heart failure. In addition, we will validate that the lack of responsiveness of group IV afferent neurons and the exaggerated responsiveness of the group III afferent neurons is maintained in culture. In this regard, we hypothesize that group III neurons will have greater excitability in heart failure rats than in normal rats, and the group IV neurons will be less excitable in heart failure than in normal rats. Rat dorsal root ganglia (L4-6) were harvested from normal and cardiomyopathic rats and plated on laminin-coated, grided glass coverslips and placed in culture for 16-18 hours. Neurons are loaded with 4.5 μl^2 of 1 mg/mL Indo-1, a calcium indicator, in 1.5 mL of HEPES solution for 45-75 minutes. Cellular responses to K+ (20 mM, 25 mM, 30 mM, and 50 mM KCl solutions) and capsaicin (250 nM and 500nM) were measured using a dual-emission microfluorimeter. Response data, in the form of intracellular calcium concentration, was compiled using Felix Software (Photon Technology International). Felix Software calculated [Ca2+] using the equation: [Ca2+]=KDß(R-Rmin)(R-Rmax), where R=405 nm/485 nm fluorescence emission ratio corrected for background fluorescence. Responses to K+ and capsaicin were considered significant when the amplitude of the response was greater than 50% of the Ca2+ baseline. Three point dose response curves for each stimulant were generated. We used size and responsiveness of neurons to capsaicin as an initial sort to differentiate between group III and group IV afferents. To further distinguish between group III and group IV afferents, we stained for IB4 and NF200 (a marker of myelin). This study will help to validate this model as an in vitro screening tool for the EPR and will serve to define a putative therapeutic target for the treatment of the exaggerated EPR in heart failure.

111.

Protein-based sarcomeric therapeutics for the diseased heart

Gabriela Ruiz-Colón, Anthony Vetter and Joseph M. Metzger
Department of Integrative Biology and Physiology
University of Minnesota Medical School

According to the World Health Organization, approximately seventeen million people die of cardiovascular diseases each year. Heart disease has been cited by the Center for Disease Control as the leading cause of death in the United States (599,413 deaths in 2009). While potential gene therapies are being developed, such as the cTnI A164H, colloquially the “Guardian Angel”, an efficient delivery mechanism is necessary, as viral delivery may require prophylactic treatment. To address alternative and complementary

delivery strategies for ischemic heart disease, adult rat cardiac myocytes were extracted and exposed to ChariotTM protein delivery reagent (Active Motif, Carlsbad, CA) in conjunction with Alexa Fluor 488 Phalloidin, a cell impermeable, fluorescent dye that binds to F-actin. The cardiac myocytes were studied ex vivo by fluorescence microscopy. Preliminary studies indicate trans-sarcolemmal delivery and sarcomeric incorporation when Alexa Fluor 488 Phalloidin is complexed with micromolar concentrations of ChariotTM. This experiment will be used as the scaffolding to design Trans-Activator of Transcription (TAT) modified sarcomeric proteins. TAT is an HIV gene that is expected to elicit a similar delivery modality as ChariotTM. The purified cardiac subunits of troponin (cTnI, cTnC and cTnT) will be covalently modified with a TAT moiety in an attempt to enhance trans-sarcolemmal translocation for the expressed purpose of endogenous troponin replacement. The “Guardian Angel”, will be one of several inotropic proteins delivered to isolated cardiac myocytes in order to study the feasibility of developing novel biological strategies featuring sarcomeric protein delivery-based therapeutics. Ultimately, if successful, this delivery mechanism could serve as a cornerstone method in protein therapeutics, leading to an effective treatment for heart disease.

112.
Genetic and environmental models of obesity: role of β-adrenergic receptors

Jacob T. McCallum, Maria Razzoli, Cheryl Cero, Ivana Ninkovic, Bradford Lowell1, Alessandro Bartolomucci.
Department of Integrative Biology and Physiology, University of Minnesota.
1 Beth Israel Deaconess Medical Center, Harvard Medical School

Gene×Environment models are the most promising avenue to study the current obesity epidemic, linking genetic predisposition and risk factors. Social stress and high fat diet (HFD) are recognized risk factors for obesity [1] but the underlying molecular mechanisms have not been fully identified yet. Beta-adrenergic receptors (βAR) are involved in sympathetic regulation of adiposity and energy balance; βless mice [2] that lack the three □AR subtypes exhibit defective adaptive thermogenesis, very low energy expenditure, and an obesity-prone phenotype exacerbated by exposure to HFD. Wild type (Wt) and βless mice were fed HFD and subjected to varying levels of social stress known to affect vulnerability to obesity in opposite directions: 1) weight loss caused by withholding social interaction in obese mice and 2) weight gain caused by chronic exposure to an aggressor. βless and Wt mice were housed in groups and fed HFD for 9 weeks and subsequently individually housed for 6 weeks under HFD. Controls remained group housed throughout. Results showed that singly housing obese mice led to body weight (BW) loss and that this effect did not require functional □AR. In expe tested the hypothesis that βless mice would be more vulnerable to chronic subordination stress (CSS)-induced obesity involving daily inescapable social defeats for 4 weeks and compared to grouped littermates while fed HFD [1]. Preliminary data in a first cohort of mice showed that CSS increased BW, calorie intake, and fat mass in Wt mice [1]. βless mice showed normal stress-induced hyperphagia but, surprisingly no BW

or fat mass gain. Lower weight gain in βless mice could be explained by a paradoxical increase in energy expenditure as determined by indirect calorimetry in absence of hyperlocomotion. These data confirm that social stressors have complex, marked effects on metabolic function. Interestingly, βless mice resisted the metabolic effects of CSS albeit fed a HFD. Further studies are needed to address the biological basis of the observed phenomenon to better understand the molecular basis of vulnerability to metabolic disorders.

113.
Chronic stress shifts the phase of adrenal clock gene rhythms

Carley Karsten, Maria Razzoli, J. Marina Yoder, Alessandro Bartolomucci, and William Engeland, Departments of Neuroscience and of Integrative Biology and Physiology, University of Minnesota

The hypothalamic-pituitary-adrenal (HPA) axis is characterized by a robust circadian rhythm in adrenal secretion of glucocorticoids such as corticosterone. The glucocorticoid rhythm that serves to synchronize other peripheral clocks and to maintain homeostasis is driven in part by adrenal clock genes. Mechanisms for entrainment of the adrenal clock, however, remain unclear. Since stress activates the HPA axis, it is possible that entrainment of the adrenal clock and, concomitantly, glucocorticoid rhythms would be susceptible to stress. The present experiment aimed to test the hypothesis that chronic stress can alter adrenal clock gene rhythms. Clock gene rhythms were assessed using mPER2::Luciferase (PER2Luc) knockin mice in which rhythms in bioluminescence reflect the expression of the Period 2 clock gene. PER2::Luc mice underwent chronic subordination stress (CSS) consisting of daily exposure to a dominant mouse for two weeks. In comparison to control mice that underwent daily handling only, CSS mice showed a robust stress phenotype consisting of increased feeding and body weight, adrenal hypertrophy, and thymic involution. Using photomultiplier tube detectors, PER2luc activity was measured in adrenal explants collected from CSS and control mice. In the CSS mice, the peak phase of the adrenal PER2luc rhythm occurred 2h earlier than that observed in control mice, while the rhythm in other tissues such as the pituitary was unaffected. In contrast, a single acute stress had no effect on the adrenal PER2luc rhythm. Basal plasma ACTH and corticosterone were unaffected by CSS. The finding that adrenal clock gene rhythmicity, but not plasma corticosterone, was shifted suggests that the corticosterone rhythm may occur independently of adrenal clock gene rhythms. These data indicate that a novel consequence of chronic activation of the HPA axis is alteration in entrainment of the adrenal clock gene rhythm. Supported in part by NSF IOS1025199.

114.
Cellular reprogramming to blood using a transcription factor cocktail

Thomas Knoedler, Jai Prakesh Richard, and Michael Kyba
Lillehei Heart Institute

During normal development, cells differentiate in a specific sequence to give rise to organs. This sequence is controlled by the spatio-temporal expression of individual transcription factors. Recent work has shown that manipulation of the expression of certain key transcription factors can modify cell fate, for example reprogramming differentiated somatic cells to pluripotent embryonic stem-like cells, or iPS cells. Our investigations indicate that it is possible to reprogram somatic cells from one fate directly into another, bypassing the pluripotent intermediate state. To investigate this, we have made use of ex vivo culture of mouse tail tip fibroblasts (TTFs) from a mouse model with conditional expression of three key hematopoietic regulators, SCL, LMO2, and GATA2. In the absence of expression of these three factors, blood is not produced. But, when the factors are induced in differentiating mES cells, they interact synergistically and even in the absence of mesoderm the majority of cells take on a hematopoietic phenotype. We present data on the effects of cytokines and differential oxygen conditions on the efficiency of reprogramming mouse embryonic fibroblasts (MEFs) and adult tail tip fibroblasts from transgenic mice with conditional expression of SCL, LMO2, and GATA2 to study reprogramming of somatic cells from an adult.

115.
Regulation of actin dynamics by cofactors within striated muscle

Praveena Narayanan1, Benjamin J. Perrin2, James M. Ervasti2
1Lillehei Heart Institute Summer Research Scholars Program, University of Minnesota – Twin Cities, Minneapolis, Minnesota
2Department of Biochemistry, Molecular Biology and Biophysics, University of Minnesota – Twin Cities, Minneapolis, Minnesota

Actin is one of the major cytoskeletal proteins found in eukaryotes, and its processes are indispensable for the generation of force and movement in striated muscle. To ensure its optimal function, actin dynamically polymerizes and depolymerizes during the assembly and maintenance of myofibrils. These complementary actions depend on the precise orchestration of a number of cofactors. Actin Interacting protein 1 (Wdr1), Coronin, and ADF/cofilin (Cofilin) have been identified as regulatory proteins and are thought to function as a tripartite complex to affect actin dynamics. However, the synergistic interplay of these proteins in the mammalian model is poorly understood. Furthermore, the activity of this complex towards different actin isoforms or bundled actin assemblies has not been determined. To address these questions, we have expressed and purified recombinant forms of the proteins by molecular cloning methods and examined their cooperative function through a cosedimentation assay. The assay involves the incubation of Cofilin, Coronin and Wdr1 with a commercial source of skeletal actin. Samples are spun at 500 x g for 30 minutes, separated by supernatant and pellet, and analyzed by coomassie staining. A shift of actin from the pellet to the supernatant relative to controls containing only actin indicates enhanced depolymerization. Because of the complexity involved with actin binding proteins, we are experimenting with multiple isoforms of Coronin (Coro1a and Coro2b) and different

modes of expression. We have already witnessed a slight shift from pellet to supernatant when Coro1a, Wdr1 and Cofilin are present together. We seek to further determine if depolymerization activity extends to actin filaments bundled by fascin. Insight into the cooperative effect of these regulatory factors provides a better picture of how small deficiencies in these cofactors may lead to striated muscle dysfunction and disease. As a next step, we have begun to characterize the skeletal muscle phenotype of mice with reduced expression of Wdr1.

116.

α-Dystrobrevin functions to reinforce the interaction between dystrophin and the membrane, loss of α-dystrobrevin results in significant loss of cardiac reserve

Jon Dean, Katharine Sharpe, and DeWayne Townsend. Integrative Biology and Physiology, University of Minnesota, Minneapolis, MN, 55455

The C-terminal region of dystrophin is highly conserved across vertebrates, but its function is largely unknown. α-Dystrobrevin (DB) is one of several proteins that bind to this region of dystrophin. Mice lacking α-DB demonstrate a mild myopathy in skeletal muscle, but the phenotype of the heart has not been fully characterized. Here we demonstrate that the loss of α-DB significantly weakens the association of cardiac dystrophin with membrane glycoproteins. In the absence of α-DB, wheat germ agglutinin pull down assay reveals a dystrophin:α-dystroglycan ratio only 13% of that observed in wildtype mice. The physiological importance of the disruption of this interaction is evident in the marked pathology induced by chronic isoproterenol administration. This challenge protocol results in significant myocardial damage and mortality >60% in mice lacking α-DB, in contrast wild type mice survived with minimal injury. The lesions and mortality observed in the α-DB null mice were not different from mice lacking dystrophin. These findings have significant implications on the design of truncated dystrophin constructs suitable for delivery via gene therapy, as many of these constructs lack the binding domain for α-DB.

117.

Coronary regulation in dystrophic cardiomyopathy

Zachary Stelter and DeWayne Townsend. Integrative Biology and Physiology, University of Minnesota, Minneapolis, MN 55455

Duchenne muscular dystrophy (DMD) is a devastating disease of both skeletal and cardiac muscle that occurs secondary to the loss of the protein dystrophin. Dystrophin is a large cytoskeletal protein that is thought to provide mechanical stability to the muscle membrane. However, much evidence also suggests that it may serve a signaling role. In skeletal muscle dystrophin has been implicated in the local control of blood flow. Here we examine the regulation of coronary blood flow in the mdx mouse, a model of DMD. Using a Langendorff perfused heart model left ventricular function, oxygen consumption, and coronary flow were monitored in the presence or absence of

dobutamine. At rest mdx mice demonstrate significant increases in coronary blood flow, but ventricular function and oxygen consumption are normal. Cardiac reserve was assessed by infusion of beta-adrenergic agonist dobutamine. In wild type mice, this treatment resulted in dramatic increases in both systolic (LVDP & max dP/dt) and diastolic (min dP/dt) function. These increase in ventricular contraction were significantly attenuated in mdx mice. In both wild type and mdx mice, coronary blood flow was significantly increased with dobutamine, although the magnitude was significantly smaller in the mdx mouse. The lusitropic actions of dobutamine were also significantly attenuated in mdx mice. Oxygen consumption was increased equally in both wild type and mdx mice following dobutamine treatment. To asses the role of nitric oxide, studies were performed in the presence of the general nitric oxide synthase inhibitor L-NAME. In wild type hearts, L-NAME generated small, but significant, increases in both systolic and diastolic function; these baseline effects are absent from mdx hearts. The presence of L-NAME significantly potentiates the response of mdx mice to dobutamine. These data suggest that in the mdx heart NO is acting as a negative inotrope and acute inhibition of NO production increases the mdx heart's contractile function.

118.

Green Fluorescent Protein membrane localization via N-terminal myristylation: proof-of-concept study for the design of a calcium buffering system at the plasma membrane

Jenny Seong, Michelle L. Asp, Joshua J. Martindale and Joseph M. Metzger

Duchenne Muscular Dystrophy (DMD) is a lethal X-linked recessive disease associated with progressive muscle weakness. It results from mutations in the dystrophin gene, which is a component of the dystrophin glycoprotein complex (DGC) present at the plasma membrane of skeletal and cardiac muscle cells. Lack of dystrophin destabilizes the DGC and creates microtears in the plasma membrane, causing calcium (Ca2+) influx and Ca2+ overload. Not surprisingly, incidence of cardiomyopathy is nearly 100% for DMD patients and it has become a major cause of mortality ever since pulmonary ventilator support and other respiratory therapies have become readily available. Now that an increasing number of DMD patients are reaching the later stages of the condition associated with the onset of cardiomyopathy, applied research on effective treatments has become vital. In an effort to reduce cellular damage caused by Ca2+ overload in cardiac muscle cells lacking dystrophin, we plan to target various low-affinity high-capacity Ca2+ binding proteins such as calreticulin, calsequestrin, Grp94 and BiP to the plasma membrane by adding one of several membrane localization sequences to the appropriate genes. Conceptually, upon Ca2+ influx, these membrane-associated binding proteins will have the capacity to "transiently trap" Ca2+ ions at the plasma membrane in order to reduce Ca2+ overload in cardiac myocytes. Here, we show the results of a proof-of-concept study in which a myristylation sequence has been cloned into the N-terminus of the GFP gene and subsequently transfected into HEK cells to determine its specificity for the plasma membrane. Long term results may hold promise for the development of a new therapy for dystrophin-associated cardiomyopathy, as

current therapies such as ACE inhibitors, β-adrenergic blockers and glucocorticoids delay the onset of cardiac complications but do not directly treat them.

119.
Characterization of myocytes derived from human inducible pluripotent stem cells

Sophie Zhang

The textbook belief regarding cardiac regenerative potential has been that no new myocytes are generated post-birth in mammals. This belief was supported by the absence of mitotic figures in cardiac myocytes, as well as the absence of new cardiac myocytes generated after acute myocardial infarction. Recent studies, however, have challenged this static theory of the heart, providing evidence that: 1.) myocytes are replaced throughout the human lifespan by a population of resident cardiac stem cells, and that 2.) the human heart contains cycling myocytes undergoing mitosis and cytokinesis under both normal and pathological conditions. From these findings, a novel strategy of managing heart failure patients is on the horizon that uses autologous cardiac progenitors to rejuvenate dysfunctional aging hearts.

From the cellular and molecular perspective, the progression of heart failure is a result of the inability of damaged and apoptotic myocytes to be replaced by new healthy myocytes. While there are a number of reports in recent literature on myocardial repair which utilize different types of adult stem cells, the underlying mechanisms of the observed improvement in cardiac contractile performance in response to cell transplantation remains largely unknown. Furthermore, the absence of a myocyte line that can model contractile abnormality in failing hearts has been a significant obstacle in characterizing mechanisms of LV chamber dysfunction in patients with heart failure. Using novel molecular and cellular technologies, the specific aims (SA) of the summer project is to compare the physiological, phenotypic, and molecular characteristics of cardiomyocytes differentiated from human inducible pluripotent stem cells (hiPSCs, derived from both DCM patients and normal controls). The results of these studies may lead to better diagnostic and therapeutic modalities for DCM

120.
Identification of regulatory region(s) for MyoD gene transcription in muscle stem cells.

Wilsen Hadiwikarsa, Atsushi Asakura

Satellite cells are a small population of myogenic stem cells located beneath the basal lamina of skeletal muscle fibers in which they are responsible for muscle repair as the skeletal muscle stem cells. Normally quiescent satellite cells are negative for MyoD, which is a muscle-specific transcription factor and regulates myogenic differentiation.

However, upon muscle injury or exercise, satellite cells are activated, enter the cell cycle, and initiate MyoD expression. However, it remains to be elucidated how MyoD expression is transcriptionally regulated during this satellite cell activation. For this purpose, we have been utilizing the technique termed Chromosome Conformation Capture assay (3C assay) in order to determine the upstream regulatory region(s) for MyoD gene transcription during satellite cell activation. The 3C assay technique was recently found by Job Dekker and is known as an approach to detect the frequency of interaction between any two genomic loci within a great distance apart, such as a promoter and enhancer region. In addition, we have made several MyoD-reporter gene constructs in which the luciferase gene will be activated by the MyoD enhancer/promoter combinations. Here we show preliminary data of the MyoD enhancer region(s) which interact with the promoter region.

121.
The effects of cyclic stretching on cell and fiber alignment and ERK pathway activation of human dermal fibroblasts entrapped in fibrin gels

Stefani Prigozhina
Summer Student w. Lillehei Summer Research Program
Mentor: Dr. Bob Tranquillo, Biomedical Engineering Department

For tissue engineered heart valves (TEHVs) to function properly in vivo, they must exhibit mechanical properties similar to those of native heart valves. Mechanical conditioning, such as cyclic stretching with bioreactors, can be used to improve properties like tensile strength, cell alignment, and collagen production in fibrin-based tissue, formed when cells entrapped in fibrin gel remodel it into a cell-produced ECM. To test how cells respond to cyclic stretching when stretched for a certain amount of time, neonatal human dermal fibroblast (nHDF) cells were cast in fibrin gel in the wells of Flexcell plates. The samples were divided into four sets and were uni-axially stretched at 8% for either 0 min, 15 min, 5 hr, or 23 hr with the Flexcell 5000 system. Thereafter, the samples were removed from the plates, imaged with polarized light microscopy, and analyzed qualitatively for cell alignment. Results show that the samples stretched for 5 and 23 hours had visibly improved cell alignment with the stretch direction compared to those stretched for 0 and 15 minutes. To test protein signaling for ERK and phosphorylated ERK (pERK) with respect to incubation time and stretch time, fibrin gel samples containing nHDF were once again cast into Flexcell plates. One set of plates was incubated for 4 days and the other set for 13 days in a cell culture incubator prior to Flexcell stretching at 8% for 15 min and 8% for 1 hour. Also, one set of plates was not stretched with the Flexcell system but incubated for the same amount of time as the stretched plates. The resulting tissues were extracted, and are currently being analyzed for ERK and pERK with Western blots to see how incubation time and stretch time impact the presence of these proteins. Varying the initial fibrin gel stiffness and the degree of stretching can provide further insights into what specific parameters produce the most ideal tissue for engineered heart valves.

Graduate Students

200.
Effect of ENDOGLIN Induction on the Generation of Hematopoeitic Progenitors from Human Embryonic Stem Cells

Kerem Fidan, Radbod Darabi, Rita CR Perlingeiro
Lillehei Heart Institute, Department of Medicine, University of Minnesota

Endoglin, an accessory receptor of transforming growth factor-β (TGF-β) superfamily, plays an important role in early hematopoietic and endothelial lineage development. Our recent studies on mouse embryonic stem (ES) cells revealed increased numbers of primitive erythroid (EryP) colonies following endoglin overexpression (see Baik's poster). However endoglin overexpression inhibited endothelial and cardiac cell differentiation. Importantly in human, ENDOGLIN mutation results in the vascular disorder hereditary hemorrhagic telangiectasia (HHT) which is characterized by abnormal blood vessel formation.

The aim of this project is to evaluate the effect of ENDOGLIN overexpression during early human hematopoietic development using the in vitro differentiation system from human ES cells. To do this, we used a human ES cell line (H1) encoding a doxycycline inducible ENDOGLIN lentiviral cassette, which allows us to overexpress ENDOGLIN during in vitro differentiation. ENDOGLIN was induced at the point of BRACHYURYexpression, which indicates mesoderm formation, using two distinct in vitro differentiation methods, embryoid body (EB) or monolayer. In the first protocol, Endoglin was induced by adding doxycycline at EB day 5, and in the monolayers, at day 6. Experimental control non-induced groups were run side-by-side.

Characterization of hematopoeitic differentiation will consist of FACS analyses for hematopoetic markers, including CD45 and Glycophorin A, as well as methylcellulose colony assays. Our preliminary results show that ENDOGLIN indeed promotes expansion of the human hematopoetic progenitor pool, as evidenced by the up-regulation of the pan-hematopoietic marker CD45, indicating a critical role for this receptor and TGF-β/BMP signaling in human hematopoietic development.

201.
Molecular Dynamics of a pH responsive histidine-modified cardiac troponin I

Evelyne M. Houanga,b ,Nathan J. Palpanta, Yuk Y. Shamb, Joseph M. Metzgera
Department of Integrative Biology and Physiologya, University of Minnesota Medical School and the Center for Drug Designb, University of Minnesota Academic Health Center, Minneapolis, Minnesota

Cardiac troponin I (cTnI) functions as the molecular switch of the thin filament. Studies have shown that a histidine button engineered into cTnI at residue 164 (cTnI A164H)

enhances inotropic function in the context of numerous pathophysiological challenges. In vitro studies of myofilament calcium sensitivity and sarcomere shortening kinetics of histidine ionization mimetics in intact and permeablized myocytes at baseline (pH 7.4) indicated similar cellular contractile function and myofilament calcium sensitivity between myocytes expressing WT cTnI and cTnI A164H while A164R (mimetic of constitutively protonated histidine) showed a hypercontractile phenotype associated with increased myofilament calcium sensitivity. Under acidic conditions, compared to depressed function in myocytes with WT cTnI, myocytes expressing cTnI A164H maintained myofilament calcium sensitivity and contractile performance similar to the constitutively protonated calcium sensitizer, cTnI A164R. The role of histidine modified cTnI was assessed by molecular dynamics (MD) simulations of WT cTnC in complex with WT and histidine-modified cTnI in the calcium saturated state. 40 ns Simulations were carried on the truncated cTnI (148-173): cTnC (1-90) based on the X-ray crystallographic structures of the full length human cardiac (PDB: 1J1E) troponin I complexed to Ca+2 bound troponin C. The cTnI A164H and cTnIA164R mutants were generated by amino acid substitution using CHARMM. Similar intermolecular atomic contacts were observed between the WT and the deprotonated cTnI A164H variant. In contrast, simulations of protonated cTnI A164H showed various potential structural configurations, one of which included a salt bridge formation between His 164 of cTnI and cTnC Glu 19. These data suggest that the molecular sensor capacity of cTnI A164H is dependent on histidine ionization state and thus responds to changes in the cytosolic milieu.

202.

Tools to Evaluate SERCA and Phospholamban Function in HEK Cells

Vaibhav Sharma, Simon J. Gruber, David D. Thomas
Biochemistry, Molecular Biology, and Biophysics, University of Minnesota

We are using fluorescent fusion proteins (FFP) expressed in HEK cells to study the relationships among the structure, dynamics, and function of the sarcoplasmic reticulum Ca-ATPase (SERCA) and its cardiac regulator phospholamban (PLB), with the goal of designing activators of SERCA for treatment of heart failure (HF) and muscular dystrophy (MD).

Heart Failure (HF) is a complex syndrome that frequently involves deficiencies in cardiac calcium cycling [1-2]. Ca2+ drives muscle contraction, and relaxation is accomplished by the sequestration of Ca2+ by the sarcoplasmic reticulum Ca-ATPase (SERCA), which is inhibited by phospholamban at submicromolar [Ca2+] in cardiac muscle. We are measuring fluorescence resonance electron transfer (FRET) using FFPs CFP-SERCA2a and YFP-PLB as well as intermolecular FRET in a doubly labeled RFP-GFP-SERCA2a. These probes make it possible to look for drugs or PLB mutants that could be therapeutic for patients with HF if they successfully activate SERCA.
In addition to FFPs, we are developing a system to purify heterologously expressed SERCA2a from mammalian (HEK) cells. Expression and purification of SERCA2a would make it possible to create a cys-null SERCA2a and introduce cysteine residues in new

locations for site-specific labeling with EPR or fluorescent probes. Cysteines are the optimal naturally occurring residues to label chemically, and SERCA has 26 in total. However, currently, only one endogenous residue can be easily labeled specifically (Cys674). Of these 26 cysteines, 11 are known to be mutable, and 2 are known to be non-mutable.
Lastly, we are using flow cytometry to evaluate new stable cell lines. Flow cytometry detects the fluorescence of single cells by passing them through a small sheath individually, and also has the capability of measuring cell size and density. Flow cytometry is being used to screen our double-fluorescent protein (RFP-GFP-SERCA2a) or cell lines expressing multiple FFPs (e.g. CFP-SERCA2a/YFP-PLB).

203.
The Atlas of Human Cardiac Anatomy

A Free-Access Educational Website
Paul A. Iaizzo1,2,3, Michael G. Bateman1,2,4, Jason L. Quill4, Christopher D. Rolfes1,2,4, Stephen Howard1,2,4, Julianne Eggum1,2, Ryan Goff1,2, Michael D. Eggen4, Gary Williams3, Alexander J. Hill4 Departments of Biomedical Engineering1, Surgery2, and Physiology3, University of Minnesota, Minneapolis, MN 55455; Medtronic, Inc4, Minneapolis, MN

The University of Minnesota's Visible Heart® Laboratory has developed a novel free-access educational website highlighting both functional and static human cardiac anatomy: The Atlas of Human Cardiac Anatomy (http://www.vhlab.umn.edu/atlas/). This website contains freely downloadable footage from over 100 human hearts, with associated text describing these anatomies, and with various related educational tutorials. To collect these images and videos, human hearts (deemed non-viable for transplant) were obtained from LifeSource (MN) or the U of MN's Bequest Program, as gifts for research from the organ donors and their families. To honor these donations, all obtained/developed educational information has and will be gifted back for the training of interested individuals: which may range from students in K-12, undergraduates, post-graduates, cardiovascular residents or fellows, physicians, or patients themselves. This library of heart images and videos, includes those obtained with videoscopes, fiberscopes, ultrasound, fluoroscopy, MRI, and/or CT: from perfusion-fixed specimens and/or from reanimated specimens using Visible Heart® methodologies (Hill et al., 2001). "The Atlas" is a living website that is updated on a monthly basis with new educational information, images, video footage, and/or requested materials.

204.

Digital Reconstructions of the Human Coronary Arteries and Cardiac Veins using Contrast-Computed Tomography

Julianne H Eggum, Matt Venegoni

Introduction

It is important to understand the relationship between the coronary arteries and cardiac veins for the development of cardiac devices. These models are of particular interest in the design of coronary sinus (CS) occulders and CS annuloplasty devices for the mitral valve. It is important that the deployment such devices do not damage the nearby coronary artery system.

Methods

First, we obtained computed tomography (CT) scans of 8 perfusion fixed human hearts while injecting contrast into the cardiac veins. Next, we obtained additional CT scans while injecting contrast in the coronary arteries. We used Mimics Software (Materialise, Leuven, Belgium) to create and then combine 3D digital reconstructions of the vessel systems.

Results

The figure displays three coronary systems of varying diseased states.

Conclusion

Using these models, device developers and clinicians can take various anatomical measurements such as the distance between a given artery and vein to optimize device design. We will continue to develop this novel database of human coronary anatomy.

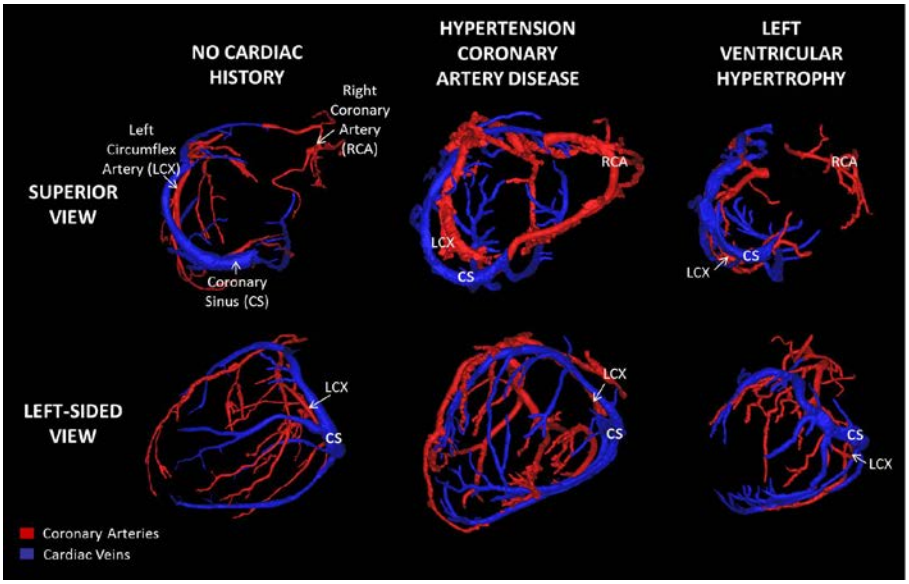

205.

3D Reconstructions of the Human Cardiac Venous System using Contrast Computed Tomography for Anatomical Evaluation

Julianne Eggum, Allison Larson, Emily Fitch, Paul Iaizzo

It is important to understand human cardiac venous anatomy for the development of cardiac devices that are deployed within such vessels. More specifically, quantification of the venous anatomy will assist in the design of cardiac resynchronization therapy devices and their delivery systems.

We obtained computed tomography scans of perfusion-fixed human hearts while injecting contrast into the cardiac veins. To date, we have generated 30 digital reconstructions from over 100 scans (Materialise, Leuven, Belgium) and measured various anatomical parameters.

The table presents the mean anatomical parameters analyzed to date. The figure displays 3D reconstructions of venous systems of varying diseased states.

We will continue to build this novel database of cardiac venous anatomy to allow device designers and clinicians to better understand the degree of anatomical variability that exists between human hearts.

Vein	Distance from the CS (mm)		Ostial Diameter (mm)		Branching Angle (□)	Arc Length (mm)	Tortuousity (Arc Length/ Linear Distance)
Posterior Interventricular							
n = 30	NA	5.0	NA	126.9	1.36		
Posterior							
	12.8	3.8	105.4	75.0	1.22		
Postero-Lateral							
n = 15	40.4	4.6	93.7	61.1	1.21		
Lateral							
n = 30	59.2	4.1	111.2	71.6	1.23		
Antero-Lateral							
n = 15		68.4	3.8	108.3	56.9	1.17	
Anterior Interventricular							
n = 30	96.0	5.1	151.2	110.2	1.41		

206.

Structural Dynamics of Calcium Transport Proteins Detected by Saturation Transfer Electron Paramagnetic Resonance

Jesse E. McCaffrey, Zachary M. James, Kurt D. Torgersen, Christine B. Karim, Edmund Howard, and David D. Thomas
University of Minnesota, Minneapolis, MN 55455, USA

We have used conventional and saturation transfer electron paramagnetic resonance (EPR) to probe the structural dynamics of the integral membrane protein phospholamban (PLB), as a function of phosphorylation and the presence of its regulatory target, the sarcoplasmic reticulum calcium ATPase (SERCA). Our goal is to elucidate the mechanism of SERCA inhibition by PLB, which is needed for the rational design of therapies to improve calcium transport in muscle cells. We used the monomeric mutant AFA-PLB, with the rigid electron spin label TOAC incorporated at position 36 in the transmembrane domain, and reconstituted the protein in lipid vesicles. EPR experiments were performed to determine the nanosecond (conventional EPR) and microsecond (saturation transfer EPR) rotational motions of PLB, as modulated by phosphorylation of PLB at serine 16 (pPLB), and/or addition of excess SERCA. Neither SERCA binding nor PLB phosphorylation caused significant changes in conventional EPR spectra of PLB, indicating no effect on the nanosecond flexibility of PLB's transmembrane domain. However, ST-EPR found that addition of SERCA caused a large decrease in microsecond rotational motion for both PLB and pPLB. Phosphorylation of PLB caused no effect in the absence of SERCA and slight immobilization in the presence of SERCA. These results indicate that both PLB and pPLB bind to SERCA, and PLB phosphorylation does not reverse this binding. Therefore, PLB phosphorylation relieves SERCA inhibition primarily by changing the structural dynamics of the SERCA-PLB complex, not by dissociation of the complex.
This work was funded by grants from NIH (R01 GM27906 and T32 AR007612).

207.

Comparable Analysis of Vasculature Functions in Mesenchymal Stem/Stromal Cells Derived from Bone Marrow, Human Embryonic Stem Cells and iPS cells

Li, Li (MS)

Mesenchymal stem/stromal cells (MSCs) are multipotent cells that have differentiation potential into forming multiple cells types of mesenchymal lineage. Moreover, their abilities to migrate to sites of injury like myocardial infraction, and stimulation of resident progenitor cells make them attractive for regenerative medicine. We have developed MSCs from human embryonic stem cell (hESC) and induced pluoripotent stem cell (iPSC), which would provide unlimited resource of MSCs for future clinical use. In order to investigate how these hESC and iPSC derived MSCs function in terms of vasculature, here we compare their migration ability in response to cytokines, permeability to large molecule as well as gene arrays to MSCs isolated from adult bone

marrow (BM-MSCs). Both phenotype and genotype analysis showed these hESC and iPSC derived MSCs had high level of similarity to BM-MSCs. Gene array identified higher expression levels of GDF-5, BGLAP and vWF in hESC-MSCs compared with iPSC-MSC and BM-MSC. Functional analysis showed like BM-MSCs, hESC and iPSC-MSCs could migrate through membrane coated with collagen and be permeable to large molecular weight molecule. In conclusion, our hESC and iPSC-MSCs are phenotypically, genotypically and functionally comparable to BM-MSCs. And the generation of MSCs from hESCs and iPSCs will facilitate the application of MSCs for clinical therapies due to their multipotency and important roles in vasculature.

208.
Local onset of Calcium Alternans precedes voltage alternans in Langendorff perfused rabbit hearts

Ramjay Visweswaran, Stephen McIntyre, Elena Tolkacheva

Introduction: Alternans, defined as a beat-to-beat alternation in the cardiac action potential duration (APD), has been considered to be a strong marker of electrical instability and a harbinger for ventricular fibrillation, which is a major cause of sudden cardiac death. Recent studies have shown that APD alternans develops locally in the whole heart, and then occupies the entire heart as the pacing rate increases. In the heart, APD alternans can be accompanied by alternans in intracellular calcium ([Ca2+]i) transients leading to electromechanical (EM) alternans. Although some techniques have been developed to predict APD alternans, the onset of [Ca2+]i and therefore, EM alternans has never been predicted. The aim of this study is to investigate the spatio-temporal evolution of EM alternans in the heart and to determine whether its local onset can be predicted. The ability to predict the onset of alternans is beneficial, since it is a precursor to various arrhythmias. Therefore, predicting alternans is a valuable clinical tool, especially for use with implantable pacemakers, paving the way for preemptive interventions.
Methods: Alternans was induced in the Langendorff-perfused rabbit hearts (n=5) by periodic pacing at progressively decreasing basic cycle length (BCL) from 300 ms to 150 ms using a perturbed downsweep protocol, and simultaneous voltage-calcium optical mapping of right ventricle (RV) was performed. Alternans in APD, [Ca2+]i amplitude (CaA) and duration (CaD) were calculated at each pixel as the difference in corresponding values between two consecutive beats, and corresponding 2-D alternans maps were constructed. Local onset of alternans (Bonset) was defined as the BCL at which at least 10% of the RV exhibited alternans. Two regions of the RV epicardial surface were defined at Bonset – the 1:1alt region, where alternans was present, and the 1:1 region exhibiting 1:1 behavior – and back projected across all prior BCLs. Statistical comparison was performed between these two regions using the t-test to investigate if any parameter could predict the local onset of EM alternans.
Results and Discussion: We found that both [Ca2+]i and APD alternans, appears locally in all 5 hearts and then occupy the entire surface of the heart as BCL decreases. We also found that the local onset of CaA alternans (Bonset = 178±4.42 ms) always

preceded the local onset of APD alternans (Bonset = 161±5.46 ms, $p<0.05$) in the same heart. Alternans in CaD occurred in 2 out of 5 hearts after both CaA and APD alternans have developed. We constructed APD and CaD dynamic and S1-S2 restitution curves (RC), and calculated their maximum slopes separately for the 1:1 (Sdyn1:1 and S12Max1:1) and 1:1alt (Sdynalt and S12Maxalt) regions. We found that the slope of APD S1-S2 RC was significantly steeper in 1:1alt region compared to the 1:1 region (S12Maxalt = 1.21± 0.07 vs. S12Max1:1= 0.85±0.01, $p<0.05$); but in the case of CaD, it was the slope of the CaD dynamic RC which was significantly different between the two regions (Sdynalt = 0.99± 0.04 vs. Sdyn1:1= 0.73±0.06, $p<0.05$). In addition, we found that CaA, normalized to the mean RV CaA (CaAN), was significantly higher in 1:1alt compared to the 1:1 region at the BCL immediately prior to onset of CaA alternans (CaANalt= 1.16±0.04 vs. CaAN1:1= 0.92±0.01, $p<0.05$).
Conclusion: Our results indicate that both APD and [Ca2+]i alternans develops locally and then spreads across the heart as BCL decreases, however the local onset of CaA alternans always precedes the local onset of APD alternans. Therefore, it is imperative to predict [Ca2+]i alternans which occurs first and then drives APD to alternate secondarily. Our results indicate that we can predict the local onset of CaA and CaD alternans by measuring the changes in CaA and slope of the CaD dynamic RC respectively. On the other hand, the onset of APD alternans can be predicted using the slopes of the S1-S2 RC.

209.
Intermittent Vagus Nerve Stimulation Reflexively Modulates Heart Rate Variability in Rats with Chronic Ischemic Heart Failure

Joseph Ippolito, Thomas Xie, Iryna Talkachova, Bruce H. KenKnight, Elena G. Tolkacheva

At rest, the heart rate of healthy individuals exhibits spontaneous variation as a result of respiratory-driven neural modulation of sinus node function (respiratory sinus arrhythmia, RSA). Heart rate variability (HRV) is defined as time-domain variations of the R-R intervals in the electrocardiogram. HRV driven primarily by RSA is strongly influenced by cholinergic nerve activity in and on the heart. Depressed parasympathetic activity within the autonomic nervous system resulting from cardiovascular disease has been linked to significantly diminished HRV in humans suffering with chronic heart failure (CHF).

Previous studies in animals and humans have shown that certain patterns (intermittent) of chronic electrical stimulation of the right cervical vagus nerve (VNS) improves plasma biomarkers, attenuates cardiac remodeling and increases survival. VNS has been shown to lower heart rate, to decrease the inflammatory response in the myocardium (aiding tissue healing), and to induce important antiarrhythmic effects. VNS may indeed present a very promising future therapy for patients suffering from CHF despite aggressive therapy, but further work is necessary to develop a reliable and efficacious treatment.

The CHF phenotype was created in rats (n=15) subjected to myocardial infarction via LCA occlusion. Subsequent to implantation of a VNS lead and pulse generator (model 103, Cyberonics) in each rat, we measured changes in HRV before (PRE), during (ON) and after (POST) episodes of right cervical VNS delivery. HRV was defined as a ratio of the standard deviation of RR intervals to the mean RR intervals during the 7-second periods of active VNS stimulation. We demonstrated that VNS is a threshold phenomenon. For a stimulation strength of 0.5 mA, the HRV between all periods (PRE: 0.39±0.013, ON: .040± 0.013, and POST: 0.4357±0.018), as well as heart rate (PRE: 373±4.49, ON: 372±4.61, and POST: 371±4.62) were statistically similar. However, for a stimulation strength of 1mA, we show that mean HRV decreases during the ON periods compared to both PRE (0.4193± 0.039 vs. 0.91± 0.155, $p < 0.05$) and POST (0.4193± 0.039 vs. 0.7452±0.13, $p < 0.05$) periods. However, no statistically significant changes in heart rate were observed (PRE: 308±1.39, ON: 308±1.31, and POST: 307±1.30). We believe that the reduction of HRV observed in our experiments can be due to periodic stimulation provided by our implantable generators, and that even in the absence of consistent heart rate changes, VNS may still effectively alleviate the effects of CHF.

210.
Towards development of a pacing protocol to mimic physiological heart rate.

Virendra Kakade, Stephen McIntyre, Elena G. Tolkachveva

Alternans, which is the beat-to-beat alternation of the action potential duration (APD) in the heart, has been considered a substrate for ventricular fibrillation and sudden cardiac death. To predict alternans formation in the heart, a restitution hypothesis has been developed, although only under assumption of periodic pacing. During periodic pacing, APD is connected to the diastolic interval (DI) through the pacing rate, thus creating feedback in the system. However, the in-vivo heart exhibits heart rate variability (HRV), therefore the restitution hypothesis has to be modified to incorporate physiological pacing rate.

Clinical ECG data from PhysioNet online database were analyzed to measure different aspects of HRV. Specifically we measured average RR interval (AVGRR), standard deviation of RR interval (SDRR) and HRV defined as (SDRR/AVGRR)*100% for two groups of patients: healthy (n=8) and those displaying T-wave alternans (TWA, n=6). In addition, we measured the amount of feedback defined as the ratio of standard deviation of DI to the standard deviation of APD calculated from the ECG.
Our results demonstrate that AVGRR (944.38±42.08 ms vs. 757.7±23.25 ms, $p<0.05$), SDRR (45.98±6.42 ms vs. 22.15±2.92 ms, $p<0.05$) and HRV (4.76±1.45% vs. 2.89±0.75%, $p<0.05$) were significantly higher in the healthy category compared to the TWA. In addition, we demonstrated that the amount of feedback is considerably higher for healthy compared to the TWA patients (5.07±1.58 vs. 2.22±0.8, $p<0.05$). Based on these data, we created two protocols: the constant-rate pacing protocol, mimicking HRV in healthy patients, and the constant-DI pacing protocol, mimicking HRV in TWA

patients. We demonstrated using numerical simulations that constant-DI protocol with no feedback leads to prevention of alternans in the isolated cardiac myocytes.

211.
The Effect of Stretch Parameters on the Contractility of Fibrin-based Myocardial Tissue Equivalents

Jacqueline Wendel

A major challenge in myocardial tissue engineering is that no approaches to date have been able to create in vitro engineered tissues with cellular densities and force generation comparable to the native myocardium. Cyclic, mechanical stretch has been shown to induce hypertrophy in cardiomyocytes in vitro, which in turn results in an increase in the magnitude of contractile response. However, optimal stretch conditions remain to be defined and characterized for maximum force generation and cellular survival. In this study, aligned myocardial tissue equivalents were created by entrapping neonatal rat cardiac cells in fibrin gel, and alignment was achieved though controlled, cell-directed compaction. Tissue equivalents were cultured statically and then transferred onto a cyclic distention bioreactor system where they were exposed to stretch regimens of varying amplitude or duration. Contractile response was found to be amplitude dependent, with 5% stretch ratio resulting in a 112% increase in measured force generation under electrical pacing, but not dependent upon duration of stretch, indicating a stimulus rather than a sustained effect of stretching. Contrary to the original hypothesis, no observable change in cellular morphology or size was seen with stretch, and no conclusive increase in gap junction formation was found. However, there was an observed change in the number and distribution of cells within the tissue equivalent, indicating that cyclic stretch may have effects on cell survival and microenvironment.

212.
Epigenetic memory and BMP4-mediated lineage specific differentiation of myoblast-derived induced pluripotent stem cells.

Jesse Mull, Yoko Asakura, and Atsushi Asakura
Stem Cell Institute, Paul and Sheila Wellstone Muscular Dystrophy Center, and Department of Neurology, University of Minnesota Medical School, Minneapolis, MN 55455

Induced pluripotent stem (iPS) cells, reprogrammed from somatic cells with defined factors such as Oct4, Sox2, cMyc and Klf4, hold the potential to produce unlimited numbers of autologous cells to treat and model a variety of muscular dystrophies. However, the derivation of myogenic pre-cursors from iPS cells remains elusive, and current differentiation protocols rely on multi-stage fluorescent cell sorting or the use of transgenes. Reprogrammed somatic cells exhibit epigenetic memory in the form of DNA methylation patterns and gene expression profiles characteristic of their tissue of origin.

Here we show that myoblast-derived iPS cells (Mb-iPS cells) maintain low level expression of myogenic markers, including MyoD, and display preferential myogenic differentiation in vitro and in vivo compared to fibroblast-derived iPS cells (Fb-iPS cells). Exploiting this epigenetic memory, we establish a simple, transgene-free method for the derivation of myogenic cells from iPS cells.

213.

Conditional Serca2 ablation impairs systolic and diastolic performance of isolated perfused hearts

Frazer I. Heinis1, Kristin B. Andersson3, Geir Christensen3, and Joseph M. Metzger1,2
1, Department of Biochemistry, Molecular Biology, and Biophysics, 2, Department of Integrative Biology and Physiology, University of Minnesota, Minneapolis, MN
3, Institute for Experimental Medical Research, Oslo University Hospital Ullevaal; Center for Heart Failure Research, University of Oslo, Oslo, Norway

Highly orchestrated contraction and relaxation of the myocardium depends on rapid release and reuptake of Ca2+ from the sarcoplasmic reticulum (SR). SERCA2a, a cardiac SR Ca2+-ATPase, is a major contributor to re-sequestration of Ca2+ and shows reduced expression with age and in heart failure. Conditional deletion of the Serca2 gene from the hearts of fl/fl mice results in progressive diastolic dysfunction, heart failure and death over a period of two months. To gain insight into the interplay between Ca2+-mishandling and the evolution of cardiac pump failure we studied mice at 1 and 4 weeks following cardiac specific cre-mediated deletion of the Serca2 gene from fl/fl mice. At each time point, isolated hearts were subjected to paced stimulation across a broad frequency range, followed by ischemia/reperfusion injury. At both 1 and 4 weeks, SERCA2a loss resulted in profound contractile deficits and diastolic impairment relative to normal hearts. Curiously, contractile dysfunction in hearts isolated from Serca2 KO mice does not correlate with the in vivo phenotype, which is mild. We are further investigating the consequences of SERCA2a loss shortly after gene deletion, at times less than four weeks after knockout, to construct a detailed dose-response relationship between titrated changes in SR Ca2+ handling and contractile function. The studies presented here focus on identifying the contribution of adrenergic stimulus to the preserved function observed in Serca2-KO mice in vivo relative to the severe ex vivo phenotypes observed. We demonstrate that KO hearts possess substantial functional reserve as revealed by heart perfusion with an inotropic agent, dobutamine.

214.

Functional β –adrenergic receptors are required for the pro-lipolytic effects of the VGF-derived peptide TLQP-21

Cheryl Cero1, Maria Razzoli1, Ivana Ninkovic1, Rana Mohammed1, Jake McCallum1, Bradford Lowell2, Alessandro Bartolomucci1
1Dept. of Integrative Biology and Physiology, University of Minnesota, MN, USA

2Dept. of Medicine, Division of Endocrinology, Beth Israel Deaconess Medical Center and Harvard Medical School, Boston, MA, USA

Norepinephrine (NE) released by the sympathetic nerve terminals is the major hormone stimulating lipolysis in adipose tissue via activation of β-adrenoreceptors (β-ARs). TLQP-21 is a Vgf peptide, expressed in sympathetic nerve terminals in the white adipose tissue (WAT) [1,2]. TLQP-21 binds adipocytes' cell membrane with high affinity and increases NE-induced lypolisis via activation of hormone sensitive lipase [1]. Importantly, TLQP-21 does not displace isoproterenol from the -AR [1], thus excluding a β-agonist mediated effect. The exact mechanism of TLQP-21 induced prolipolytic effects has not been identified yet. Our hypothesis is that functional β-ARs are required for the pro-lipolytic effects of TLQP-21. To test this hypothesis we used -less knockout mice, which lack the β1-β2-β3 ARs, and thier wild type (wt) control mice [3]. Obese - less and wt mice were chronically treated with either TLQP-21 (5mg/kg) or saline daily for 28 days. TLQP-21-treated wt but not -less mice showed a decrese in body weight and fat mass without any diffrence in food efficiency. Moreover there was no diffrence in energy expenditure and locomotor activity mesured with indirect calorimetery. Furthermore adipocytes of β -less and wt mice were cultured in vitro with TLQP-21 in presence or absence of the b-agonist isoproterenol and glycerol release in the media used as an indirect measure to assess lypolisis [1]. TLQP-21 potentiated ISO-induced glycerol release in wt but not β-less adipocytes further supporting our in vivo observation. In conclusion, our preliminary results further support an anti-obesity role for TLQP-21 and demonstrate that functional β-ARs are required for the pro-lipolytic effects of TLQP-21.

References and Notes

[1]. Possenti R, et al. Characterization of a novel peripheral pro-lipolytic mechanism in mice: role of VGF-derived peptide TLQP-21. Biochem J. 2012; Jan 1; 441(1):511-22.
[2]. Bartolomucci A, et al. The extended granin family: structure, function, and biomedical implications. Endocr Rev. 2011 Dec; 32(6):755-97.
[3]. Bachman ES, et al. betaAR signaling required for diet-induced thermogenesis and obesity resistance. Science. 2002 Aug 2; 297(5582):843-5.

This research is supported in part by the Minnesota Partnership for Biotechnology and Medical Genomics and the Decade of Discovery in Diabetes Grant.

215.

Dystrophin and Utrophin: Interaction with Microtubules

Joseph J. Belanto1,2, Davin M. Henderson1, Michele A. Jaeger1, and James M. Ervasti1,2
1Department of Biochemistry, Molecular Biology, and Biophysics
2Program in Molecular, Cellular, Developmental Biology, and Genetics

The dystrophin gene resides on the X chromosome and, in striated muscle, encodes a 427 kD cytoplasmic protein responsible for linking the intracellular actin cytoskeleton to

the extracellular matrix via the associated dystrophin-glycoprotein complex. Mutations in dystrophin that abolish or reduce its expression lead to Duchenne muscular dystrophy (DMD) or Becker muscular dystrophy (BMD), respectively. Patients with DMD succumb to fatal cardiac and/or respiratory arrest in their late teens to early twenties. There is currently no effective or widely available treatment for DMD.
Recently, our lab reported that dystrophin, present at the muscle plasma membrane (sarcolemma), directly binds to microtubules and organizes them along the sarcolemma. Microtubules are composed of α- and β-tubulin monomers arranged in heterodimeric protofilaments which form a hollow, cylindrical coil along which the cell transports intracellular cargo using the motor proteins dyneins and kinesins. Mice lacking dystrophin (mdx mice) present with a disorganized microtubule lattice at the sarcolemma, the consequence of which is unknown. Using in vitro microtubule cosedimentation assays, we show that dystrophin binds to microtubules with strong affinity (KD=0.33μM). The region currently proposed to be the major contributor of this binding is contained between spectrin-like repeats 20 and 24 of the dystrophin protein based on cosedimentation assays of various dystrophin isoforms.
Many therapies for treating dystrophin deficiency aim at upregulating its autosomal homolog, utrophin, due to its structural similarity and ability to bind many proteins that dystrophin binds. We show that in vitro utrophin binds microtubules with far less affinity (KD=2.34μM) than does dystrophin, which is not sufficient to rescue the disorganized microtubule network in utrophin-transgenic (Fiona-mdx) mice. Moreover, transgenic expression of dystrophin on the mdx mouse background results in rescue of microtubule lattice organization. These results suggest that any deficiency in microtubule trafficking or function caused by loss of dystrophin may not be fully restored upon upregulation of utrophin. Therefore, it is of great importance to determine what, if any, specific pathologies can be attributed to loss of microtubule organization secondary to the pathology caused due to the loss of the dystrophin protein itself.
This work was supported by the NIH Training Program in Muscle Research AR007612 and NIH RO1 AR042423.

216.
Effect of Selective Afferent Renal Denervation by Periaxonal Application of Capsaicin on Salt Sensitivity of Arterial Pressure

Jason D. Foss, W. E. Engeland and John W. Osborn
Departments of Integrative Biology and Physiology and Neuroscience
University of Minnesota Medical School

Renal nerves contribute to some forms of hypertension, but the differential role of afferent and efferent renal nerves remains unclear. It has been proposed that afferent renal nerves modulate arterial pressure (AP) since rats subjected to dorsal rhizotomy (DRX) at spinal levels T9-L1 exhibit salt-sensitive hypertension. Since DRX is not selective for renal afferents, we developed a novel method for selective ablation of calcitonin gene-related peptide (CGRP) positive sensory fibers in the kidney and tested the hypothesis that, as with DRX, our method of afferent renal denervation (ARDN)

causes salt-dependent hypertension in rats. Male Sprague Dawley rats were implanted with radiotelemeters to measure AP and heart rate (HR) and underwent either ARDN (renal-CAP) or sham surgery (SHAM). In renal-CAP rats, the renal nerves were exposed to a 33 mM capsaicin solution for 15 minutes. The rats were housed in metabolic cages, fed a 0.1% NaCl diet and allowed to recover for 10 days. After a 4 day baseline period, the diet was increased to 4% NaCl for 3 weeks then 8% NaCl for 2 weeks. At the end of the protocol the rats were euthanized and immunohistochemistry (IHC) was performed on the kidneys labeling for CGRP, as a marker of afferent renal fibers, and tyrosine hydroxylase, as a marker of efferent renal fibers. Baseline mean AP (mmHg) was slightly higher in renal-CAP (103 ± 2) than SHAM rats (97 ± 3) whereas HR (BPM) was similar (399 ± 11 vs. 395 ± 10). Increasing salt intake caused a similar increase in MAP in both groups, but HR decreased more in SHAM than renal-CAP rats (358 ± 6 vs. 385 ± 3 BPM). Sodium and water intake, excretion and balance were not different between the two groups. IHC confirmed the selective destruction of renal afferent fibers. These data suggest that: 1) renal-CAP treatment is an effective method for ARDN, 2) afferent renal nerves play a minimal role in the regulation of AP or sodium and water balance in normotensive rats, regardless of salt intake and 3) afferent renal nerves appear to mediate sodium dependent decreases in HR. The discrepancy between these results and those of previous studies may be due to the non-selective nature of DRX.

217.
Interstitial Flow Improves Lumen Formation in Aligned Engineered Microvasculature

Kristen T. Morin and Robert T. Tranquillo
Department of Biomedical Engineering

The need for microvascular networks in engineered tissue, especially highly metabolic tissue such as myocardium, is well documented. In addition, perfusion of such a network in vitro prior to implantation to provide nutrients to the maturing tissue would be optimal, if not required. To this end, we hypothesized that cell-induced gel compaction would cause alignment of microvascular structures formed from circulating endothelial cells, which would provide natural inlet and outlet ends for perfusion. Initial results indicated that lumen formation was impaired in the aligned tissue, so interstitial flow was investigated as a means to improve lumen formation.
Human blood outgrowth endothelial cells (BOECs; 2 M/ml) and GFP-labeled human brain pericytes (PCs; 0.4 M/ml) were entrapped in 2.5 mg/ml fibrin gel which contained SCF, IL-3 and SDF-1α at 200 ng/ml each. The gel was cast in a custom built perfusion chamber, which consisted of an ultem well (0.5 cm x 2 cm) with glass capillary tubes extending through the shorter sides of the chamber. After casting the bottom of the chamber was removed, and the chamber placed in a dish filled with culture medium. After 5 days of culture, the gel was detached from the walls of the chamber, so that it was only adherent to the glass capillary tubes. This enabled compaction and alignment of the gel into a tissue strip between the glass tubes, which occurred over the course of 3 days. On day 8 of culture, the tissues were embedded in 5% agarose in the perfusion

chamber, which included the bottom and top pieces to form a fully enclosed chamber. The glass capillary tubes were connected to a syringe pump, which generated flow through the tissue for 3 or 6 days. Fluid did not leak from the tissue due to the high density agarose that surrounded it. Flow rates of 0.015 µl/min ("ultra low") and 0.105 µl/min ("low") were used. Control tissues, which were cultured statically and not embedded in agarose, were harvested at the same time point.
Fluorescent images of CD31-immunostained longitudinal tissue sections were quantitated with a custom Matlab script. This analysis revealed that the endothelial structures had become highly aligned during gel compaction, and that flow did not compromise this alignment. In addition while the use of low flow appeared to reduce PC recruitment to microvessels, ultra low flow maintained PC recruitment. In addition, substantial improvements in lumen formation were observed with ultra low flow, but not low flow. These improvements were present after 3 days of flow, and maintained, but not further improved, after 6 days of flow. Therefore, culture of these tissues under ultra low flow conditions for 3 or 6 days yields a tissue containing highly aligned vascular structures with a large number of lumens.

218.
The Effect of Continuous Flow Left Ventricular Assist Device (CF-LVAD) Implantation on Serum Uric Acid Levels

Andrew N Rosenbaum1, Sue Duval2, Muhammad Bilal Salman Khan1, Marc Pritzker1, Ranjit John3, and Peter M Eckman1.

Introduction: Hyperuricemia is common in patients with severe heart failure. Change in uric acid level following continuous flow ventricular assist device (CF-VAD) placement has not previously been reported. We hypothesized that uric acid levels would decrease following CF-VAD implant.
Methods: 238 consecutive patients undergoing implantation of a CF-LVAD at a single center between 6/2005 and 11/2011 were identified. Retrospective chart review was conducted in the 23 patients who were noted to have serum uric acid values measured prior to and following CF-LVAD implant. Baseline characteristics and follow-up data were obtained via chart review.
Results: Mean age was 56.7 ± 9.4 years; 18 were male. Serum uric acid values decreased significantly from 9.7 ± 2.6 to 6.5 ± 3.0 following implant (p=0.02). Mean RA pressure remained unchanged after implant, while PA and PCW pressures decreased significantly (p=0.02 and p=0.02). No significant change in mean furosemide-equivalent diuretic daily dose was seen. However, there was a correlation between uric acid level changes and diuretic dose changes post-implant (r^2=0.33, p<0.01). Improvement in serum uric acid values was associated with improvements in renal function, decreased diuretic dosing, improved hemodynamics (all p<0.01).
Conclusions: Serum uric acid values decreased after LVAD implant, although several mechanisms may be operative. Further work may clarify the mechanism(s) by which uric acid levels decrease following CF-LVAD .

219.

Noninvasive Imaging of the Three-dimensional Ventricular Activation Sequence of Paced Rhythm and Ventricular Tachycardia in the Canine Heart

Chengzong Han1, Steven Pogwizd2, Cheryl Killingsworth2, Bin He1
1. Department of Biomedical Engineering, University of Minnesota
2. Department of Medicine, University of Alabama at Birmingham

Introduction—Imaging myocardial activation is important for the study of mechanisms and for aiding in the clinical management of cardiac arrhythmias. In the present study, we evaluate the performance of a novel noninvasive 3D cardiac electrical imaging (3DCEI) technique with the aid of simultaneous 3D intra-cardiac mapping during pacing and ventricular tachycardia (VT) in the canine heart.
Methods—Body surface potentials (from up to 124 ECG electrodes) were measured simultaneously with bipolar electrical recordings (from up to 216 intramural sites) in a closed-chest condition in healthy canines. CT images were obtained after the mapping study to construct realistic geometry models. Data analysis was performed on paced rhythms and VTs induced by norepinephrine (NE).
Results—The noninvasively reconstructed activation sequence was in good agreement with the simultaneous measurements from 3D intra-cardiac mapping with a correlation coefficient of ~0.70 averaged over both the paced beats and ectopic beats including premature ventricular complexes, couplets, and nonsustained monomorphic VTs and polymorphic VTs. The NE-induced ectopic beats initiated in the subendocardium by a focal mechanism. Sites of initial activation were estimated to be ~7mm from the measured initiation sites for both the paced beats and ectopic beats. For the polymorphic VTs, beat-to-beat dynamic shifts of initiation site and activation pattern were characterized by the reconstruction.
Conclusions—3DCEI can non-invasively image the 3D activation sequence and localize the origin of activation of paced rhythms and NE-induced VTs in the canine heart with good accuracy. It offers the potential to aid catheter ablation procedures for treating ventricular arrhythmias and to non-invasively assess the mechanisms of ventricular arrhythmias.

220.

Noninvasive imaging of atrial arrhythmias in humans

Zhaoye Zhou1, Jorge Pedrón Torrecilla1, Jian Sun2, Dakun Lai1, Yigang Li2, Bin He1
1 Department of Biomedical Engineering, University of Minnesota, Minneapolis, Minnesota, USA.
2 School of Medicine, Xinhua Hospital Affiliated to Shanghai Jiao Tong University, Shanghai, China.

Introduction

The study aims to evaluate a novel noninvasive cardiac electric imaging (NCEI) technique to image atrial electrical activity during arrhythmia from body surface potential maps (BSPMs).
Methods
BSPMs were measured on 4 patients (pts) with paroxysmal atrial fibrillation (AF) or atrial flutter (AFL), and 4 healthy subjects (sbj) during sinus rhythm (SR). Equivalent current densities (ECD) were estimated from BSPMs and sbj' CT-determined heart-torso models. Activation sequences (AS) of AFL and SR were reconstructed from the time instant corresponding to the peak magnitude of ECD. For AF, the dominant frequency (DF) map was reconstructed from highest-amplitude frequency.
Results
Spectral analysis identified maximum DF site in right superior pulmonary vein (PV, 8.8 Hz) on AF patient. A remarkable left-to-right atrial DF gradient was identified, with DF highest at right superior PV (8.8Hz), intermediate at coronary sinus ostium (6.2Hz), lowest at posterior right atrium (4.8Hz). Circumferential PV isolation set the patient AF free. NCEI imaged counterclockwise typical AFL and identified tricuspid isthmus as critical zone. AFL was abolished after linear ablation at the isthmus. The imaged SR is consistent with literature.
Conclusions
This pilot study suggests the feasibility to image atrial AS during SR and AFL, and DF maps in humans. The present results correlated well with catheter ablation outcome in pts, and suggest atrial electric source imaging may facilitate clinical treatment of atrial arrhythmia.

221.
Noninvasive Imaging of the Three-dimensional Ventricular Activation Sequence of Paced Rhythm and Ventricular Tachycardia in the Canine Heart

Chengzong Han1, Steven Pogwizd2, Cheryl Killingsworth2, Bin He1
1. Department of Biomedical Engineering, University of Minnesota
2. Department of Medicine, University of Alabama at Birmingham

Introduction—Imaging myocardial activation is important for the study of mechanisms and for aiding in the clinical management of cardiac arrhythmias. In the present study, we evaluate the performance of a novel noninvasive 3D cardiac electrical imaging (3DCEI) technique with the aid of simultaneous 3D intra-cardiac mapping during pacing and ventricular tachycardia (VT) in the canine heart.
Methods—Body surface potentials (from up to 124 ECG electrodes) were measured simultaneously with bipolar electrical recordings (from up to 216 intramural sites) in a closed-chest condition in healthy canines. CT images were obtained after the mapping study to construct realistic geometry models. Data analysis was performed on paced rhythms and VTs induced by norepinephrine (NE).
Results—The noninvasively reconstructed activation sequence was in good agreement with the simultaneous measurements from 3D intra-cardiac mapping with a correlation coefficient of ~0.70 averaged over both the paced beats and ectopic beats including

premature ventricular complexes, couplets, and nonsustained monomorphic VTs and polymorphic VTs. The NE-induced ectopic beats initiated in the subendocardium by a focal mechanism. Sites of initial activation were estimated to be ~7mm from the measured initiation sites for both the paced beats and ectopic beats. For the polymorphic VTs, beat-to-beat dynamic shifts of initiation site and activation pattern were characterized by the reconstruction.
Conclusions—3DCEI can non-invasively image the 3D activation sequence and localize the origin of activation of paced rhythms and NE-induced VTs in the canine heart with good accuracy. It offers the potential to aid catheter ablation procedures for treating ventricular arrhythmias and to non-invasively assess the mechanisms of ventricular arrhythmias.

222.
Stability of human dystrophin constructs skipped around exon 45

Jackie McCourt, Michele A. Jaeger, Joseph J. Belanto, Dana Strandjord, Davin M. Henderson and James M. Ervasti

Exon-skipping therapeutics are under investigation to delete disease-causing mutations from dystrophin transcripts. We showed that internal sequence deletions can result in dystrophin instability and aggregation (Henderson *et al *2011), raising question of whether exon skipping affects dystrophin stability. To address this question, we compared the biophysical properties of purified full-length human dystrophin with proteins deleted for exons 44-45 (hDys-ex44/45), or exons
45-46 (hDys-ex45/46). By circular dichroism spectroscopy and differential scanning fluorimetry, hDys-ex44/45 and hDys-ex45/46 both showed thermal stabilities equivalent to full-length dystrophin. In contrast, a dystrophin deleted for exons 43-44 (hDys-ex43/44) was too unstable to be expressed and purified for further characterization. While our results suggest that exon
45 skipped dystrophins are stable, a remaining caveat is that each of the dystrophins analyzed were contaminated by a large N-terminal fragment that may have influenced the biophysical analyses. Therefore, we are currently optimizing a dual affinity purification strategy employing distinct N- and C-terminal epitope tags.

223.
Single amino acid changes in distinct domains of dystrophin can affect protein folding and cause disease, but not always.

Dana M. Strandjord, Davin M. Henderson, Bin Li, James M. Ervasti

Advancements in sequencing technology have revealed several Duchenne and Becker Muscular Dystrophy patients who encode only a single amino acid change in their DMD gene. Additionally, large amounts of single nucleotide variant (SNV) data are being generated from projects such as International HapMap and 1000 genomes. We have compared the amino acid changes reported and have identified many originally

associated with disease but now listed as SNVs. There are still mutations only associated with disease and they are differentially distributed in the protein. Both the N- and C-terminal domains present with significantly greater proportions of disease-causing changes compared to the central rod domain, indicating they are less tolerant to primary sequence changes. Consistent with the concentration of disease-causing mutations in the dystrophin termini, we have previously shown that missense mutations in the N-terminal actin-binding domain cause thermal instability in vitro. We have now engineered amino acid changes located in the C-terminal or central rod region. Our biochemical analyses demonstrate that disease-causing changes significantly decrease the solubility and thermal stability of dystrophin while population changes do not.

224.
Spectroscopic Design of SERCA Activators for Drug or Gene Therapy

Simon J Gruber1, Suzanne Haydon1, Razvan L Cornea1, Bengt Svensson1, Dongzhu Jin2, Jiqui Chen2, Joseph M Muretta1, Gregory D Gillispie1,3, and David D Thomas1
1Department of Biochemistry, Molecular Biology, and Biophysics, University of Minnesota, Minneapolis, MN 55455, USA
2Cardiovascular Research Center, Mount Sinai School of Medicine, New York, NY 10029, USA
3Fluorescence Innovations, Inc., Bozeman, MT 59718, USA

We have used spectroscopic probes (small molecule and fluorescent fusion proteins) to study the relationships among structure, dynamics, and function of the sarcoplasmic reticulum Ca-ATPase (SERCA) and its cardiac regulator phospholamban (PLB), with the goal of designing activators of SERCA for treatment of heart failure (HF) and muscular dystrophy (MD).
Heart Failure (HF) is a complex syndrome that frequently involves deficiencies in cardiac calcium cycling [1-2]. Ca2+ drives muscle contraction, and relaxation is accomplished by the sequestration of Ca2+ by the sarcoplasmic reticulum Ca-ATPase (SERCA), which is inhibited by phospholamban at submicromolar [Ca2+] in cardiac muscle. We are using spectroscopic probes of both SERCA and PLB to design LOF-PLB mutants (PLBM) that can compete with WT-PLB (PLBW) and thus relieve SERCA inhibition. Our ideal mutant is partial loss-of-function, binds tightly to SERCA2a, and remains phosphorylatable via β-adrenergic pathways (BBRC 408: 388–392). We have developed a system for examining the function and interactions of SERCA and PLB in living HEK cells to examine the ability of PLBM to compete with PLBW, thus rescuing SERCA activity. Active human SERCA2a and PLBW, tagged with fluorescent proteins (e.g., CFP and YFP), are co-expressed in stable cell lines followed by transient co-expression with PLBM. The effects of PLBM on Ca-ATPase activity and FRET are measured to determine the mutant's ability to compete with PLBW, both physically and functionally. Optimal mutants are being tested in a rat model of heart failure.
A similar SERCA-PLB FRET assay is being used to screen for small molecular activators of SERCA. Some of these are being developed as promising drugs for HF therapy and other applications (collaboration with Celladon, Inc.). Surprisingly, some of

these drugs are direct SERCA activators that are also effective in rescuing the muscular dystrophy phenotype in dystrophic mice.

225.
Guanylyl Cyclase A and B Are Asymmetric Dimers That Are Allosterically Regulated by ATP Binding to the Catalytic Domain

Jerid W. Robinson, Dr. Lincoln R. Potter

226.
Title: In Vitro Modeling of Duchenne Muscular Dystrophy Cardiomyopathy Using Human Induced Pluripotent Stem Cells

Forum D.K. Kamdar, Michelle J Doyle, Christopher S Chapman, Jaime Lohr, Daniel J Garry
Division of Cardiology, Lillehei Heart Institute, University of Minnesota, Minneapolis, MN

Duchenne Muscular Dystrophy (DMD) is the most common and severely debilitating X-linked muscular dystrophy that leads to devastating skeletal and cardiac muscle damage. The treatment of pulmonary complications of DMD has improved survival, however DMD associated cardiomyopathy has emerged now as the leading cause of death. Despite significant advancements in the understanding of the skeletal muscle disease of DMD has been achieved, there is limited knowledge of the pathophysiology and effective treatment of DMD cardiomyopathy. While many mouse models of muscular dystrophy exist, they do not fully approximate human disease especially DMD cardiomyopathy. In order to overcome this limitation, the development of novel and improved models is necessary.

Induced pluripotent stem cells (iPSC) are a significant advance in stem cell biology that allows the reprogramming of adult somatic cells into a pluripotent state. The iPSC technique can be used to provide cellular models to explore pathological mechanisms of many human diseases in vitro, such DMD cardiomyopathy. We hypothesize that the pathophysiology of DMD cardiomyopathy can be modeled by differentiating DMD iPSC to cardiomyocytes and interrogating them at the cellular and molecular level. To evaluate this hypothesis, we will utilize and derive human iPS lines from patients with DMD cardiomyopathy and their unaffected age-matched relative controls and differentiate the hiPSC to cardiomyocytes. In vitro differences in the disease and control cardiomyocytes will be elicited using molecular biological and physiological techniques including electrophysiology, calcium imaging, and contractile force assays. This approach will serve as a platform for developing novel therapeutic regimens for patients with muscular dystrophy cardiomyopathies.

227.
The title is Effect of Endoglin overexpression during embryonic body development

June Baik

Increasing evidence points to endoglin (Eng), an accessory receptor for the TGF-beta superfamily commonly associated with the endothelial lineage, as an important regulator of the hematopoietic lineage. We have shown that lack of Eng results in reduced numbers of primitive erythroid (EryP) colonies as well as down-regulation of key hematopoietic genes. To determine the effect of endoglin overexpression in hematopoietic development, we generated a doxycycline-inducible ES cell line. Our results demonstrate that induction of endoglin during embryoid body (EB) differentiation leads to a significant increase in the frequency of hematopoietic progenitors, in particular the erythroid lineage, which correlated with up-regulation of Scl, Gata1, Runx1 and embryonic globin. Interestingly activation of the hematopoietic program happened at the expense of endothelial and cardiac cells, as differentiation into these mesoderm lineages was compromised. Endoglin-induced enhanced erythroid activity was accompanied by high levels of Smad1 phosphorylation. This effect was attenuated by addition of a BMP signaling inhibitor to these cultures. Among the BMPs, BMP4 is well-known for its role in hematopoietic specification from mesoderm by promoting expression of several hematopoietic genes, including Scl. Since Scl is considered the master regulator of the hematopoietic program, we investigated whether Scl would be capable of rescuing the defective hematopoietic phenotype observed in Eng-/- ES cells. Scl expression in endoglin-deficient ES cells resulted in increased erythroid colony-forming activity and up-regulation of Gata1 and Gata2, positioning endoglin upstream of Scl. Taken together, these findings support the premise that endoglin modulates the hematopoietic transcriptional network, most likely through regulation of BMP4 signaling.

228.
Platform for small molecular discovery in “titratable” cardiac inotropic therapy.

Anthony Vetter, Brian Thompson, Joe Muretta, Yuk Sham, David D. Thomas, Joseph M. Metzger
Department of Integrative Biology and Physiology
University of Minnesota Medical School

Ischemic heart disease is a leading cause of morbidity and mortality in the world. According to the World Health Organization it accounts for approximately 12.2% of all deaths. Myocardial infarction is a common presentation of the disease; it is characterized as the obstruction of adequate blood supply to the heart and ultimately results in the death of cardiac myocytes. Penultimate to cell death is an alteration of the biochemical milieu of the sarcomeric apparatus. The sarcomere undergoes acidification and subsequent uncoupling of the calcium-force relationship. The neonatal cardiac isoform of cTnI, ssTnI, shows reduced pH sensitivity compared with the adult cTnI isoform. Functional studies have shown this pH insensitivity to stem from H132 of

ssTnI. Alignment of ssTnI and cTnI reveals H132 corresponds with an alanine in cTnI at amino acid position 164. Substitution in cTnI with the respective ssTnI residue (A164H) is capable of sustaining the calcium-force relationship in lieu of acidosis without deleterious effects at baseline pH. We are establishing a high-throughput FRET experiment to assay thin filament proteins under various pathophysiological states with both the intent of discovering novel small molecule therapeutics capable of recapitulating the cTnI A164H phenotype, but also gaining useful insight to the conformational dynamics which regulate contraction.

229.

Structure of the Phospholamban/Ca2+-ATPase membrane protein complex in lipids by hybrid solid-state NMR methods

Martin Gustavsson1, Raffaello Verardi1, Nathaniel J. Traaseth1, and Gianluigi Veglia1
1Department of Biochemistry, Molecular Biology and Biophysics, University of Minnesota, Minneapolis, MN 55455

Sarcoplasmic reticulum (SR) Ca2+-ATPase (SERCA) and phospholamban (PLN) form a 116 kDa membrane protein complex that transports Ca2+ from the cytosol into the SR of cardiomyocytes. Owing to their importance for cardiac muscle function, PLN and SERCA have been targeted in therapeutic studies aimed at relieving heart failure. PLN consists of a transmembrane helix (domain Ib and II, residue 23-52) connected to a cytoplasmic region (domain Ia, residue 1-16) by a short loop (residue 17-22). Domain Ia is in a conformational equilibrium between an unfolded, solvent-accessible R state and a helical, membrane-associated T state. Despite the wealth of structural information about PLN (from NMR) and SERCA (from X-ray crystallography), there is still no high resolution structure of the SERCA/PLN complex.
Here, we co-reconstituted SERCA and PLN into native-like lipid bilayers under fully functional conditions and utilized hybrid solid-state NMR methods to characterize the SERCA/PLN complex. Magic angle spinning (MAS) NMR was used to determine the complete secondary structure of PLN. Paramagnetic relaxation enhancement (PRE) experiments, utilizing nitroxide spin labels covalently attached to SERCA and to the bilayer lipids, provided multiple inter-protein distances. Membrane topology was determined by oriented NMR in aligned bicelles. Finally, these restraints were implemented into XPLOR-NIH to determine the structure of R and T states of PLN in complex with SERCA. Our results show that the transmembrane domain is helical between residues 23-50 and binds to SERCA at a ~40° tilt angle with respect to the membrane bilayer. Domain Ia interacts with the cytoplasmic region of SERCA in an extended, unfolded conformation (R state) while still remaining in equilibrium with the membrane-attached helical T state. These studies show the application of hybrid solid-state NMR methods for large membrane protein complexes in lipid bilayers.

230.

Oriented Solid State NMR Reveals the Molecular Mechanism by which Sarcolipin Inhibits SERCA

Kaustubh R. Mote1 and Gianluigi Veglia1,2
Departments of Chemistry1 and Department of Biochemistry, Molecular Biology & Biophysics2
University of Minnesota, Minneapolis, MN 55445

Sarcolipin (SLN) is small, 31 amino-acid transmembrane protein that regulates Sarco(endo)plasmic Ca(II) ATPase (SERCA), the calcium ion pump of cardiac and skeletal muscle, by inhibiting its Ca2+ uptake in atria and slow/fast-twitch skeletal muscle cells1, 2. Biophysical and biochemical evidence in vitro3, 4 and in vivo5, 6 show that a direct association of SLN transmembrane domain with the transmembrane helices of SERCA as the driving force behind this functional interaction. Understanding the mechanism of this inhibition and defining the SLN-SERCA complex will allow us to better understand the SERCA regulation of function and possibly design SLN mutants to restore SERCA activity in failing heart or skeletal muscle cells.
Crystal structures of SERCA in absence of SLN show significant rearrangements in transmembrane M1/M2 helices upon nucleotide binding7. These helices are adjacent to the proposed SLN binding grove, which also forms a posterior interface to the intra-membrane calcium binding site8. We mapped the changes in the topology of SLN using oriented solid state NMR (Oss-NMR) upon binding to SERCA in the presence of nucleotide, under high and low calcium concentrations. As shown in the Figure 1, SLN tilt angle changes by 10˚-15˚ upon the binding of calcium to SERCA. This indicates that SLN inhibits SERCA by modulating the change in M2 helix conformation upon ATP binding. With this topological-allosteric mechanism of inhibition, SLN can act on both, the coupling between the ATP hydrolysis and calcium transport, and calcium binding. In order to fully understand the effect of SLN binding, we determined the structure of the 114 kDa SLN-SERCA complex by combining restraints from MAS-ssNMR (which provided the binding interface and relevant changes in side chains) and Oss-NMR (which provided the orientation of SLN relative to the bilayer and SERCA). The complex explains a host of previous biophysical data obtained pertaining to the inhibitory effect of SLN and SLN-mutants on SERCA. This study forms the first step towards a rational design of mutants to alleviate SERCA dysfunction in diseased muscle cells.

Post Doc/Research Associate/Scientist

300.
Characterization of Pseudotyped and Inducible Adeno Associated Virus Vectors in Cardiac Gene Transfer

Erik Arden, Qingli Lu, Martina Maerz Mary Garry and Joseph Metzger, Integrative Biology and Physiology, University of Minnesota, Minneapolis, MN, USA 55419

Adeno Associated Virus (AAV) is a viable cardiac gene delivery system that can potentially remediate cardiac dysfunction. However, expression cassettes pseudotyped with alternative serotypes display variable cardiac transduction. Here, we compare the ability of AAV 1, 6, 8, and 9 capsids to effectively transduce cardiac and skeletal tissues using a constitutively expressed (CMV) Luciferase reporter system. AAV2/1 provided little cardiac transduction, while AAV2/9 demonstrated a dose dependent response and AAV2/6 and AAV2/8 illustrated the most robust constitutive Luciferase cardiac expression. Similar trends were observed in skeletal muscle. We further characterized AAV2/6 gene delivery efficacy using a muscle specific Myosin Heavy Chain-Creatine Kinase (MHCk7) fusion promoter driving Luciferase expression. The MHCk7 construct displayed reduced expression levels compared to the constitutive reporter system, however, expression was localized to muscle tissue. Lastly, we investigated AAV2/6 in the context of a Double Oxygen Sensing Vector System (DOSVs) capable of in trans gene expression during hypoxic challenge. Mice injected with the DOSVs displayed robust expression levels when confronted with hypoxic challenge in distressed cardiac tissue compared to normoxic controls. This reduced oxygen response system demonstrates in vivo delivery of a long term, inducible expression system in the context of hypoxic cardiac events.

301.
The C-terminal fragment of dystrophin cleavage by enteroviral protease 2A causes dystrophic cardiomyopathy

Matthew S. Barnabei and Joseph M. Metzger
Department of Integrative Biology and Physiology

Cardiac enterovirus (EV) infection is a clinically relevant disease state which causes cardiomyopathy and heightened susceptibility to ischemic injury. Previously, it has been shown that dystrophin is targeted for cleavage by the 2A protease (2Apro) expressed by enteroviruses. This has led to the hypothesis that dystrophin cleavage contributes to the cardiomyopathy of EV infection. However, because 2Apro cleaves numerous substrates, it is unclear if dystrophin contributes to cardiomyopathy during EV infection or is a byproduct of other pathological processes. To address this question, transgenic mice were created expressing the N- and C-terminal products of 2Apro-mediated dystrophin cleavage (NtermDys and CtermDys, respectively). CtermDys transgenic mice show a dystrophic cardiomyopathy as shown by enhanced Evans blue

dye (EBD) uptake during isoproterenol stress, enhanced myocardial fibrosis, and increased susceptibility to ischemic injury. CtermDys transgenic mice also show ~70% reduction in expression of dystrophin along with a ~5-10 fold increase in other DGC proteins. Conversely, NtermDys transgenic mice show no dystrophic cardiomyopathy as indicated by normal EBD uptake during isoproterenol stress and express normal levels of dystrophin and other DGC proteins. To more accurately simulate EV infection, double transgenic mice were generated which also show a dystrophic cardiomyopathy as shown by EBD uptake during isoproterenol stress that is similar to CtermDys mice. Collectively, these results show that expression of CtermDys is sufficient to cause a dystrophic cardiomyopathy with the NtermDys protein having no detrimental effects. These findings provide evidence that CtermDys acts as a dominant negative to DGC function and, therefore, could contribute significantly to the cardiomyopathy of EV infection.

302.

MIR-208A TARGETED SUPPRESSION OF PDE4D DIRECTLY ENHANCES MYOCYTE CONTRACTILE FUNCTION VIA PKA-MEDIATED PHOSPHORYLATION OF CTNI AND PLN

Fikru Belema-Bedada and Joseph M. Metzger
Department of Integrative Biology and Physiology, University of Minnesota
6-125 Jackson Hall, 321 Church Street SE, Minneapolis, MN 55455 U.S.A.

Molecular inotropy refers to cardiac myocyte contractile status that can be titrated, positively or negatively, to affect overall heart pump performance. Although inotropic drugs have been in clinical practice for many decades, there is an urgent need to discover new inotropes with unique mechanisms of action for the treatment of heart failure. Here, we investigate the prospect of micro-RNAs to directly modify downstream inotropic signaling pathways for improving contractile function. We focused on miR-208a owing in part to its known restricted expression profile in the myocardium. Results show that acute miR-208a expression, at 4-5 fold over endogenous miR-208a and independent of altered host myosin gene expression, confers significant positive inotropy and faster relaxation compared to miR-208a-mutant and untreated control adult cardiac myocytes ($P<0.05$). Using in vitro cardiac stress testing, miR-208a amplified the inotropic and relaxation responses to increased stimulation frequency. MiR-208a also promoted fast calcium transient decay with no change in peak calcium accounting in part for enhanced relaxation. To gain insight into mechanism, we analyzed in silico putative miR-208a targets, focusing on potential inotropic signaling targets. Interestingly, we provide evidence that miR-208a has a direct effect to negatively regulate expression of PDE4D, but does not affect PDE5A in myocytes. Consistent with these findings, phosphorylation of cTnI and PLN at PKA sites was increased in myocytes after acute miR-208a expression. Taken together, we show for the first time that miR-208a confers positive inotropy and enhances relaxation in myocytes by PKA mediated phosphorylation of cTnI and PLN through a mechanism of direct suppression of PDE4D. Because heart failure is associated with decreased phosphorylation of cTnI

and PLN, miR-208a may represent a new therapeutic modality for enhancing ventricular myocyte performance via the PDE4D-cAMP-PKA signaling pathway.

303.

Pouya Hematti, MSII, Lee Pyles, MD

MyEIF.org a Hybrid Personal and Medical Health Record with an Emergency Focus

Purpose: The website www.MyEIF.org has been developed to host individual instances of an emergency-focused hybrid personal and medical health record. This database uses an Emergency Information Form (EIF) template formulated and promoted by the American College of Emergency Physicians and AAP Committees on Pediatric Emergency Medicine. Our hypothesis is that emergency and disaster care for children with special health care needs can be improved by implementing and updating a tool that facilitates emergent access to individualized clinical summaries. This report will present how continued cycles of evaluation and improvement of the MyEIF.org website impacts parents, special needs children, and health care providers.
Methods: The website was built using Microsoft SQL®, Adobe ColdFusion®, and SAP CrystalReports®. The EIFs have been collaboratively completed and updated by health care providers, site administrators, parents, and other family members since 2002, when patients began enrolling in MyEIF.org. The UM IRB approved protocol for the website outlines informatics features such as family self-registration, role-based privileges for access, family options to control levels of regular access and family control of break-the-glass emergency access. Database features include constrained options for choices of diagnoses, procedures and medications; ability to build custom templates for personalized family and physician decision support; and novel templates that document technologic devices such as pacemakers and home ventilators. One of the essential features is a virtual tour that introduces potential users to the site. In addition, a survey engine allows design, delivery and collation of user surveys. Compliance features include a UM IRB approved consent for research, role-based security and a notification of Privacy Practices. The operation and usability of the website has been investigated during actual emergency visits and in a live disaster simulation. An icon system attributes the source of medical data; provider, parent or administrator.
Results: There are 272 patients currently enrolled and emergent EIF use has been reported 33 times. Family users have accessed the website on 1562 patient days since inception on 8/15/2002. The site tour (www.myeif.org/tour) has been accessed 274 times by visitors from 33 US states since it was created in 11/12/2003. Since 6/15/2006, the website has been used for 29,663 total minutes (average session time of 17.23 minutes) with users logging in an average of 11.5 times. Reasons for the 2242 webpage active sessions include new enrollment (637), clinic visit (607), telephone call (282), family update (253), MD/Nurse update (210), hospital discharge (123), emergency department discharge (18) and home health visit (10). A unique features of the EIF template is an advice section in the medical summary that outlines appropriate responses to emergencies related to a child's specific health problem.

Conclusions: Hosting the emergency-focused clinical summaries, MyEIF.org has elucidated an understanding of the public's attitudes and beliefs regarding personal health records .Web accesses and updates are documented. Improvements have addressed concerns for attribution of data and time expenditure by health care workers. Emergency access continues to evolve. The innovative advice section of MyEIF.org promotes patient-specific decision support for families and providers. The MyEIF.org website serves as a model instrument to house medical information critical to emergency and disaster management for patients with complex medical histories. Exposure to the website changes family outlook regarding their special needs child by fostering "normalization", the feeling of reassurance that the family is regaining control of their lives. The parent website experience brings to light the need for emergency and disaster health information for special needs children.

304.

Etv2-regulated microRNAs are essential for endothelial development

Bhairab N. Singh, Xiaozhong Shi, Tara L. Rasmussen, Alicia Wallis, Kathy Bowlin, Naoko Koyano-Nakagawa and Daniel J. Garry*
Lillehei Heart Institute, University of Minnesota, USA

Precise regulation of the fate of endothelial precursors is critical for vascular development. Currently, no known microRNAs have been shown to have a functional role in the specification of the endothelial progenitor cell fate during early embryogenesis. To decipher the requirement of miRNAs during endothelial and vascular development, we disrupted Dicer in a tissue-specific manner, utilizing the Etv2-Cre transgenic mouse model that we engineered to ablate microRNA biogenesis in endothelial progenitors. Using this strategy, we determined that miRNA biogenesis is essential for vasculogenesis as Etv2-Cre:DicerF/F embryos are lethal by E11.5-12.5. Histological analysis reveals that the Dicer conditional knockout embryos have severe vascular defects and hemorrhage compared to the wildtype littermates. We have previously reported enrichment of a Pdgfr-□+ cell population in the Etv2 mutant embryos; however the mechanistic regulation is unclear. In the present study, we have identified miR-27a and miR-130a as Etv2 downstream target genes. Using transcriptional assays, we observed that Etv2 transactivated both miR-27a and miR-130a in a dose-dependent manner. Further, we have identified and mapped the miR-27a and miR130a binding sites on the Pdgfr-□□ 3-UTR. Our transcriptional assays indicate that miR-27a and miR-130a attenuate the expression of Pdgfr-□□. Collectively, these findings identify novel microRNA-mediated mechanisms that govern lineage decisions of mesodermal progenitors and ultimately impact cardiovascular development.

305.

An ex vivo Gene Therapy Approach to Treat Muscular Dystrophy Using iPS cells

Antonio Filareto1, Sarah Parker1, Radbod Darabi1, Luciene Borges1, Michelina Iacovino2, Tory Schaaf1, Timothy Mayerhofer1, Jeffrey S Chamberlain3, James M. Ervasti4, R. Scott McIvor5, Michael Kyba2 and Rita C.R. Perlingeiro1

1Lillehei Heart Institute, Department of Medicine, University of Minnesota, Minneapolis, MN USA, 2Lillehei Heart Institute, Department of Pediatrics, University of Minnesota, Minneapolis, MN, USA 3Department of Neurology, University of Washington School of Medicine, Seattle, WA, USA, 4Department of Biochemistry, Molecular Biology, and Biophysics, University of Minnesota, Minneapolis, MN, USA, 5Department of Genetics, Cell Biology and Development, University of Minnesota, Minneapolis, MN, USA.

Duchenne muscular dystrophy (DMD) is a progressive and fatal neuromuscular disease caused by genetic and biochemical defects of the dystrophin-glycoprotein complex (DGC). To date, there is no cure for DMD. A strategy that holds promise is the direct reprogramming of adult fibroblasts to a pluripotent state, generating patient- and disease- specific stem cells, and correcting these in vitro prior to transplantation. Here we show the regenerative potential of myogenic progenitors derived from corrected dystrophic iPS cells generated from fibroblasts of mice lacking both dystrophin and utrophin (dKO). We corrected the phenotype of these dystrophic iPS cells using a Sleeping Beauty transposon carrying the micro-utrophin (μUTRN) gene, differentiated these cells into skeletal muscle progenitors, and assessed whether their transplantation back into dystrophic mice would ameliorate the muscle wasting phenotype. Engrafted muscles displayed large numbers of μ-UTRN+ myofibers, with biochemically restored DGC, and significantly improved contractile strength. Notably transplanted corrected cells seeded the satellite cell compartment, and responded properly to injury. We show that systemic delivery of these corrected progenitors results in widespread muscle engraftment, including TA and gastrocnemius muscles. Thus, these results represent an important advance toward a potential future treatment of muscular dystrophies using genetically corrected autologous iPS cells.

306.

Endoplasmic reticulum stress sensor PERK protects against pressure overload induced heart failure

Xiaoyu Liu, Xin Xu, Huan Wang, Dongmin Kwak, Xinli Hu, John Fassett, Ping Zhang, Robert J. Bache, Yingjie Chen

Studies have reported that development of congestive heart failure (CHF) is associated with increased endoplasmic reticulum (ER) stress. Double stranded RNA activated protein kinase-like endoplasmic reticulum kinase (PERK) is a major transducer of the ER stress response and directly phosphorylates eIF2α, resulting in translational

attenuation. However, the effect of PERK on the development of ventricular hypertrophy and CHF has not been studied. Global PERK gene deficiency is embryonic lethal, so in order to study the effect of PERK on ventricular structure and function.we generated inducible cardiac specific PERK gene deficient mice using MerCreMer system.Under unstressed conditions, selective gene deletion of PERK in cardiac myocytes had no effect on left ventricular mass or its ratio to body weight, myocyte size, or left ventricular function. However, in response to chronic transverse aortic constriction (TAC), cardiac specific PERK-deficiency significantly worsened reductions in ejection fraction and LV contractility, and exacerbated pulmonary congestion in comparison to wild type mice. PERK deficiency also significantly exacerbated TAC-induced increases of ventricular fibrosis and atrial natriuretic peptide, but caused no more cardiac myocyte hypertrophy than wild type mice. Interestingly, PERK deficiency significantly increased TAC-induced myocyte apoptosis and caspase-3 activation. Collectively, our data indicate that PERK protects against LV myocyte apoptosis and LV contractile dysfunction. Our findings suggest PERK is required to protect the heart from pressure overload induced congestive heart failure.

307.
A novel role for Pax3 as regulator of the skeletal versus cardiac myogenic program during mesoderm formation

Alessandro Magli, Erin Schnettler and Rita Perlingeiro
Lillehei Heart Institute, Dept. of Medicine, University of Minnesota, Minneapolis

The paired box transcription factor Pax3, a major regulator of embryonic myogenesis, is first expressed in the developing somites and then becomes restricted to the dermomyotome of the mature somites. To better understand the role of Pax3 during these early stages, we analyzed its function in differentiating mouse ES cells. Our results show that, during Embryoid Body (EB) development, Pax3 up-regulates several paraxial mesoderm and skeletal myogenic markers. This is consistent with the generation of a robust cell population that mimics the events occurring from the epithelial somite to the myotome stage. Taking advantage of this system, we performed a systematic analysis of Pax3 requirement during the induction of the myogenic lineage, focusing particularly on the identification of the domain that account for Pax3 functions. Notably, we found that as induction of Pax3 leads to specification of the skeletal myogenic cell fate, characterized by up-regulation of Myf5 and MyoD, there is simultaneous repression of the cardiac cell fate, as evidenced by reduced expression of several cardiac genes, including Gata4, Tbx5 and cTnI. These findings are corroborated by our studies using deletion mutants of Pax3, which differentially affect its transcriptional activity and therefore its ability to switch between the skeletal and the cardiac program. Importantly, we show that Tbx5 is directly down-regulated by Pax3 as evidenced by short time induction experiments. Co-expression of Tbx5 and Pax3 leads to the rescue of the cardiac differentiation and repression of skeletal myogenesis. Thus our in vitro system allowed the identification of an unexpected role of Pax3 in repressing the cardiac myogenesis. Ongoing in vivo studies in Pax3-null animals will provide a

better comprehension of Pax3 function by enhancing our knowledge of its role in determining cell fate during embryonic development.

308.
Nucleotide activation of the Ca-ATPase

J. Michael Autry, John E. Rubin, Bengt Svensson, Ji Li, and David D. Thomas
Department of Biochemistry, Molecular Biology, and Biophysics, University of Minnesota

Background: FITC is a useful but underutilized covalent probe of the Ca-ATPase nucleotide-binding site.
Result: We measured fluorescence lifetime, anisotropy, and quenching of FITC-labeled Ca-ATPase. We used enzyme reverse mode to synthesize FITC monophosphate as a fluorescent ATP analog tethered to the active site of the Ca-ATPase.
Conclusion: The Ca-ATPase active site exhibits increased dynamics when enclosed with bound ATP.
Significance: Fluorescence spectroscopy bridges enzyme kinetics and crystal structures.

We have used time-resolved fluorescence spectroscopy, molecular modeling, and limited proteolysis to examine structural dynamics of the sarcoplasmic reticulum Ca-ATPase (SERCA). The Ca-ATPase in sarcoplasmic reticulum (SR) vesicles from skeletal muscle (SERCA1a isoform) was selectively labeled with fluorescein isothiocyanate (FITC), a probe that specifically reacts with Lys-515 in the nucleotide-binding site. We used enzyme reverse mode to synthesize FITC monophosphate (FMP) on SERCA, producing a phosphorylated pseudosubstrate tethered to the nucleotide-binding site. Conformation-specific proteolysis demonstrated that FMP acts as an ATP analog but FITC does not. Subnanosecond-resolved detection of fluorescence lifetime, anisotropy, and quenching was used to characterize FMP-SERCA in the Ca-free state (ATP.E2) as compared to FITC-SERCA in Ca-free, Ca-bound, and actively-cycling phosphoenzyme states (E2, E1, EP). Fluorescence results reveal that FMP-SERCA exhibits increased probe dynamics but decreased probe accessibility compared to FITC-SERCA, indicating that the ATP.E2 state exhibits active-site disorder within a closed cytoplasmic headpiece. Molecular modeling of FMP and FITC in crystal structures of SERCA was used to calculate solvent-accessible surface area (SASA) of bound fluorescent probes, providing independent support for a closed cytoplasmic headpiece in ATP.E2. We conclude that active-site dynamics is critical for ATP hydrolysis and phosphoenzyme formation.

Acknowledgments: This work was supported by NIH grants to D.D.T. (R01 GM27906, P30 AR0507220, T32 AR007612). J.L. was supported by a University of Minnesota Doctoral Dissertation Fellowship. Spectroscopy was performed in the Biophysical Spectroscopy Center. Computational resources were provided by the Minnesota Supercomputing Institute.

309.

Double-strand RNA–dependent Protein kinase deficiency protects the heart from systolic overload-induced congestive heart failure

Huan Wang; Xin Xu, Dongmin Kwak, John Fassett, Xinli Hu, Ping Zhang, Haipeng Guo, Jennifer Hall, Robert J. Bache, and Yingjie Chen
Cardiovascular Division, University of Minnesota Medical School, Minneapolis, MN

Double-strand RNA–dependent protein kinase (PKR) is an eIF2 □ (the alpha s eukaryotic initiation factor 2) kinase, that can selectively attenuate mRNA translation in response to inflammation or stress through eIF2 □. Development failure (CHF) is associated with myocardial inflammation and increased phosphorylation of eIF2 □. However, it ventricular (LV) hypertrophy or heart failure. Interestingly, we found that myocardial PKR protein expression was significantly increased in heart failure samples obtained from human subjects and experimental animals. Furthermore, PKR was predominantly localized in the nuclei in heart failure samples as compared to normal heart samples, suggesting increased activation of PKR in the failing heart. To further understand the physiological role of PKR on LV structure and function, PKR knockout mice and control wild type mice were studied under control conditions and in response to chronic pressure overload produced by transverse aortic constriction (TAC). Under unstressed conditions PKR deficiency had no effect on LV mass or its ratio to body weight, myocyte size, or LV function. However, in response to chronic TAC, PKR-deficient mice developed significantly less reduction of ejection fraction, less reduction of LV contractility and less pulmonary congestion than wild type mice, although they had the same level of LV hypertrophy. PKR deficiency also remarkably attenuated TAC-induced increases of ventricular fibrosis and atrial natriuretic peptide. Although PKR deficiency significantly attenuated ventricular p-eIF2 □ content, it had no expression. Interestingly, PKR deficiency significantly attenuated TAC-induced myocyte apoptosis as indicated by TUNEL staining. This was associated with reduced Bax expression and reduced inflammatory cytokines in PKR deficient hearts. Consistent with the protective effects observed in PKR deficient mice, selective gene silencing of PKR in cultured rat neonatal cardiac myocytes significantly attenuated LPS and TNF □ induced expression of inflammatory cytokines and cardiac myocyte apoptosis. Collectively, our data indicate that in the setting of pressure overload, PKR activity is detrimental. By promoting expression of pro-apoptotic proteins (Bax) and inflammatory cytokines, PKR contributes to left ventricular myocyte apoptosis and LV contractile dysfunction. These findings suggest that modulating PKR signaling might be a novel therapeutic approach for treating congestive heart failure.

310.

Multiple DDAH1 knockout strains reveal abnormal vascular endothelial DDAH1 function as the major contributor for exacerbated hypoxia-induced pulmonary artery hypertension in mice

Dongmin Kwak, Xin Xu, Dachun Xu, Haipeng Guo, Xinli Hu, Ping Zhang, Zhongbing Lu, E. Kenneth Weir, Yingjie Chen
Cardiovascular Division, University of Minnesota Medical School, Minneapolis, MN

Pulmonary artery hypertension (PAH) is a progressive disease with a very poor prognosis. Recent studies have demonstrated that PAH is associated with diminished nitric oxide bioavailability and increased levels of endogenous nitric oxide synthase (NOS) inhibitor ADMA. We have demonstrated that dimethylarginine dimethylaminohydrolase-1 (DDAH1) is essential for degradation of endogenous NOS inhibitor ADMA, and is important for optimal endothelial NO production. PAH is associated with decreased lung DDAH activity. However, it is not clear whether decreased DDAH activity and ADMA accumulation can exacerbate the development or progression of PAH. In addition, the impact of endothelial specific DDAH1 dysfunction on PAH development is unknown. Using global DDAH1 gene deficient mice, we first demonstrate that chronic ADMA accumulation by DDAH1 gene deletion does not cause significant PAH under control conditions, but significantly exacerbates chronic hypoxia-induced PAH, as indicated by significantly increased right ventricular (RV) pressure, more RV hypertrophy, and exacerbated pulmonary vascular remodeling in DDAH deficient mice as compared to wild type mice. Similar to global DDAH1 deficiency, endothelial specific DDAH1 gene deletion also significantly exacerbated hypoxia induced increases in systolic RV pressure, RV hypertrophy and lung vascular remodeling as compared to wild type littermates. This suggests that DDAH1 deficiency specifically localized to the vascular endothelium is sufficient to exacerbate hypoxia-induced PAH in mice, and suggests exacerbated PAH observed in global DDAH1 KO mice could be due primarily to reduced endothelial DDAH1 activity. In support of this concept, cardiomyocyte specific disruption of DDAH1 did not exacerbate hypoxia induced increases in RV pressure or vascular remodeling in comparison to wild type littermates. Collectively, our data indicate that DDAH1, localized specifically in the vascular endothelium, plays a critical role in protection against hypoxia-induced PAH.

311.
Microtubule Actin Cross linking Factor(MACF1/ACF7) gene disruption causes cardiomyocyte microtubule disorganization and exacerbates pathological hypertrophy

Rational: In response to ventricular wall stress, cardiomyocytes reorganize the extra-sarcomeric cytoskeleton (β-actin filaments, intermediate filaments, microtubules). MACF1/ACF7 is a ~600 kd spectraplakin that coordinates the cytostructural response to external stimuli by stabilizing microtubules(MTs) and guiding MT growth along actin filaments. ACF7 is expressed in the heart, but its role in cardiomyocyte cytoskeletal organization and adaptation to stress is not known.
Objective: Determine the role of ACF7 in cardiomyocyte cytoskeletal organization and adaptation to hypertrophic stress.
Methods and Results: In neonatal rat cardiomyocytes, ACF7 RNAi treatment severely disrupted normal microtubule trajectories and blocked cell spreading. In adult mice, cardiac-specific inducible disruption of ACF7 had no effect on heart size or function

under basal conditions. However, in response to pressure overload(transverse aortic constriction; TAC), ACF7 KO significantly exacerbated cardiac hypertrophy, LV dilation, and contractile dysfunction as compared to WT mice. ACF7 KO mice exhibited increased levels of PKC alpha expression and reduced levels of caveolin 3 and serca2A in response to TAC as compared to WT mice. While β-actin, desmin and tubulin increased to a similar extent in WT and ACF7 KO mice after TAC, microtubule distribution was altered, so that MTs accumulated more with the cell membrane in ACF7 KO mice. Furthermore, increased tubulin content in the cell membrane fraction was closely correlated with the degree of contractile dysfunction in both WT and ACF7 KO mice($r=0.799$, $p=.001$). These findings support a role for ACF7 in maintaining MT organization during adaptation to hypertrophic stress, and identify increased membrane association of microtubules as a novel predictive factor in pressure overload induced contractile dysfunction.

312.
Reduced translocation of the TRPv1 receptor in afferent neurons of cardiomyopathic rats

Minh M. Nguyen, Laurence E. Stout, Qinglu Li, and Mary G. Garry
University of Minnesota, School of Medicine

Heart failure (HF) patients exhibit an abnormal exercise pressor reflex (EPR) in response to exercise. Previous studies have implicated the TrpV1 receptor, a vanilloid receptor and transmembrane ion channel, as a mediator of the EPR. A necessary step in activation of TRPv1 is translocation to the membrane. To determine if the translocation of TRPv1 is affected in HF, we compared the subcellular localization of TRPv1 in primary cultures of dorsal root ganglia (DRG) from normal and cardiomyopathic rats. DRGs (L4-L6) of normal or cardiomyopathic rats were evaluated in the presence or absence of NGF. Cells were stained for TrpV1 and fluorescence intensities of membrane and cytoplasm were quantified. Normal NGF treated DRG cells showed an increased ratio of membrane to cytoplasmic TrpV1 staining as compared to normal untreated control. Conversely, in HF, the ratio of membrane to cytoplasmic TrpV1 decreased in response to NGF treatment. These results suggest that HF DRGs are impaired in their ability to recruit TrpV1 to the membrane. Furthermore, this suggests that abnormal EPR response in HF patients may be due, in part, to decreased TrpV1 activity due to reduced TrpV1 membrane localization.

313.
Validation of systemic cell delivery and generation of integration free human ES/iPS derived myogenic precursors

Radbod Darabi and Rita C.R. Perlingeiro
Lillehei Heart Institute, Department of Medicine, University of Minnesota

We have been the first group to report successful generation of myogenic progenitors from mouse ES/iPS cells by controlled expression of Pax3/Pax7. These cells have the ability to promote in vivo skeletal muscle regeneration following transplantation in mdx mice, which is accompanied by functional recovery. Importantly, we have also shown that ES/iPS-derived engrafted cells have the ability to seed the muscle adult satellite cell compartment, confirming the in vivo self renewal potential of myogenic precursors obtained from pluripotent cells.

However, efficient generation of engraftable skeletal myogenic progenitors from human ES/iPS cells is not a straightforward task. In continuation of our works on using ES/iPS cells, we have recently developed a very efficient protocol for derivation of engraftable human ES/iPS derived myogenic precursors. We have shown that by controlled over expression of Pax7- using a doxycycline inducible lentiviral system- during human ES/iPS derived EB differentiation, skeletal myogenic progenitors can be specified and sorted out. These cells show uniform myogenic surface markers and can be expanded exponentially in vitro. Moreover, these human ES/iPS derived myogenic progenitors show great regeneration potential after intra muscular transplantation into immunodeficient NSG-mdx mice and are able to differentiate into mature and functional myofibers expressing human dystrophin as well as seeding satellite cells.
However to apply this strategy to human patients, we need further studies in the mouse model to maximize engraftment potential as well as to develop non-integrating viral/non-viral gene expression systems to deliver safe cell preparations for clinical application. Here we evaluate strategies that will allow us to maximize the engraftment ability of human ES/iPS- derived myogenic progenitors. Specifically we test systemic delivery (intra-arterial transplantation) to see if the human ES/iPS derived progenitors are able to home and engraft into muscle, which would be a great advantage from a clinical stand point. Our second aim is to establish a safe method to induce Pax7, using non-integrating episomal DNA vectors (Minicircle) or synthetic modified mRNA transduction. This study will help us to move this technology one step closer to clinical trials.

314.
DDAH1 protects the heart from systolic overload-induced ventricular hypertrophy and heart failure

Ping Zhang, Xin Xu, Xinli Hu, Dorothee Atzler, Dongming Kwak, Haipeng Guo, Dachun Xu, Zhongbing Lu, Edzard Schwedhelm, Rainer H. Böger, Yingjie Chen, Robert J. Bache

ADMA is the strongest independent predictor of both mortality and major nonfatal cardiovascular events in patients after myocardial infarction. While studies indicated that accumulation of ADMA is associated with congestive heart failure, it is not clear whether chronic ADMA accumulation can cause or exacerbate the development of congestive heart failure. Here we demonstrated that chronic ADMA accumulation by global DDAH1 gene deficiency (DDAH1-/-) caused aging-dependent moderate left ventricular hypertrophy with no apparent left ventricular dysfunction/failure under unstressed

conditions, indicating that chronic accumulation of ADMA alone is insufficient to cause left ventricular dysfunction. In addition, using an inducible cardiac specific DDAH1 gene deficient strain, we demonstrated that selective DDAH1 gene deletion in cardiac myocytes (cardio-DDAH1-/-) had no effect on circulating ADMA and left ventricular hypertrophy, suggesting that left ventricular hypertrophy observed in DDAH1-/- mice is mainly due to the moderate systolic hypertension in this strain. However, cardio-DDAH1-/- significantly exacerbated transverse aortic constriction-induced left ventricular hypertrophy, left ventricular dilatation and pulmonary congestion, indicating that DDAH1 distributed in cardiac myocytes is important in protecting the heart from systolic pressure overload-induced left ventricular hypertrophy and heart failure.

315.

The Chemical Membrane Sealant Poloxamer 188 Ameliorates Myocardial Ischemia/Reperfusion-induced Injury by Preventing Sarcolemmal Permeability

Joshua J. Martindale, Martina Maerz, Joseph M. Metzger, Department of Integrative Biology & Physiology, University of Minnesota, Minneapolis, MN 55455

Compromised sarcolemmal integrity is a feature of myocardial ischemia/reperfusion (I/R) injury leading to necrotic cell death. We hypothesized that the chemical membrane sealant Poloxamer 188 (P188) could prevent I/R-induced sarcolemmal permeability, thus preventing cell death and improving functional recovery. In an in vitro model of I/R, isolated adult rat ventricular myocytes were exposed to 1 hour hypoxia (0.2% O2) followed by 1 hour reoxygenation (H/R). Sarcolemmal permeability was assessed by measuring myocyte release of lactate dehydrogenase (LDH) or uptake of a membrane impermeant fluorescent dextran. H/R caused a significant increase in LDH release (15.5±0.6 fold, $p<0.05$), which was reduced nearly to control levels by 10uM P188 (2.6±0.01 fold). In addition, H/R induced the uptake of fluorescent dextran (2.3±0.4 fold), which was reduced by P188 (0.2±0.1 fold). To determine the effects of P188 in a whole organ model, isolated mouse hearts were exposed to 15 minutes ischemia followed by 60 minutes reperfusion (I/R). Control hearts exhibited recovery of left ventricular developed pressures of 24.1±5.6 mmHg at 60 minutes reperfusion, which was improved to 39.43±3.7 mmHg by P188, a nearly 2-fold increase in function ($p<0.05$). I/R caused a significant increase in LDH release into the perfusate (6.9±1.9 fold, $p<0.05$), which was reduced by P188 (3.3±1.4 fold). I/R induced a significant increase in fluorescent dextran uptake (4.3±0.8 fold, $p<0.05$), which was reduced nearly to control levels by P188 (1.5±0.2 fold). These data support the hypothesis that prevention of sarcolemmal permeability by P188 can reduce I/R-induced myocardial injury and improve function at the cellular and organ levels.

316.

Dominant effect of histidine modified troponin to normalize SR Ca2+ load and rescue ischemia/reperfusion deficits in phosholamban deficient hearts.

Joshua J. Martindale, Todd J. Herron, Sharlene M. Day, Joseph M. Metzger,
Department of Integrative Biology & Physiology, University of Minnesota, Minneapolis, MN 55455

Genetic modification of cardiac Ca2+ handling has been proposed to improve functional deficits in the failing heart. For example, ablation of phospholamban (PLN), a key inhibitor of the sarcoplasmic reticulum Ca2+ - ATPase (SERCA2a), causes enhanced cardiac contractility and faster relaxation. However, phospholamban deficient hearts (PLN KO) are highly susceptible to increased ischemia/reperfusion (I/R) injury. We hypothesized that histidine-modified cardiac troponin I, cTnI (A164H), which has increased Ca2+ sensitivity especially during ischemia/acidosis, could rescue PLN KO hearts from I/R mediated functional deficits. Isolated PLN KO hearts exposed to I/R exhibited dramatically reduced recovery after 1 hr of reperfusion compared to controls (2.5% +/- 1.4% recovery vs 32.5% +/- 9.3%, $P<0.05$), highlighting a major deficiency in PLN KO hearts. Interestingly, expression of cTnIA164H had nearly a 14-fold improvement and restored functionality to PLN KO hearts (34.7% +/- 8.5% recovery). As PLN KO hearts have been shown to have increased SR Ca2+ load, we sought to determine whether cTnIA164H has an effect on Ca2+ dynamics. PLN KO myocytes have a nearly two-fold increase in caffeine-induced SR Ca2+ release compared to control, consistent with previous results. Surprisingly, PLN KO myocytes expressing the cTnI A164H transgene had normalized caffeine-releasable SR Ca2+ load, yet still maintained the rapid SR Ca2+ uptake characteristic of PLN KO myocytes. These findings suggest a new paradigm of Ca2+ handling in the heart by indicating a dynamic interplay between SR and myofilaments, with cTnIA164H myofilaments having a dominant effect to normalize SR Ca2+ load and rescue ischemia/reperfusion deficits in hearts with dysregulated Ca2+ pumps.

317.

Loss of the eIF2 kinase GCN2 protects mice from pressure overload induced congestive heart failure

Xin Xu, Zhongbing Lu, John Fassett, Ping Zhang, Xinli Hu,
Dongmin Kwak, Huang Wang, Robert J. Bache, Yingjie Chen

Nutrient deprivation or stress enhances phosphorylation of the alpha subunit of eukaryotic initiation factor 2 (eIF2 ☐) by General Co
(GCN2). Phosphorylation of eIF2 ☐ inhibits trans
containing 5'TOP motifs, but can facilitate translation of some mRNAs associated with the cell stress response. Phosphorylation of eIF2 ☐ is increase
is not known whether GCN2 plays a role in the development of left ventricular (LV) hypertrophy or heart failure. To understand the physiological role of GCN2 on LV structure and function, GCN2+/+ and GCN2-/- mice were studied under control

conditions and in response to chronic transverse aortic constriction (TAC). Under unstressed conditions GCN2 deficiency had no effect on LV mass or its ratio to body weight, myocyte size, or LV function. However, in response to chronic TAC, GCN2-deficient mice developed more LV hypertrophy, but less reduction of ejection fraction and less pulmonary congestion than wild type mice. GCN2 deficiency also significantly attenuated TAC-induced increases of ventricular fibrosis and atrial natriuretic peptide. Although loss of GCN2 expression significantly attenuated ventricular p-eIF2 ☐ content, it had no effect on total eIF2 ☐ expression o deficiency significantly attenuated TAC-induced myocyte apoptosis and caspase-3 activation, in association with reduced Bax expression and increased Bcl2 expression. Bcl2 mRNA levels were similar in WT and GCN2-/- mice, suggesting GCN2 deficiency improved Bcl2 translation. GCN2 also significantly attenuated the TAC-induced increase of CHOP, but had no effect on ventricular ATF4 or GADD34 expression. Collectively, our data indicate that GCN2 deficiency increased TAC-induced LV hypertrophy, but attenuated LV myocyte apoptosis and LV contractile dysfunction by selectively enhancing mRNA translation of a set of protective genes. Our findings suggest GCN2 signaling might be a novel therapeutic approach for treating congestive heart failure.

318.
Transcriptional regulation of Etv2 gene expression governs vasculogenesis

Tara L. Rasmussen, Naoko Koyano-Nakagawa, Alicia Wallis, Xiaozhong Shi, Christine Wasylyk, Bohdan Wasylyk, and Daniel J. Garry

Etv2 is an Ets related transcription factor that is essential for the specification of the endothelial lineage. We have previously demonstrated that Etv2 mutant mouse embryos are lethal by E9.5 and the entire endothelial lineage is absent. The purpose of the present study is to define the upstream transcriptional regulators that activate and repress Etv2 gene expression. Using an array of techniques, we demonstrate that Etv2 expression in vivo is dependent upon Flk1 expression. Using transcriptional assays, we show that the Etv2 promoter is activated in a dose dependent fashion by Vegf/Flk1. We further demonstrate that the Vegf/Flk1 activation is mediated, in a dose dependent fashion, by Creb and p38-MAPK. Creb binding to evolutionary conserved binding motifs within the Etv2 promoter was verified using EMSA and ChIP assays. However, while these upstream activators (Vegf/Flk1/Creb) are continuously expressed throughout development and into adulthood, Etv2 expression is limited to a narrow developmental window. Therefore, we examined candidates that may function to repress and/or extinguish Etv2 gene expression. In previous studies, we have shown that there is an increase in the Etv2 promoter-EYFP reporter in Etv2 mutant embryos, suggesting that Etv2 may activate a repressor of itself. We have identified Elk3 as a downstream target of Etv2 using microarrays of Etv2 knockout embryos and Etv2-overexpressing EBs. Elk3 is an Ets factor that functions as a transcriptional inhibitor in the vascular system. Therefore, we examined whether Elk3 can function as a transcriptional repressor of Etv2. We observed that Etv2 is overexpressed three fold in Elk3 mouse knockouts compared to the wildtype littermates at E8. We identified evolutionarily conserved Ets

binding elements (EBEs) within the 3.9kb upstream regulatory region of the Etv2 gene. Using transcriptional assays, we observed that Elk3 transcriptionally represses Etv2 gene expression ten fold. In summary, our data demonstrate that Flk1 and VEGF activate Etv2 in a Creb dependent manner. Etv2 activates Elk3, which in turn, represses Etv2 transcription. We suggest that Etv2 and Elk3 form an essential feedback loop which governs the short temporal expression pattern of Etv2 and thus vasculogenesis.

319.

Tamoxifen has acute inhibitory effects on contractility in isolated adult rat cardiac myocytes

Michelle L. Asp, Joshua J. Martindale, and Joseph M. Metzger

Spatiotemporal cardiac gene targeting featuring α-MyHC-MerCreMer (MCM) transgenic mice is an important approach for studying heart-specific gene function. The modified estrogen receptor (MER) is activated by the selective estrogen receptor modulator (SERM) tamoxifen. MER activation by tamoxifen results in nuclear translocation of MCM, and Cre-mediated excision of loxP-flanked genes. A drawback to tamoxifen-dependent Cre translocation is transient cardiomyopathy, which is suggested to be independent of gene excision and dependent on the presence of MCM. However, studies using isolated cardiac myocytes reveal the presence of an acute non-genomic inhibitory effect of tamoxifen on several types of ion channels, suggesting tamoxifen also may have an effect in the absence of MCM. The goal of the present study was to determine whether the inhibition of ion channels found in previous studies translates to changes in contractility and calcium transients in isolated adult rat cardiac myocytes. One day after cell isolation, we found an acute decrease in the peak height of contraction with tamoxifen at concentrations of 5 and 10μM. This was accompanied by slowed relaxation and diminished calcium transient amplitude. Additionally, the percentage of rod-shaped cells that visibly contract dose-dependently decreased over the course of 45 minutes of pacing with tamoxifen. Raloxifene, also in the SERM class of drugs, had acute effects on cardiac myocytes that included hypercontractility and slowed relaxation. In conclusion, the acute tamoxifen and raloxifene-induced alteration of cardiac myocyte contractility may contribute to the transient cardiomyopathy seen in MCM transgenic mice. The results of this study emphasize the importance of using the minimum dose of tamoxifen or raloxifene required for gene excision in MCM transgenic mice, as well as incorporating appropriate control groups to address acute cardiomyopathy in this model.

320.

Heart function following exposure to bile acids during cold storage

Karen Porter PhD1, Tyler Mingo1, Glynnis Garry1, Peter I. Dosa PhD2, and Mary G. Garry PhD1

Department of Medicine1 and Medicinal Chemistry2 and Lillehei Heart Institute, University of Minnesota, Minneapolis, MN

Bile acids have been used to improve various liver conditions and are now being investigated as putative therapies for neurological and cardiovascular pathologies. Tauroursodexycholic acid (TUDCA), a taurine conjugate of ursodeoxycholic acid (UDCA), has been demonstrated to reduce scar size and apoptosis resulting from myocardial infarction. Since TUDCA has been shown to protect against acute tissue injury, we hypothesized that addition of TUDCA to the cold storage solution, University of Wisconsin (UW), will improve heart function during reperfusion and lengthen the time the heart can be stored. Male rat hearts were explanted and perfused with UW alone, UW+TUDCA (1 mM), or UW+Pyruvate+TUDCA then stored in the solution for 4 hours at 4°C. Following cold storage the hearts were reperfused with Krebs-Henseleit buffer via a Langendorff isolated heart apparatus to measure cardiovascular function. A second study was conducted to determine if the addition of Compound E, a UDCA pro-drug (1 mM) to UW would improve function following cold storage. Hearts stored in UW+Pyruvate+TUDCA did not show improvement of left ventricular developed pressure (LVDP) or coronary flow compared to UW alone. Exposure to Compound E did show a significant improvement in LVDP compared to UW alone, however, there was no improvement in coronary flow. The data presented suggests Compound E provides some recovery of heart function following cold storage compared to TUDCA.

321.

Circadian and infradian rhythms of some parameters of the ECG on days with or without examination

Lyazzat Gumarova
Visiting scholar, Halberg Chronobiology Center

Seasonal rhythms of an organism are an important tool to adapt to the environment. As part of the problem of adjustment to a load (“stress”), infradian (including seasonal) biorhythms deserve special attention, notably in a climate with a strong contrast between summer and winter. Evolutionary circannual rhythms contribute to the survival of individuals, species and populations of different animals in the face of seasonal changes in habitat. The changing of seasons imposes great demands on organisms, especially in the continental climate of Kazakhstan. This investigation examines any influence of seasons on the daily dynamics of some ECG parameters (notably endpoints of heart rate variability, HRV) in association with the load of an examination in this Central Asian region. All exams were conducted in the morning (at 09:00). Circadian rhythm characteristics of ECG endpoints were compared between days with vs. without exam, when exams were taken either during winter or summer. In summer, on days with an examination, 24-hour means of SDNNidx and rMSSD (HRV parameters) were decreased, more so at night, when the parameters SDNNidx, rMSSD, pNN50, pNN100, pNN200 undergo statistically significant changes. Changes of lesser extent were observed in winter. In both seasons, the load of an examination was

associated with a shift in the circadian acrophase (phase of maximum of cosine curve approximating the data) that was more pronounced in summer than in winter. On days with an exam, the harmonic content increased, components with a frequency higher than 1 cycle per day (ultradians) becoming more prominent.
Responses of blood pressure and heart rate to a load can vary greatly as a function of the circadian stage when the stimulus is applied. Recently, cycles other than circadian and circannual also have been reported, notably components with periods of about 5 and 16 months, detected in longitudinal records of blood pressure and heart rate as well as in mortality statistics from myocardial infarction and sudden cardiac death in different geographic locations. Whether the response to a load such as an examination is also characterized by such non-photic infradian components deserves further investigation.

322.
Combating Adaptation to Stretch Conditioning Through Prolonged Activation of Extracellular Signal-Regulated Kinase

Justin Weinbaum, Jill Schmidt, Robert Tranquillo

In developing an implantable tissue-engineered artery based on cellular remodeling of a fibrin scaffold, a key measure of success is high final collagen content. Cellular collagen synthesis is promoted by cyclic distension during the remodeling process but is limited by adaptation to the stretching stimulus (Syedain et al. PNAS 2010). Cellular adaptation to stretching is mediated by deactivation of extracellular signal-regulated kinase (ERK); therefore a chemical method for prolonging ERK activation should improve stretch-induced collagen production and accelerate the development of a strong bioartificial artery. The hypothesis of this study is that p38 mitogen activated protein kinase (p38) activation by stretching inhibits ERK and that a chemical inhibitor of p38, SB 203580, will therefore lead to higher ERK activation and subsequent collagen production. Inhibition of p38 during cyclic stretching of cell monolayers increased ERK activation in a dose responsive manner; one of the effective inhibitory doses, 5 uM, was selected for studies using cells in fibrin scaffolds. Pretreatment with the p38 inhibitor increased short-term ERK activation in biaxially- stretched, but not static, fibrin-based tissue constructs. When constructs were exposed to three weeks of incremental amplitude cyclic stretching, p38 inhibition led to an increase in total collagen versus untreated controls. Future studies will investigate whether SB treatment will also lead to increased collagen content and superior mechanical strength in stretch- conditioned bioartificial arteries. In conclusion, we have found a chemical method to circumvent adaptation that may be useful in engineering tissues where collagen-endowed mechanical strength is a priority.

323.
Maternal stress, NPY system and adult metabolic syndrome.

Ruijun Han, Xinying Wang, Joanna Kitlinska1, Aiyun Li1, G Ian Gallicano1 and Zofia Zukowska. Depts of Integrative Biology & Physiology, University of Minnesota,

Minneapolis MN 55455, and 1Physiology & Biophysics, Georgetown University, Washington DC 20057, USA

Prenatal and early postnatal stress, psychologically and metabolically, increases the risk of obesity and diabetes in the progeny, while mechanisms are unknown. In adult mice, stress activated NPY and its Y2R in a glucocorticoid-dependent manner in the abdominal fat. This increased adipogenesis and angiogenesis leading to abdominal obesity and metabolic syndrome which were inhibited by intra-fat Y2R inactivation. Here we studied long-term effects of prenatal low protein diets (LPD) stress on the offspring's obesity and effects of NPY system in adipogenic lineage commitment in murine embryonic stem cells (mESC). Male offspring of mice stressed by LPD during pregnancy had lower birth weight but quickly caught up before weaning. Male offspring developed abdominal adiposity, elevated circulating NPY levels, Y2R up-regulation specifically in the abdominal fat and impaired glucose tolerance on high fat diets (HFD). To determine whether stress elevates NPY system and accelerates adipogenic potential of embryo, we "stressed" mESC with epinephrine during their adipogenic differentiation. Epinephrine-induced stress dramatically amplified adipogenic differentiation detected by increasing the adipocyte markers FABP4 and PPARγ mRNAs and Oil-red O-staining. Stress markedly up-regulated the expression NPY and the Y1R at the commitment stage, followed by increased Y2R mRNA peaking later at differentiation stage. Epinephrine-induced adipogenesis was completely prevented by antagonists of the NPY receptors (Y1R+Y2R+Y5R). Taken together, our data suggested that NPY system mediates stress induced adipogenic commitment in embryo, and thus play an important role in prenatal stress programmed abdominal obesity and metabolic syndrome in offspring.

324.

Modeling Cardiac Differentiation in Human Induced Pluripotent Stem Cells (hiPSC)

Michelle J Doyle, Jamie L Lohr, Christopher Chapman, Forum D Kamdar, Naoko Koyano-Nakagawa, Daniel J Garry. Lillehei Heart Institute, University of Minnesota, Minneapolis, MN.

During organogenesis, cardiomyocytes are derived from distinct heart fields that differ in their position, cellular context, molecular signaling and timing of differentiation. Disruption of normal heart field development is associated with specific forms of congenital heart disease, in humans and in animal model systems. Human embryonic and induced pluripotent stem cells (hiPSC) can be directed to a cardiac fate, but the molecular networks and timing of the intermediate steps of differentiation have not been well defined. We hypothesize that manipulation of hiPSC cardiomyocyte differentiation can be used to model the development of specific heart fields. To test this hypothesis, we utilized a monolayer differentiation assay with the addition of timed growth factors to direct hiPSC to a cardiac fate. Differentiation proceeds through a stage specific manner with mesoderm induction, characterized by robust MESP1 expression by day 2. Expression of the early cardiac transcription factors Nkx2.5 and Isl1 is detected

between day 4 and 6, followed closely by expression of structural proteins cTNT and Myh6. An increased number of cardiomyocytes and increased contractility, as well as a decrease in smooth muscle cells is observed with the addition of Wnt3a compared to Activin A alone at day 0. Furthermore, we observe expression of transcription factors and signaling molecules associated with second heart field development in cardiomyocyte culture. This will facilitate utilization of the hiPSC system to study the molecular networks involved in heart field development and to differentiate subsets of cardiomyocytes representative of a specific developmental field.

325.

A novel automated method for the morphological analysis of adipocytes: preliminary evidence

Ivana Ninkovic, Rana Mohammed, Cheryl Cero, Alessandro Bartolomucci
Department of Integrative Biology and Physiology, University of Minnesota

Obesity is often associated with an increase of adipocyte diameter. The direct measurement of adipocyte size thus far has been done by microscopy and various immunohistochemical methods are widely used [1]. These methods are very accurate but are slow and require extensive expertise in histology and morphology of the adipose tissue. Development of a new method allows a rapid and accurate determination of adipocyte size may have a major impact in the obesity field. Here, we report a preliminary assessment of a new automatic method for determining adipocyte size and number. This method allows a large number of adipocytes to be measured rapidly through the Vision Cell Analyzer and the dedicated software (Nexcelom, MA). This system is an automated cell counter and cell analyzer that combine bright field microscopy and multi-channel fluorescence images generating cell count and fluorescence data. Preliminary data were obtained in both primary adipocytes from obese and lean mouse as well as in 3T3-L1 adipocytes. In each mouse strain as well as in the model cell line, enlargement of the fat cells in observed adipose depot led to fat cell populations that were more normally distributed. The degree of precision of various operations involved and of the final estimates of adipocyte size and diameter distribution was evaluated and found to be within expected limits previously described by literature. 3T3-L1 is fibroblast-like cells that can be differentiated in adipocytes following a specific and well established protocol. 3T3-L1 cells are extensively used as a model of adipocytes and are sensitive to lipogenic and lipolytic agents, including epinephrine, isoproterenol, and insulin [2]. During differentiation from fibroblasts into adipocytes, 3T3-L1 cells were measured for diameter change over a period of 12 days. At maturity, they were treated for 3 hours to 3 days with several concentrations of a lipolytic agent. Individual adipocyte size (diameter in microns), relative distribution in cell size, and cell number utilizing method based in direct microscopic determination was performed. Developmental diameter change of 3T3-L1 cells increased over time averaging an increase of 12 microns. Different lipolytic agents induced diameter decrease in 3T3-L1 mature adipocytes in parallel with an increase in free glycerol in the media, an indirect measur of lipolysis. In addition, adipocytes from obese mice were enlarged and

enriched in large size cells when compared to lean mice. Our findings indicate general applicability of this methodology for accurately and rapidly determining adipocytes size and number. In addition, results from this method suggest that heterogeneity in size of a fat cell population is a measurable parameter which should be studied further as a clue to the expansion of the adipose organ.

[1] Cinti S. The Adipose Organ. In 'Adipose Tissue and Adipokines in Health and Disease' Edited by: G. Fantuzzi and T. Mazzone. Humana Press Inc., Totowa, NJ 2007
[2] Green H, Kehinde O (1975). "An established preadipose cell line and its differentiation in culture. II. Factors affecting the adipose conversion". Cell 5(1): 19–27.
Acknowledgements: Alnoor Pirani, Benjamin Paradis and Timothy Smith from Nexcelom are acknowledge for their technical support.

326.

Molecular Mechanisms of A164H cTnI.

Brian Thompson1, Evelyne Houang1,2, Yuk Sham2, Joseph Metzger1

Department of 1Integrative Biology and Physiology and 2Center for Drug Design, University of Minnesota, Minneapolis, MN 55455

Troponin I (TnI) has a central, isoform-dependent role in ischemic contractile failure. The fetal heart expresses the slow skeletal TnI (ssTnI) isoform which confers protection from ischemia-mediated contractile failure relative to the adult expressed cardiac TnI (cTnI) isoform. A single codon substitution in cTnI, A164H, reverts significantly to an ssTnI phenotype, in specifics, conferring protection from ischemia-mediated contractile failure. Importantly, unlike ssTnI, cTnI A164H does not alter contractile performance under baseline conditions. The molecular mechanisms for the marked enhancement in myocyte function under pathophysiological conditions with no detected effects under baseline conditions have yet to be determined. Isoform specific residues in helix 4 of TnI were investigated through structure/function analysis to gain insight into this mechanism. Molecular dynamics simulation for cTnI, Q157R/A164H/E166V/H173N cTnI (QAEH), A164H cTnI, and ssTnI in complex with cTnC, showed that substitution of cTnI with the ssTnI residues alters the intermolecular interactions between TnI and cTnC. These findings suggest that these residues are important for the conformation of helix 4 in regards to cTnC. To investigate if these substitutions alter function, adult cardiac myocytes were transduced with adenovirus expressing QAEH cTnI and sarcomere dynamics were analyzed. QAEH cTnI showed a similar phenotype to ssTnI, increasing sarcomere shortening and slowing relaxation at pH 7.4 while maintaining normal contractile function under acidic conditions. To elucidate this further, double and triple mutants were analyzed to determine the importance of each of the three residues to baseline contractility. The data show that H173 and Q157 are necessary for the reduced contractility at baseline while E166 exerts the opposite effect. Taken together, these new findings suggests that the conformation of helix 4 in TnI is an important determinate of contractility in ischemia.

327.
A focused region of D4Z4 demethylation in FSHD2

LM Hartweck1, LJ Anderson1, RJ Lemmers2, A Dandapat1, S Grindle1, EA Toso1, JC Dalton3, R Tawil4, JW Day5, SM van der Maarel2, M Kyba1;
UMN Department of Pediatrics and Lillehei Heart Institute University of Minnesota1, Leiden University Medical Center, Department of Human Genetics, Albinusdreef 2, 2333ZA Leiden, Netherlands 2 Academic Health Center and Wellstone Muscular Dystrophy Center UMN3, Neuromuscular Disease Center, University of Rocherster Medical Center4, Department of Neurology and Institutes of Human Genetics and Translational Neuroscience and Wellstone Muscular Dystrophy Center UMN5

Facioscapulohumeral muscular dystrophy (FSHD) is a neuromuscular disease with an unclear genetic mechanism. Most patients have a contraction of the D4Z4 macrosatellite repeat array at 4qter which is thought to cause partial demethylation (FSHD1) on the contracted allele, however <5% of patients (FSHD2) show hypomethylation of D4Z4 throughout the genome, including both alleles on chromosome 4 and highly related repeats on chromosome 10. Previous studies on D4Z4 methylation changes in FSHD1 surveyed 3 or 4 methylation sensitive restriction sites in the first D4Z4 repeat. Our objective was to take advantage of the global D4Z4 chromatin changes seen in FSHD2 to evaluate D4Z4 for evidence of domain-specific differential epigenetic deregulation using bisulfate sequencing. We analyzed FSHD2 and control blood samples and cultured myoblasts for methylation levels over three disparate regions within D4Z4 encompassing 74 CpG sites. We have identified a 5' domain with a 75% reduction in methylation in FSHD2. We have also identified a 3' domain within the DUX4 ORF which is not severely hypomethylated in FSHD2 and a domain between these that shows intermediate demethylation. Demethylation of D4Z4 is therefore remarkably non-homogeneous in FSHD2. In a related study with mouse embryonic stem cells, we found that the number of arrayed repeats may also influence methylation at the identified 5' domain. D4Z4 is a complex element with domains of differential methylation in controls, and differential sensitivity to FSHD2-associated hypomethylation. We postulate that the key D4Z4 chromatin regulatory factors that go awry in FSHD2 are likely to be found within the zone of greatest differential methylation, ie. near the 5' hypomethylated domain.

328.
In vitro characterization of DUX4c, a gene involved in FSHD

Megan Roth, Robert W. Arpke, Darko Bosnakovski, Megan M. Multhaup, Michael Kyba
Lillehei Heart Institute, University of Minnesota, Minneapolis MN

Facioscapulohumeral muscular dystrophy (FSHD) is caused by a contraction that deregulates D4Z4 transcription, leading to DUX4 expression. This contraction also alters regulation of an inverted orphaned D4Z4 repeat approximately 40 kb upstream of the main tandem repeat array, resulting in transcription of DUX4c, a gene identical to

DUX4 but lacking the C-terminus due to a frameshift mutation. While over-expression of DUX4 in vitro is associated with cytotoxicity, impaired differentiation, and cell death; over-expression of DUX4c in vitro appeared was non-toxic in C2C12 myoblasts, but blocked their differentiation. We have generated an inducible mouse model that expresses DUX4c upon administration of doxycycline. We find unexpectedly that although DUX4c is not cytotoxic in vitro, it is organismically toxic: upon doxycycline induction, DUX4c animals present facial swelling, ichthyosis, hair loss, hunching, and ultimately die. This response is dependent on the dose of doxycycline delivered. These mice also show a delay to repair following cardiotoxin-mediated muscle damage. Further, Pax7+ satellite cells isolated from DUX4c+ mice subjected to a single cell cloning assay demonstrated a lower plating efficiency, fusion index, and differentiation potential. Together, these results suggest that misregulation of DUX4c in myogenic progenitors is profoundly disruptive, and might therefore contribute to FSHD pathology. Together, these results suggest that misregulation of DUX4c is profoundly disruptive, and is deleterious to myogenic regeneration. It may therefore contribute together with DUX4 to FSHD pathology.

329.
Functional improvement after satellite cell transplantation into NSG-mdx4Cv mice.

Robert W. Arpke1,2, Radbod Darabi1,3, Tara Mader4,5, Kerri T. Haider1,2, Akira Toyama1,2,
Cara-lin Lonetree1,2, Nardina Nash1,2, Dawn Lowe4,5, Rita Perlingeiro1,3 and Michael Kyba1,2

1Lillehei Heart Institute, 2Department of Pediatrics, 3Department of Medicine, 4Program in Physical Therapy, 5Department of Physical Medicine & Rehabilitation, University of Minnesota.
We have developed a profoundly immunodeficient, dystrophin-deficient transplant recipient model: NOD/SCID;IL2Rg-mdx4Cv (NSG-mdx4Cv) mice. The scid mutation knocks out T and B cells, while the IL2Rg (common gamma chain for the IL2 receptor) mutation knocks out NK cells, involved in rejection of non-self MHC-expressing tissue, and for this reason is preferred for human to mouse hematopoietic stem cell transplantation studies. The mdx4Cv mutation is reported to have a 10 fold reduced rate of revertant fibers. As expected, when peripheral blood profiles of these mice were analyzed, the NSG-mdx4Cv mice lacked T cells and B cells while granulocytes were still observed. At both 6 and 15 weeks of age, the NSG-mdx4Cv mice had fewer revertant fibers than similar age mdx mice. Maximal isometric torque was 48% lower in 6 week NSG-mdx4Cv and mdx mice than in wildtype mice. Maximal eccentric torque generation was also equally low in NSG-mdx4Cv and mdx mice relative to wildtype. Specific force generation was ~34% lower in all EDL muscles lacking dystrophin compared to wildtype, with no difference between NSG-mdx4Cv and mdx mice at 6 or 15 weeks of age. The NSG-mdx4Cv mice function as both a xenogeneic and an allogeneic transplant recipient animal model. We observed engraftment of pig and dog gastrocnemius mononuclear cells into irradiated and cardiotoxin-injured muscle. To test

for allogeneic transplantation potential, satellite cells isolated from a fluorescent reporter mouse strain were intramuscularly injected into irradiated and injured tibialis anterior muscle of NSG-mdx4Cv mice. When maximal isometric tetanic force was examined one month after transplantation, Pax7-ZsGreen+ cells injected into the TA nearly doubled force generation compared to that of the contralateral leg PBS-injected control. Laminin and dystrophin staining indicated an average of 55% of the muscle fibers of the TA were donor-derived based upon dystrophin positivity.

330.

Cardiac Myosin Binding Protein-C Restricts Intrafilament Torsional Dynamics of Actin in a Phosphorylation-Dependent Manner

Colson, Brett A.‡#, Inna N. Rybakova§, Ewa Prochniewicz‡, Richard L. Moss§, and David D. Thomas‡

‡Dept. of Biochemistry, Molecular Biology and Biophysics, University of Minnesota 312 Church St. SE, Minneapolis, MN 55455; §Department of Cell and Regenerative Biology, University of Wisconsin School of Medicine and Public Health, Madison, WI 53711.

We have determined the effects of myosin binding protein-C (MyBP-C) and its domains on the microsecond rotational dynamics of actin, using time-resolved phosphorescence anisotropy (TPA). MyBP-C is a multi-domain thick filament-associated modulator of striated muscle contraction, interacting with myosin, titin, and possibly actin. Cardiac and slow skeletal MyBP-C are known substrates for protein kinase-A (PKA), and phosphorylation of the cardiac isoform alters contractile properties and myofilament structure. To determine the effects of MyBP-C on actin structural dynamics, we labeled actin at C374 with erythrosine iodoacetamide and performed TPA experiments. The interaction of all three MyBP-C isoforms with actin increased the final anisotropy of the TPA decay, indicating restriction of the amplitude of actin torsional flexibility by 15-20° at saturation of the TPA effect. PKA phosphorylation of slow skeletal and cardiac MyBP-C relieved the restrictive effect on actin torsional flexibility, and at the same time decreased the rate of intrafilament motion. In the case of fast skeletal MyBP-C, its effect on actin dynamics was unchanged by phosphorylation. Effects of truncated cardiac MyBP-C on actin anisotropy revealed that the C-terminal half C5-C10 has partial effects of full-length cardiac MyBP-C on rate and amplitude, and binds actin more tightly than the N-terminal half C0-C4, which does not affect amplitude but increases the rate of actin intrafilament motion. We propose that these MyBP-C-induced changes in actin dynamics play a role in the known effects of MyBP-C on the functional actin-myosin interaction.

331.
Context-dependent lineage determination by Mesp1

Sunny Sun-Kin Chan,1,2 Xiaozhong Shi,1,3 Akira Toyama,1,3 Robert W. Arpke,1,3 Abhijit Dandapat,1,2 Michelina Iacovino,1,3 Jin-Joo Kang,1,2 Gengyun Le,1,2 Hannah R. Hagen,1 Daniel J. Garry,1,3 and Michael Kyba1,2,*

1Lillehei Heart Institute, 2Department of Pediatrics, and 3Department of Medicine, University of Minnesota, Minneapolis, MN 55455, USA.

Mesp1 is regarded as the master regulator of cardiovascular development, initiating the cardiac transcription factor cascade to direct the generation of cardiac mesoderm. To define the early embryonic cell population that responds to Mesp1, we performed inductions of gene expression over tight temporal windows following embryonic stem cell differentiation. Remarkably, instead of promoting cardiac differentiation, Mesp1 binds to the Tal1 (Scl) +40k enhancer and induces the initial wave of mesoderm into Flk-1+ precursors expressing Etv2 (ER71) and Tal1 that undergo hematopoietic differentiation. The second wave of mesoderm responds to Mesp1 by differentiating into PDGFR □+ precursors tha
absence of serum-derived factors, Mesp1 promoted skeletal myogenic differentiation. Lineage tracing revealed that the majority of yolk sac and many adult hematopoietic cells derive from Mesp1+ precursors. Thus, Mesp1 is not a cardiac master regulator, but rather a context-dependent determination factor, integrating stage of differentiation and signaling environment to specify different lineage outcomes.

332.
Heterogeneity of ATP turnover rates in the LV of swine hearts with post-infarction remodeling

Qiang Xiong, Pengyuan Zhang, Lei Ye, Albert Jang, Jianyi Zhang

Rationale and Objective Alterations in ATP synthetic capacity is thought to contribute to the dysfunction of the failing heart. However, in in vivo hearts, low myocardial inorganic phosphate (Pi) levels limit direct measurement of these rates with magnetic resonance spectroscopy-magnetization saturation transfer (MRS-MST) method. In current study, we have developed a novel indirect MRS-MST technique and demonstrated for the first time the measurement of ATP→ADP+Pi unidirectional rate (kr,ATP) in both normal and diseased swine hearts in vivo.
Methods and Results The indirect MRS-MST method was validated on swine skeletal muscle (n=5). kr,ATP was measured at the remote (RZ) and peri-infarct (BZ) regions of swine heats with post-infarction left ventricular remodeling (LVR, n=9, 4 weeks post infarction) as well as age and sex-matched normal hearts (NL, n=11). In NL hearts, kr,ATP (which is the sum of mitochondrial and cytosolic ATP→Pi rate constants) was linearly related to the rate-pressure-product (RPP) during the catecholamine stimulation. In BZ (but not in RZ) of LVR hearts, kr,S was significantly reduced at

baseline (LVR-BZ-0.06±0.02 vs.NL-0.17±0.03 s-1, p<0.05) and became nonresponsive to catecholamine stimulation although the overall RPP responses to catecholamine stimulation are comparable between LVR and NL hearts. Notably, the rate constants of the creatine kinase (CK) reaction (PCr→ATP) were comparable (NL-0.37±0.03 vs. LVR-BZ-0.34±0.03 s-1, p=NS). The regional abnormality of ATP turnover rate in LVR-BZ was accompanied with contractility reduction (BZ thickening fraction), wall stress elevation and impairment of vascular structure and perfusion.

Conclusion The novel MRS-MST measurements of kr,ATP have shown that non-failing LVR hearts are metabolically heterogeneous and that kr,ATP reductions in BZ precede that of CK rates and the overall decline of LV metabolic and mechanical performance as LVR progresses. The down-regulation of kr, ATP in the BZ may reflect greater wall stresses and concomitantly greater activation of adverse molecular signaling pathways in that region. The data supported the hypothesis that metabolic dysfunction in LVR hearts progresses circumferentially as LVR worsen.

333.

Genetic down-regulation or pharmacological inhibition of Flt-1 ameliorates the muscular dystrophy phenotype by increasing the vasculature in DMD model mice

James Ennen, Mayank Verma, Yoko Asakura, Hiroyuki Hirai, Shuichi Watanabe, Jarrod A Call, DeWayne Townsend, Dawn A Lowe, Atsushi Asakura

Duchenne Muscular Dystrophy (DMD) is a X-linked recessive genetic disorder caused by mutations in the gene coding for the protein dystrophin. Dystrophin has a structural role as a cytoskeletal stabilization protein and protects cells against contraction-induced damage. Dystrophin also has a signaling role through mechanotransduction of forces and localization of neuronal nitric oxide synthase (nNOS), which produces nitric oxide (NO) to facilitate vasorelaxation. Lack of dystrophin in vascular smooth muscle impairs blood flow in response to metabolic demands and creates a damaging state of functional ischemia. The two-hit hypothesis explains that the myofiber damage seen in dystrophic muscle is due to a combination of functional ischemia and the inherent weakness of the dystrophin deficient muscle. This implies that myofiber damage can be attenuated through therapy focused on improving blood flow and tissue perfusion, and this project utilized a pro-angiogenic approach that increases vascular density in order to achieve this goal. Vascular endothelial growth factor (VEGF) is a prominent regulatory molecule for angiogenesis and induces angiogenic signals through the Flt-1 and Flk-1 receptors. Flk-1 is a low affinity receptor for VEGF but contains an active tyrosine kinase domain, whereas Flt-1 is a high affinity receptor for VEGF but contains a weaker tyrosine kinase domain. A soluble form of Flt-1 (sFlt-1) also exists but lacks a signaling domain. So, Flt-1 and sFlt-1 act as competitive inhibitors to Flk-1 for VEGF binding and consequent angiogenic induction. This makes inhibition or quantitative reduction of Flt-1 and/or sFlt-1 potential targets for DMD pro-angiogenic therapy. To assess the utility of pro-angiogenic DMD therapy through developmental down-regulation of ¬Flt-1, we crossed DMD model mdx mice with Flt-1 knockout mice to

create double mutant mdx:Flt-1+/- mice. The resulting phenotype from the mdx:Flt-1+/- mice displayed a happloinsufficient scenario with increased vascular density, improved muscle histology, and greater number of satellite cells compared to mdx mice. Functionally, the mdx:Flt-1+/- had increased anterior crural muscle torque production, improved blood flow, and no adverse outcomes in myocardial hemodynamic studies compared to mdx mice. To replicate this phenomenon in a drug inducible model, we utilized a synthetic hexapeptide that antagonizes the Flt-1 receptor. We found that the mdx mouse muscle injected with the anti-Flt-1 peptide had increased capillary density, higher muscle blood flow, lower membrane permeability, and decreased fibrosis compared to the vehicle only control. Combined, these data strongly suggest that increasing the vasculature in dystrophic muscle may ameliorate the histological and functional phenotypes seen in DMD patients.

334.
Cellular reprogramming to blood using a transcription factor cocktail

Jai Richard1, Ismail Ismailoglu1, Michelina Iacovino1 & Michael Kyba1
1Lillehei Heart Institute, Dept. of Pediatrics, University of Minnesota.

During normal development cells follow a pre-determined path to give rise to various organs. This path is controlled by the spatio-temporal expression of individual transcription factors. Recent work has shown that manipulation of the expression of certain key transcription factors can modify cell fate, for example reprogramming differentiated somatic cells to pluripotent embryonic stem-like cells, or iPS cells. We have been investigating whether it is possible to reprogram cells directly from one fate to another without going through a pluripotent intermediate state. To investigate this, we have made use of in vitro differentiation of mES cells. Using a 2D culture model, we have coexpressed three early blood-specific transcription factors: SCL, LMO2, and GATA2. In the absence of expression of these three factors, blood is not produced. But, when the factors are induced in differentiating mES cells, they interact synergistically and even in the absence of mesoderm the majority of cells take on a hematopoietic phenotype. We present investigations into the mechanism of this conversion, and describe ongoing studies to reprogram mouse embryonic fibroblasts (MEFs) and adult tail tip fibroblasts from transgenic mice with conditional expression of SCL, LMO2, and GATA2 to study reprogramming of somatic cells from an adult.

335.
Identification of a Novel microRNA-Protease Signaling Pathway in Symptomatic Carotid Plaques

Neeta Adhikari1, Marjorie Carlson1, Darrell Loeffler2, Dinesha Walek3, Jerry Daniel3, Mark J Lawson4 Aaron J Mackey4, Amir Lerman2 and Jennifer L. Hall1
1 Lillehei Heart Institute, Department of Medicine, University of Minnesota, MN 55455
2 Division of cardiovascular Diseases, Mayo Clinic Rochester, MN 55905
3 Biomedical Genomics Core Facility, University of Minnesota, MN 55455

4 Center for Public Health Genomics, University of Virginia, VA 22904

MicroRNAs are a class of small non-coding RNAs that regulate gene expression by binding to discrete sites of genes and inhibiting translation. The objective of this study was to identify microRNAs and downstream enriched targets associated with symptomatic carotid plaques. Carotid plaque samples from patients were defined as symptomatic if they were associated with a prior ischemic stroke or transient ischemic attack or as asymptomatic if there were no prior ischemic events. Digital microRNA profiling was performed on from symptomatic (n=6) and asymptomatic (n=6) carotid plaques utilizing the nCounter analysis system (NanoString Technologies, Seattle, WA) The BioConductor/R package "edgeR" was used to perform moderated-ANOVA testing for differences in gene abundance between groups, assuming a negative binomial distribution of gene counts, with Benjamini-Hochberg multiple hypothesis correction to control false discovery rate. Analysis revealed enrichment of five microRNAs including miR-16 (p=0.0003) which was confirmed by RTqPCR (n=6, p=0.02). Predicted downstream targets of the miR-16 family were enriched for proteases including Cathepsin L, Cathepsin B and heparanase. RTqPCR demonstrated upregulation of Cathepsin B transcript in a larger cohort of symptomatic patients (n=45-50, p=0.02). However, Cathepsin L (n=45-50) and heparanase (n=45-50) transcripts were not significantly different between symptomatic and asymptomatic carotid plaques. Also, Cathepsin L enzyme activity was not significantly different in symptomatic cohort (n=12, p=ns). Taken together, these findings suggest that miR-16 and Cathepsin B may be unique to symptomatic carotid plaques.

336.

Title: Mouse model to understand the role of Dux4 in Facioscapulohumeral muscular dystrophy

Abhijit Dandapat, Darko Bosnakovski, Kristen A. Baltgalvis, Lynn Hartweck, Cara-lin Lonetree, Nardina Nash, Dawn A. Lowe, and Michael Kyba,
Lillehei Heart Institute and Department of Pediatrics, University of Minnesota, Minneapolis

Facioscapulohumeral muscular dystrophy (FSHD) is an autosomal dominant disease that affects 1:20 000 individuals. Mapping studies have associated the disease with a reduced number (1-10) of the D4Z4 macrosatellite repeats from the usual ~100. These repeats lie adjacent to the telomeres and are usually present in a highly silenced epigenetic state. It is not clear which genes are affected or how DNA methylation patterns affect the disease. Within the D4Z4 repeat is an ORF encoding a putative transcription factor named Dux4, containing two homeodomains. Although the function of Dux4 is unknown, the Dux4 homeodomains are similar to those of Pax7, a protein known to be involved in muscle development, proliferation and differentiation. We have previously reported that Dux4 is toxic when misexpressed at high levels in many cell types, and blocks differentiation of myoblasts when expressed at low levels, and competes with Pax7 for regulation of myogenic target genes. To model Dux4 function in vivo, we made a Dux4-inducible mES cell line by inserting a doxycycline-inducible

Dux4 allele (iDux4+3'UTR) onto the X chromosome at a euchromatic region (HPRT). High-level induction of the Dux4 was toxic to mES cells but low-level induction resulted in altered differentiation. When iDux4+3'UTR mice where generated and bred, this allele demonstrated leaky phenotypes in females, and male-specific lethality. Rare live-born males were small and underdeveloped with abnormal skin and defective sperm development and showed changes to muscle fibers, but no overt muscle degeneration. However, mice died within 1 month, well before the stage when degeneration usually begins in FSHD. Dux4 protein could be induced and observed in cultured primary cells, and we are evaluating pups and embryos for Dux4 expression in vivo. Dux4 carrier females were smaller and displayed the skin phenotype in transverse stripes. We hypothesize that the 3' UTR contains an enhancer which drives leaky expression in some embryonic cell types and that X chromosome inactivation combined with selective survival of XDux4-inactive cells protects the females from the lethality. To test for selectively biased X inactivation, we crossed Dux4 carrier females with XGFP males. Upon FACS analysis of the GFP+ cells in XGFP/ X+ vs. XGFP/ XDUX4 female progeny, we found that the latter had an elevated frequency of GFP positive cells in most tissues, including the satellite cell compartment of skeletal muscle, confirming our hypothesis of selective XDux4 inactivation. This mouse model suggests that Dux4 is a dominant lethal gene even when expressed at very low levels and can cause a variety of developmental defects in EBs and in embryo development.

337 .

Smooth Muscle Specific Deletion of N-deacetylase-sulfotransferase1 (Ndst1) Results In Altered Arterial Elasticity

Kim Ramil C Montaniel1, Neeta Adhikari1, Spencer P Lake2, Marie Billaud3 Marjorie Carlson1, Brant E Isakson3, Victor H Barocas2, Jennifer L Hall1
1 Lillehei Heart Institute, University of Minnesota, Minneapolis, MN 55455
2 Department of Biomedical Engineering, University of Minnesota, Minneapolis, MN 55455
3 Robert M Berne Cardiovascular Research Center, School of Medicine, University of Virginia, Charlottesville, VA 22908

Ndst1 is a rate-determining heparan sulfate proteoglycan (HSPG) biosynthetic enzyme that regulates the sulfation pattern of heparan sulfate side chains attached to proteoglycan core proteins. We previously published that a mouse model with smooth muscle specific deletion of Ndst1 (SM22αcre+Ndst1-/-) exhibited the expected significant reduction in HSPG sulfation and an unexpected significant reduction in vessel size. Despite this, SM22αcre+Ndst1-/- exhibited no change in systemic or diastolic blood pressure compared to WT. This led us to hypothesize that these phenotypic changes could have influenced arterial elasticity. This is important, as loss of arterial elasticity is an early predictor of cardiovascular disease such as hypertension and atherosclerosis. To test this, we measured elastic modulus and circumferential compliance in aorta and thoracodorsal arteries (TDA), respectively. Aortas from 2-5 month old male WT and SM22αcre+Ndst1-/- were clamped and stretched longitudinally and circumferentially (i.e., ring tests) using an Instron test machine. SM22αcre+Ndst1-/-

exhibited a decreased longitudinal tangent modulus of 0.69 ± 0.12 MPa (n=5) compared to WT with 2.01 ± 0.17 MPa (n=11, P<0.01). However, circumferential moduli values did not differ (n=3, P=0.32). To measure compliance, TDA from WT (n=6) and SM22αcre+Ndst1-/- (n=8) were mounted onto an arterial myograph and perfused with Kreb's Buffer at a pressure range of 10 to 140 mmHg. SM22αcre+Ndst1-/- TDA exhibited a decreased vessel lumen but maintained compliance similar to WT. At 110 mmHg, compliance was 86.92 ± 21.07 (WT, n=6) and 121.19 ± 26.17 (SM22αcre+Ndst1-/-, n=8) μm2/mmHg (P=0.32). In conclusion, compliance in TDA or circumferential tangent modulus in aorta was unaffected in SM22αcre+Ndst1-/-. In contrast, SM22αcre+Ndst1-/- exhibited increased compliance (decreased modulus) in response to longitudinal stretch. This suggests that loss of HSPG sulfation may affect elastin fiber organization and/or properties given elastin's predominant role in longitudinal stretch.

338.

An evidence-based score to detect prevalent peripheral artery disease (PAD)

Sue Duval1, Joseph M Massaro2, Michael R Jaff3, William E Boden4, Mark J Alberts5, Robert M Califf6, Kim A Eagle7, Ralph B D'Agostino Sr8, Alison Pedley2, Gregg C Fonarow9, Joanne M Murabito10, P Gabriel Steg11, Deepak L Bhatt12 and Alan T Hirsch13 on behalf of the REACH Registry Investigators

1 Lillehei Clinical Research Unit, Cardiovascular Division, University of Minnesota Medical School, Minneapolis, MN, USA
2 Biostatistics, Boston University School of Public Health and Harvard Clinical Research Institute, Boston, MA, USA
3 Medicine, Massachusetts General Hospital, Boston, MA, USA
4 Medicine, Samuel S Stratton VA Medical Center and Department of Medicine, Albany Medical Center, Albany, NY, USA
5 Neurology, Northwestern University Feinberg School of Medicine, Chicago, IL, USA
6 Cardiology, Duke University Medical Center and Duke Translational Medicine Institute, Durham, NC, USA
7 Internal Medicine, University of Michigan Cardiovascular Center, Ann Arbor, MI, USA
8 Mathematics, Boston University School of Public Health and Harvard Clinical Research Institute, Boston, MA, USA
9 Medicine, David Geffen School of Medicine at University of California Los Angeles, Los Angeles, CA, USA
10 Medicine, Boston University School of Medicine, Boston, MA, USA
11 INSERM U-698, Univ Paris 7, Paris, France
12 Cardiology, VA Boston Healthcare System, Brigham and Women's Hospital and Harvard Medical School, Boston, MA, USA
13 Medicine, Epidemiology and Community Health, Cardiovascular Division, University of Minnesota Medical School and School of Public Health, Minneapolis, MN, USA

Abstract

Detection of peripheral artery disease (PAD) typically entails collection of medical history, physical examination, and noninvasive imaging, but whether a risk factor-based model has clinical utility in population screening is unclear. Our objective was to derive and validate a new score for estimating PAD probability in individuals or populations. PAD presence was determined by a history of previous or current intermittent claudication associated with an ankle–brachial index (ABI) of < 0.9 or previous lower extremity arterial intervention. Multivariable stepwise logistic regression identified cross-sectional correlates of PAD from demographic, clinical, and laboratory variables. Analyses were derived from 18,049 US REACH (REduction of Atherothrombosis for Continued Health) Registry outpatients with a complete baseline risk factor profile (enrolled from December 2003 to June 2004). Model performance was assessed internally using 10-fold cross validation, and effect estimates were used to generate the score. The model was externally validated using the Framingham Offspring Study. Age, sex, smoking, diabetes mellitus, body mass index, hypertension stage, and history of heart failure, coronary artery disease, and cerebrovascular disease were predictive of PAD prevalence. The model had reasonable discrimination on derivation and internal validation (c-statistic = 0.61 and 0.60, respectively) and external validation (c-statistic = 0.63 [ABI < 0.9] or 0.64 [clinical PAD]). The model-estimated PAD prevalence varied more than threefold from lowest to highest decile (range, 4.5–16.7) and corresponded closely with actual PAD prevalence in each population. In conclusion, this new tool uses clinical variables to estimate PAD prevalence. While predictive power may be limited, it may improve PAD detection in vulnerable, at-risk populations.

339.
Trends in Utilization of the Ankle-Brachial Index (ABI) in the US Medicare Population: 1998 to 2008

Sue Duval, PhD, Stephen T. Parente, PhD, MPH, MS, Niki C. Oldenburg, DrPH, and Alan T. Hirsch, MD.

The ankle-brachial index (ABI) has long represented the gold standard for the non-invasive, cost-effective diagnosis of PAD. Evidence of marked underdiagnosis of PAD was established in 2001. National evidence-based clinical care guidelines in 2005 defined targeted ABI use as a Class 1B diagnostic tool, followed by an NHLBI supported national PAD public awareness campaign. We assessed the temporal rates of use of physiologic PAD tests in the US Medicare population.

Methods
We analyzed annual Medicare data from a 5% sample of the Part B CMS administrative database. We evaluated annual rates of use of single-level ABI and multi-level segmental pressure (SP) tests to determine trends in utilization of PAD diagnostic tests over the years 1998 to 2002 and 2007 to 2008.

Results
There has been a marked rise in use of ABI and SP diagnostic PAD tests during the eleven year period from 1998 to 2008. Rates of either PAD test increased by 63%, from 131/10,000 in 1998 to 214/10,000 in 2008. The number of individuals having either test rose from 533,940 in 1998 to 1,021,500 in 2008. ABI use has risen faster than SP use over this time period (by 146% and 51%, respectively). The number of ABI or SP tests performed in those tested was similar during the study period (mean 1.3 tests/year). In a Medicare population in which PAD prevalence is 15-20%, in 2008 only 2.1% of this high risk cohort had a PAD diagnostic test performed.

Conclusion
From 1998 through 2008, there was substantial growth in the use of PAD diagnostic testing in the US Medicare population. Despite this increase, these data do not demonstrate “overutilization” as ABI usage rates remain very low compared to the potential Medicare “PAD population at risk”.

340.
NF-κB-mediated degradation of the coactivator RIP140 regulates inflammatory responses and contributes to endotoxin tolerance.

Ping-Chih Ho, Yao-Chen Tsui, Xudong Feng, David R Greaves & Li-Na Wei
Department of Pharmacology, University of Minnesota Medical School, Minneapolis,Minnesota, USA.

Endotoxin tolerance (ET), triggered by prior exposure to TLR ligands provides a mechanism to dampen inflammatory cytokines. Receptor-interacting protein 140 (RIP140) interacts with NF-kB to regulate the expression of proinflammatory cytokine genes. Here, we identify LPS stimulation of Sky-mediated tyrosine phosphorylation on RIP140 and RelA interaction with RIP140. These events increase recruitment of SOCS1-Rbx1 E3 ligase to tyrosine-phosphorylated RIP140, thereby degrading RIP140 to inactivate inflammatory cytokine genes. Macrophages expressing a non-degradable RIP140 were resistant to the establishment of ET in a gene-specific manner. The results reveal RelA as an adaptor for SCF ubiqutin ligase to fine tune NF-kB target genes by targeting specific co-activator RIP140, and unexpected role for RIP140 protein degradation in resolving inflammation and ET.

Acknowledgements: this study is supported by NIH grants DK60521 and DK54733.

341.

Rational Structure-Based Design of PLN Mutants to Tune SERCA Function

Kim N. Ha1, Martin Gustavsson1, Raffaello Verardi1, Gianluigi Veglia1,2
University of Minnesota
Department of Biochemistry, Molecular Biology and Biophysics1 and Department of Chemistry2

Phospholamban (PLN) is the endogenous inhibitor of the sarco(endo)plasmic reticulum Ca2+ ATPase (SERCA), the enzyme that regulates cardiac muscle relaxation. In its phosphorylated state (pS16-PLN, pT17-PLN, and pS16pT17-PLN), PLN does not inhibit SERCA. Dysfunctions in SERCA:PLN interactions and in the PLN phosphorylation mechanism have been implicated in cardiac disease, and targeting PLN is becoming a promising avenue for treating cardomyopathies. Innovative gene therapy treatments using recombinant adeno-associated virus (rAAV) vectors to deliver S16E-PLN, a pseudo-phosphorylated form of PLN, have shown a remarkable efficacy in reducing the progression of cardiac failure in both small and large animals. We seek to further develop PLN species to tune SERCA function by rationally designing mutations based on the structural and biophysical data available on the system. Using a combination of NMR spectroscopy and biochemical assays, we have built a structure-dynamics-function correlation that shows PLN can be tuned to augment SERCA function by acting on the conformational coupling between the cytoplasmic and transmembrane domain and by altering the charge through pseudo-phosphorylation. Additionally, to better understand the role of mutation in PLN:SERCA interactions, we also investigated a mutant of PLN (R9C) known to be linked to hereditary dilated cardiomyopathy, showing that the mutation disrupts the pentamer-monomer equilibrium, and that these effects are exacerbated under oxidizing conditions. Insights to these issues will provide better paradigms with which to design therapeutic mutants of PLN for treatment of heart failure, and also demonstrate a model by which an enzyme can be controlled through tuning the allosteric regulation of an inhibitor.

Clinical Fellows

400.
Dexmedetomidine may unmask atrioventricular node disease

Kalpana Thammineni, M.D., M.P.H.
Division of Pediatric Cardiology
University of Minnesota,
East Bldg, 5th Floor,
2450 Riverside Avenue
Minneapolis, MN 55454

Arif Somani, M.D.
Division of Pediatric Critical Care Medicine
University of Minnesota,
East Bldg, 5th Floor,
2450 Riverside Avenue
Minneapolis, MN 55454

Parvin Dorostkar, M.D., M.S., M.B.A.
Division of Pediatric Cardiology
University of Minnesota,
East Bldg, 5th Floor,
2450 Riverside Avenue
Minneapolis, MN 55454

401.
Risk of Acute Kidney Injury is Not Higher in Patients Who Undergo Coronary Angiography and Cardiac Surgery in Close Succession

Byungsoo Ko, MD, Salima Mithani, MD, Santiago Garcia, MD, Venkat Tholakanahalli, MD, and Selcuk Adabag, MD, MS

Background Cardiac surgery and coronary angiography are both associated with higher risk of acute kidney injury (AKI). We hypothesized that the risk of postoperative AKI increases when coronary angiogram and cardiac surgery are performed in close succession, without sufficient time to allow kidney function to recover from the adverse effects of intravenous contrast.
Methods We included 2133 consecutive patients who underwent cardiac surgery at the Minneapolis Veterans Administration Medical Center from 2004 to 2010. The outcome variable was AKI as defined by the AKI network (increase in creatinine >0.3 mg/dl or >50% from baseline 48 hours after surgery or hemodialysis) and the Risk, Injury, Failure, Loss, End-stage (RIFLE) criteria. Estimated glomerular filtration rate (eGFR) was calculated by the Modification of Diet in Renal Disease (MDRD) method.

Multivariable logistic regression analysis was used. Number of days between coronary angiogram and cardiac surgery was analyzed as a continuous variable.
Results Patients were 66±10 years old. Mean preoperative creatinine and eGFR were 1.1±0.4 mg/dl and 75±22 ml/min/1.73 m2, respectively. Cardiac surgery was performed after a median 14 days (range 0-235) following coronary angiography. Of the 2133 patients, 680 (32%) met the AKI network definition, and 390 (18%) and 111 (5%) met the RIFLE risk and injury criteria of AKI, respectively. Age, body mass index, diabetes mellitus New York Heart Association class III/IV, cardiopulmonary bypass time, and impaired preoperative renal function (eGFR < 60 ml/min/1.73m2) were independent predictors of AKI. However, the time between coronary angiogram and cardiac surgery was not associated with AKI in univariable and multivariable analyses. Frequency of AKI was 35% in 433 patients who were operated within 3 days of coronary angiogram vs. 31% in 1700 patients who were operated after 3 days (p=0.17). Results were the same in subgroups of patients with impaired preoperative renal function and those who had contrast-induced nephropathy.
Conclusion Risk of AKI after cardiac surgery is not influenced by the time between coronary angiogram and cardiac surgery. There is no need to delay cardiac surgery for the sole purpose of renal recovery after coronary angiogram.

402.
Utility of Claims Based Data to Identify Critical Limb Ischemia Patients
Wobo Bekwelem, Lindsay G. Smith, Niki C. Oldenburg, Tamara J. Winden, Hong H. Keo, Alan T. Hirsch, Sue Duval

Background: It is challenging to identify patients with critical limb ischemia (CLI) for research and clinical purposes. Administrative data are increasingly being used to identify patients with specific diseases; the utility of this approach varies widely by disease state. No study has determined the validity of using ICD-9 billing codes from a claims database to identify patients with CLI.

Methods: CLI cases (n = 126), diagnosed by a vascular specialist during a hospital admission, were enrolled in a dedicated registry. Patients without CLI in their electronic problem list were frequency matched to cases on age, sex and admission date in a 2:1 ratio. Billing codes for all patients were extracted. Algorithms were developed on the basis of ICD-9 diagnosis and procedure codes using frequency distributions of codes in any position for the cases, and on the basis of clinical knowledge of the condition. The sensitivity, specificity, positive and negative predictive values were calculated for each algorithm.

Results: The sensitivity of the algorithms ranged from 0.29 to 0.92 (Table); the specificity was at least 0.99 for each algorithm. Algorithm 5, based on a combination of diagnosis and procedure codes exhibited the best overall performance with a sensitivity of 0.92, specificity of 0.99, positive predictive value of 0.98, and a negative predictive value of 0.96.

Conclusion: Billing codes can be used effectively and efficiently to identify CLI patients for population-based surveillance, epidemiological studies and recruitment for clinical trials. An algorithm based on a combination of diagnosis and procedure codes has the best utility in identifying these patients.

Algorithm*	Sensitivity	Specificity	PPV	NPV
1. Any one of (440.22, 440.23, 440.24, 443.9)	0.75	1.00	1.00	0.89
2. Algorithm 1 AND any one of (84.xx, 39.29, 39.5, 38.18)	0.59	1.00	1.00	0.83
3. Algorithm 1 AND any one of (250.xx)	0.33	1.00	1.00	0.75
4. Algorithm 1 AND Algorithm 2 AND Algorithm 3	0.29	1.00	1.00	0.74
5. Algorithm 1 OR Algorithm 2	0.92	0.99	0.98	0.96
6. Algorithm 3 OR any one of (84.xx, 39.29, 39.5, 38.18)	0.80	0.99	0.98	0.91

*Algorithms use ICD-9 CM diagnosis and procedure codes; PPV: positive predictive value; NPV: negative predictive value

403.

Incidence of Appropriate Shock in Implantable Cardioverter-Defibrillator Patients with Improved Ejection Fraction

Niyada Naksuk, MD, Ali Saab, DO, Jian-Ming Li, MD, PhD, FHRS, Viorel Florea, MD, PhD, Inder S. Anand, MD, DPhil, David G. Benditt, MD, FHRS, and Selcuk Adabag, MD, MS
Division of Cardiology, Veterans Administration Medical Center and Cardiac Arrhythmia and Syncope Center, Cardiovascular Division, Department of Medicine, University of Minnesota

Background: Ejection fraction (EF) is a key element in the decision for initiating implantable cardioverter-defibrillator (ICD) therapy. However, management of ICD patients whose EF has improved to >35% when ICD reaches elective device replacement indicator is unclear. Thus we sought to examine the incidence of appropriate ICD shocks in patients with vs. without EF improvement.
Methods: We included 121 consecutive patients who underwent ICD generator replacement at the Minneapolis Veterans Affairs Medical Center from 2006 to 2010. Patients with cardiac resynchronization therapy were excluded. EF was measured at initial implant and at generator replacement. Improved EF was defined as EF >35% and an increase in EF >10% from baseline (both conditions had to be met).
Results: Patients were 69±10 years old, 99% were male and 76% had ischemic cardiomyopathy. ICD indication was primary prevention in 75%. At generator replacement, 32 (26%) patients had improved EF (0.51±0.08 vs. 0.32±0.09 at baseline; $p<0.0001$). These patients were more likely to have non-ischemic cardiomyopathy than those with unchanged EF (37% vs. 19%; $p=0.037$). Over 6.2±2.3 years of follow-up after initial device implantation, 13 (41%) patients with improved EF vs. 27 (30%) patients with unchanged EF had appropriate ICD shocks ($p=0.29$). The incidence of appropriate ICD shocks was similar between the two groups before ($p=0.64$) and after ICD generator replacement ($p=0.92$). In 6 of the 13 patients with improved EF, ICD shock

occurred after EF improvement. Three of these patients had their first appropriate shock after EF improvement.
Conclusions: ICD patients whose EF improves to >35% remain at risk for appropriate ICD shocks.

404.

Resource Utilization in HeartMate II Left Ventricular Assist Device Patients with Gastrointestinal Bleeding

Niyada Naksuk, MD, Prangthip Chareonpong, MD, Eva Tone, MBA, Andrew Rosenbaum, Brian S Milavitzl, Ranjit John, MD, and Peter M Eckman, MD
Division of Cardiology and Division of Cardiothoracic Surgery, University of Minnesota

INTRODUCTION: Gastrointestinal (GI) bleeding is a common complication of continuous-flow left ventricular assist devices (LVADs), but there is little data on the resource needs of its evaluation and management. We examined resource utilization of LVAD patients who were admitted for GI bleeding.
HYPOTHESIS: Management of GI bleeding in LVAD patients is resource intensive and financial unfavorable.
METHODS: Twenty-four consecutive patients who were admitted for GI bleeding were identified from retrospective chart review of all HeartMate II (HMII) implants at our center. Transfusions, procedures, length of stay (LOS), and cost were evaluated to estimate resource utilization. LOS and cost are represented as median (25th; 75th % tile).
RESULTS: Mean age was 64±9 years, with 42% destination therapy. During their first admission for GI bleeding, 4.3±4.2 (range 0-18) units of red cells were transfused, 1.8±1.4 procedures were performed (range 0-6), and LOS was 7 (2;9) days. The estimated direct cost to the hospital for these admissions was $9,765 ($5,563;$16,693) with median loss of $4,635 per admission. Bleeding etiology was arteriovenous malformation (AVM) in 16 (67%); estimated direct cost in this cohort was $11,101 ($6,671;$17,544), in contrast to $4,919 ($3,601;$7,016) for the 8 who experienced non-AVM bleeding (p=0.13 for comparison). Net income was negative in AVM bleeding whereas positive in non-AVM bleeding (table). Higher cost in AVM bleeding was driven by higher transfusion and lodging costs, whereas other costs including procedures were comparable.

	All patients n=24	Patients with AVM bleeding n=16	Patients with non-AVM bleeding n=8	P value
Procedures	1.8±1.4	2.0±1.7	1.6±0.9	0.63
Red cell transfusion, units	4.3±4.2	5.5±4.3	1.6±2.4	0.03
LOS, days	7.0 (2.0;9.2)	8.0 (4.5;9.3)	3.5 (2.0;9.0)	0.53

Hospital cost, $ (3,601;7,016)	9,765 (5,563;16,693)	11,101 (6,671;17,544)	4,919 0.13
Net income, $ (n413;8,305)	n4,635 (n15,560;6,244)	n9,043 (n19,297;n561)	3,509 0.33

CONCLUSIONS: Admission of HMII patients for GI bleeding is resource intensive, particularly in AVM bleeding. This finding highlights the importance of strategies to minimize bleeding in improving the cost effectiveness of this therapy, and reinforces the need for improved understanding of the pathophysiology of AVM bleeding.

405.
Ultrafiltration Therapy for Heart Failure Patients with Preserved and Reduced Ejection Fraction Results in Similar Morbidity and Mortality

Niyada Naksuk, MD, Monica Colvin-Adams, MD, MS, Prangthip Charoenpong, MD, Michael Petty, PhD, RN, Marc Priztker, MD and Sofia Carolina Masri, MD.
Cardiology Division and Department of Medicine, University of Minnesota

Introduction: Ultrafiltration therapy (UF) has been used increasingly for acute decompensated heart failure (ADHF) patients who failed diuretic therapy. However little is known about the outcomes of UF in heart failure patients refractory to standard medical therapy with preserved ejection fraction (pEF).
Hypothesis: Patients with pEF who require UF therapy experience morbidity and mortality similar to heart failure patients with reduced EF (rEF).
Method: We retrospectively studied 57 consecutive ADHF patients who required UF at University of Minnesota Medical Center from 2006 to 2011. All patients had a trial of loop diuretics. Selection of UF as the treatment method was made by the attending cardiologist. Subjects were divided into two groups: pEF (EF>0.45) and rEF (EF<0.45).
Results: Of a total of 57 patients, mean age was 67±14 years. Seventeen (30%) had pEF. Mean EF was 0.57±0.06 in the pEF group versus 0.25±0.11 in the rEF group (p <0.0001). Patients with pEF were more likely to be female compared to patients with rEF (p=0.02). Otherwise, characteristics including age, weight, right ventricular function and baseline creatinine (p=0.60) were equal in the two groups. During UF therapy, fluid removal rate, total fluid removal, documented weight lost and delta hematocrit were also similar (p=ns for all). At time of discharge, creatinine (p=0.07) was not different between patients with pEF and rEF. Similarly, 90-day readmission (53% vs. 51%, respectively, p=0.90) and mortality (40% vs. 43%, respectively, p=0.87) were comparable.
Conclusions: ADHF patients who are not responsive to conventional medical therapy have a high 90-day readmission rate and mortality despite improvement in weight and fluid removal with UF. Interestingly, these outcomes are similar among heart failure patients with pEF and rEF. Further studies are required to clarify the role of UF in patients refractory to conventional treatment since it is unlikely to change the natural history of ADHF.

Baseline characteristics, ultrafiltration therapy and outcomes of study patients

	Patients with pEF n=17	Patients with rEF n=40	P value
Characteristics			
Age, years	70 ± 16	66 ± 13	0.37
Female,%	53	22	0.02
Left ventricular ejection fraction	0.57 ± 0.06	0.25 ± 0.11	<0.0001
Moderate-severe RV function,%	47	63	0.31
Baseline creatinine, mg/dL	2.2 ± 0.8	2.1 ± 0.9	0.43
UF therapy			
UF rate, ml/hr	153 ± 49	153 ± 61	0.83
Total fluid removal, L	10 ± 9	12 ± 9	0.40
Total weight lost, kg	8.3 ± 9.5	7.1 ± 5.0	0.62
Delta hematocrit, %	1.9 ± 3.6	2.7 ± 3.5	0.44
Outcomes			
Creatinine at discharge, mg/dL	2.9 ± 1.8	2.2 ± 0.9	0.15
90-day readmission, %	53	51	0.90
90-day death,%	40	43	0.87

Abbreviations: pEF=preserved ejection fraction; rEF=reduced ejection fraction

406.

Novel transcripts and pathways identified in blood one week following implant of continuous-flow left ventricular assist device (CF-LVAD)

Adam Mitchell, Rodney Staggs, Weihua Guan, Suzanne Grindle, Neeta Adhikari, Sameh Hozayen, Peter Eckman and Jennifer L. Hall

Bleeding, thrombosis and infection are common adverse events following placement of continuous-flow left ventricular assist devices (CF-LVADs). We performed RNA sequencing to identify novel genes and pathways that may be involved. RNA was extracted from blood samples taken from 9 heart failure patients (8 male) prior to and 7 days after implant of a CF-LVAD. Libraries were sequenced on an Illumina Hiseq2000 and sequences mapped to the human ensembl GRCh37.67 genome assembly using TopHat. Annotations were assigned using the ensembl gene transfer format (GTF) reference. Cufflinks, Cuffmerge and Cuffdiff were used to generate FPKM values. All called gene FPKM values and upper, lower confidence interval bounds were analyzed with a Paired T-test and q-values generated to estimate the false discovery rate. Ingenuity Pathway Analysis was used to investigate pathways. Four of the top ten differentially expressed genes are related to hematopoiesis, neuronal edema, and leukocyte trafficking (see Table). Of the major pathways represented two involved T cell signaling (see Table).

To our knowledge this is the first characterization of changes in the human transcriptome in blood one week after LVAD insertion. These findings may represent new pathways for exploration to define mechanisms underlying the adverse events in this patient population.

Gene	Fold change	p value	q value

CA1 (carbonic anhydrase – associated with neuronal edema) 7.062 0.0010036 0.035
AHSP (alpha hemoglobin stabilizing protein – key protein during erythropoiesis) 6.056 0.0015853 0.043
ABCG2 (stem cell marker for blood, may be a marker for injured cardiac muscle) 5.697 0.0006194 0.029
FAM20A (secreted protein expressed during hematopoietic differentiation) 4.608 0.000331 0.024
CXCL9 (ligand mediating leukocyte interaction) -4.023 0.000554 0.028

Pathway	Genes involved (%)	p value
CD28 Signaling in T Helper Cells	21/132 (15.9)	0.00000338
CTLA4 Signaling in Cytotoxic T Lymphocytes	18/98 (18.4)	0.00000539

407.

Survey of Treatment Choices in Acute Decompensated Heart Failure Suggests Vasodilators Underused Compared to Guideline Recommendations

Authors: Michelle D Carlson, MD1,† and Peter M Eckman, MD1. 1Medicine, Division of Cardiology, University of Minnesota Medical School, Minneapolis, MN, United States, 55455. †Presenting author; corresponding author (phone: 952-210-3997; e-mail: carl2452@umn.edu).
Category: Graduate student (Internal Medicine resident)
Introduction: Vasodilators are vital for ADHF management and prominent in professional society guidelines, but use is variable. We hypothesized that self-reported vasodilator use in ADHF is lower than guideline recommendations.

Methods: A web-based survey of treatment options and rationale in 6 clinical scenarios was distributed to 996 physicians; 227 responded.

Results: Respondents were mostly trainees (38%) or in practice less than 10 years (37%) and worked at academic centers (61%). Non-cardiologists preferred nitroglycerin (65%) and dobutamine (85%); cardiologists were comfortable with most vasoactive therapies. Compared to other cardiologists, self-identified heart failure (HF) physicians were more likely to use milrinone (84 vs 48%) and digoxin (64 vs 44%) and less likely to use dopamine (33 vs 70%) ($p<0.05$ for all). Patient characteristics were the most cited rationale for therapeutic choice (76%); guidelines less so (60%). HF physicians relied heavily on personal experience (72%), and many cardiologists cited EBM (78%). Most chose vasodilators for normo- and hypertensive patients and inotropes for hypotensive, underperfused patients. For normotensive patients who failed one vasodilator and hypotensive patients with adequate perfusion, most chose an inotrope, contrary to HFSA guidelines (table 1). Most thought guidelines and RCTs were inadequate to guide

therapy (table 2), yet rated these factors as influential. Those who rated guidelines as adequate were more likely to select the correct vasoactive medication than other participants only for scenario B ($p<0.05$).

Conclusions: Clinicians cite clinical guidelines and EBM as important factors in therapy choices, but often regard these resources as inadequate. Vasodilators are underused compared to guideline recommendations, regardless of specialty. The reasons for divergence from guidelines warrants further study.

Vasoactive Therapy Selection

Scenario

(A-F) A: Normotensive B: Normotensive, failed 1st tx C: Hypotensive, adequate perfusion D: Hypotensive, inadequate perfusion E: Hypotensive, inadequate perfusion, failed 1st tx F: Hypertensive

Correct* Answer (%)	Vasodilator	Vasodilator	Vasodilator	Inotrope	Inotrope	Vasodilator
Overall	70	32	22	89	81	96
Cardiologists	67	33	23	89	78	96
Non-cardiologists	68	21	16	72	49	84
HF physicians	62	34	25	87	72	94

*Per 2010 HFSA guidelines

Factors Guiding Vasoactive Therapy

	Guidelines Adequate (%)	RCTs Adequate (%)
Overall	43	26
Cardiologists	34	21
Non-cardiologists	59	38
HF physicians	22	9

408.

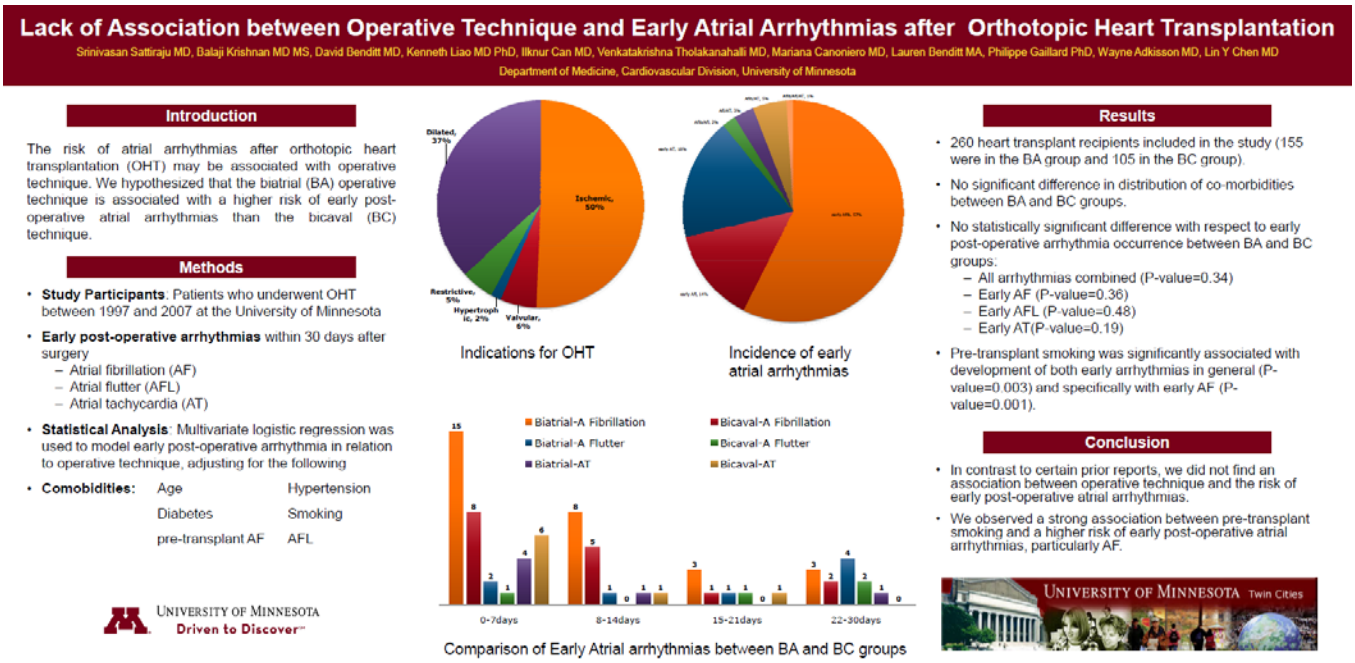

409.

Association of Common Variations on Chromosome 4q25 and Left Atrial Volume in Patients with Atrial Fibrillation

Hirad Yarmohammadi, MD, MPH, Hana Hoyt, MD, Irfan M. Khurram MD, Rozann Hansford, RN, MPH, Menekhem M. Zviman, PhD, Stefan L. Zimmerman, MD, Steven J. Steinberg, PhD, Daniel P. Judge, MD, Gordon F. Tomaselli, MD, Henry R. Halperin, MD, MA, Alan Cheng, MD, David D. Spragg, MD, Charles A. Henrikson, MD, Sunil Sinha, MD, Joseph E. Marine, MD, Ronald Berger, MD, PHD, Hugh Calkins, MD, Saman Nazarian, MD
Johns Hopkins University, Baltimore, Maryland, US

Background
The incidence of atrial fibrillation (AF) is strongly associated with two non-coding single nuclear polymorphisms (SNPs) on chromosome 4q25 (rs2200733 and rs10033464).(1) Both SNPs are adjacent to the paired-like homeodomain transcription factor 2 (PITX2) gene which has a major role in cardiac development.
PITX2 appears to be involved in left atrial and pulmonary vein inflow morphogenesis. Recent studies have demonstrated that reduced PITX2 expression is associated with progressive enlargement of the murine left atrium .(2)

The study included 100 patients referred for catheter ablation of drug-resistant AF.

4 patients were excluded because a three-dimensional image of the LA prior to their first ablation was unavailable.
After providing written informed consent, all patients had blood drawn for genotyping. Computed tomography angiograms (CTA) or magnetic resonance angiograms (MRA) obtained prior to the patient's first procedure were used for analysis.

Genotyping:
DNA was extracted from blood samples using Qiagen's Puregene DNA extraction kit.
Genotyping of SNPs rs10033464 and rs2200733 was performed with the MassARRAY system of the Sequenom genotyping platform as part of a single multiplex SNP analysis (Sequenom, San Diego, CA).
Ea
ch sample was tested at least three times and at least two concordant results were required.
Image acquisition :
Image analysis was performed by Investigators were blinded to genotyping results.
All individuals had either cardiac CTA or MRA to delineate end diastolic left atrial dimensions.
All scans were ECG-gated and were acquired at atrial end-diastole, just before opening of the mitral valve.
Of all scans, 24 (25%) were obtained during atrial fibrillation and the remaining scans were acquired during sinus rhythm.
Measurement of Left Atrial Volume:
The anterior- posterior (AP)
and longitudinal (LO)
diameters were
measured at the midpoint
of the transverse (T)
diameter in oblique axial and sagittal images. These dimensions were then entered into the prolate ellipsoid formula:
Left atrial volume = (T × AP × LO) × (0.523)

Conclusion
Polymorphism at rs10033464 but not rs2200733, near the PITX2 locus on chromosome 4q25 is significantly associated with increased left atrial volume. Left atrial dilatation may mediate the association of common variants at 4q25 with AF.

410.

Long-term Prognosis of Patients with Ventricular Arrhythmias After Cardiac Surgery

Farzad Azimpour, MD, Henri Roukoz, MD, Selcuk Adabag MD, MS

Division of Cardiology, Veterans Administration Medical Center, Minneapolis, MN and the Division of Cardiology, University of Minnesota, Minneapolis, MN

Background

- More than 285,000 cardiac surgical operations performed in the US in 2010
- Postoperative period following cardiac surgery known to predispose patients to ventricular tachyarrhythmias
- Long-term prognosis of patients with non-sustained ventricular tachycardia (NSVT) after cardiac surgery in the contemporary era of implantable cardioverter-defibrillators, wearable defibrillators, and state-of-the-art medical therapy is unclear
- **Objective:** To determine the long-term prognosis of patients with NSVT or cardiac arrest from ventricular tachycardia/fibrillation (VT/VF) after cardiac surgery

Methods

- 2271 patients underwent cardiac surgery at the Minneapolis VA Medical Center from 2004 to 2011
- Postoperative in-hospital cardiac arrests with VT/VF were identified from cardiac surgery database
- Patients with NSVT were identified by revision of all cardiology and cardiac electrophysiology consultations that originated from cardiac surgery service
- **Primary Outcome**: Operative (30-day) and long-term mortality, assessed by the VA vital status files and captured in the cardiac surgery database
- Kaplan-Meier survival curves were generated to compare survival of patients with and without ventricular tachyarrhythmias

Results

Table 1: Baseline characteristics of post-cardiac surgery patients with and without ventricular arrhythmias

Variable	Ventricular Arrhythmia (n=66)	No Ventricular Arrhythmia (n=2205)	P value
Age (years)	68 ± 9	66 ± 10	0.17
Male Gender	64 (97%)	2189 (99%)	0.09
Diabetes Mellitus	24 (36%)	766 (35%)	0.79
Hypertension	51 (77%)	1868 (85%)	0.10
COPD	20 (30%)	615 (28%)	0.67
CVD	15 (23%)	532 (24%)	0.79
Current Smoker	13 (20%)	446 (20%)	0.95
Prior MI	37 (56%)	896 (41%)	0.04
Prior Cardiac Surgery	7 (11%)	151 (7%)	0.24
LV Ejection Fraction <55%	41 (62%)	897 (41%)	<0.0001
NYHA III/IV	49 (74%)	1332 (60%)	0.02
CABG only	38 (58%)	1497 (68%)	0.05
Ischemic time (minutes)	105 ± 42	96 ± 40	0.09
CPB time (minutes)	148 ± 45	137 ± 48	0.07

Table 2: Characteristics of the study patients with NSVT vs. VT/VF

Variable	VT/VF (n=31)	NSVT (n=22)	P value
Age (years)	67 ± 11	67 ± 8	0.83
Male Gender	31 (100%)	21 (96%)	0.42
Diabetes Mellitus	14 (45%)	7 (32%)	0.33
Hypertension	24 (77%)	16 (73%)	0.69
COPD	14 (45%)	3 (14%)	0.02
CVD	6 (19%)	5 (23%)	0.77
Current Smoker	8 (26%)	3 (14%)	0.33
Prior MI	19 (61%)	11 (50%)	0.06
Prior Cardiac Surgery	1 (3%)	2 (9%)	0.56
LV Ejection Fraction <55%	20 (65%)	15 (68%)	0.78
NYHA III/IV	26 (84%)	14 (64%)	0.09
CABG only	22 (71%)	8 (36%)	0.02
Ischemic time (minutes)	96 ± 34	122 ± 53	0.03
CPB time (minutes)	140 ± 38	164 ± 56	0.06

Table 3. Mortality after cardiac surgery by ventricular arrhythmia type

Variables	VT/VF n=31	NSVT n=5	No arrhythmia n=298	P value (NSVT vs No arrhythmia)	P value (VT/VF vs No arrhythmia)
Operative Mortality	14 (45%)	1 (4%)	35 (2%)	0.46	<0.0001
Long-term Mortality	17 (55%)	4 (14%)	263 (12%)	0.5	<0.0001

Figure 1. Kaplan-Meier survival curve comparing patients with NSVT, VT/VF, and no arrhythmia

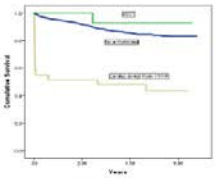

Conclusions

- Ventricular tachyarrhythmias (NSVT and VT/VF) are uncommon after cardiac surgery
- Postoperative cardiac arrest due to VT/VF portends high mortality
- However, NSVT after cardiac surgery is not associated with long-term mortality except in patients with left ventricular dysfunction, EF <55%
- These patients may be considered for risk stratification with EP study, and potentially evaluated for wearable defibrillator or ICD implantation for prevention of sudden cardiac death

411.

Comorbidities and Physical and Cognitive Impairments in Elderly Heart Failure Patients: Impact on Total Mortality: The Cardiovascular Health Study (CHS)

Khalil Murad; Timothy M Morgan; Gregory L Burke; David C Goff, Jr.; Dalane W Kitzman
Division of Public Health Sciences, Department of Epidemiology and Prevention
Department of Internal Medicine, Section of Cardiology

Background
Comorbidities and physical and cognitive impairments are common in patients with heart failure (HF) and often associated with greater mortality risk. However, the prevalence of these conditions and their associated mortality risk in elderly patients with incident HF is unknown.
Method
We examined the prevalence of 9 comorbidities and 4 measures of physical and cognitive impairments among the Cardiovascular Health Study (CHS) participants with incident HF at the time of their HF diagnosis. Participants were followed prospectively to determine the associated mortality risk.
Results
We included 558 CHS participants with incident HF (table 1).

The burden of comorbidities and physical and cognitive impairments was high; 60% of participants had ≥ 3 comorbidities, and only 2.5% had none. 22.5% and 43.7% of participants had ≥ 1 activity of daily living (ADL) and ≥ 1 instrumental activity of daily living (IADL) impaired respectively. 17% of participants had modified mini-mental state exam (3MSE) score < 80.
During follow up, which lasted until June 2008, 504 participants, (90.3%) died. Estimated 1-year and 5-year mortality rates were 19% and 56% respectively.
Diabetes mellitus, chronic kidney disease, cerebrovascular disease, depression, cognitive impairment, and certain measures of physical impairments were associated with greater mortality risk while higher body mass index was associated with lower mortality risk (table 2).
Other comorbidities including hypertension, coronary heart disease, atrial fibrillation, peripheral vascular disease, and obstructive airway disease did were not associated with mortality in elderly patients with incident HF (table 2).
Conclusion
Elderly patients with incident HF have a high burden of comorbidities and physical and cognitive impairments, and some of these conditions are associated with greater mortality risk.

412.
3-D TTE Calculation of Stroke Volume: a Comparison to 2-D and Thermal Calculations

Matthew Chu M.D. and Richard Madlon-Kay M.D.
University of Minnesota Cardiovascular Disease Fellowship, University of Minnesota Physicians Heart, and the University of Minnesota Medical Center, Fairview

University of Minnesota Cardiovascular Disease Fellowship, University of Minnesota Physicians Heart, and the University of Minnesota Medical Center, Fairview
Limitations to stroke volume calculation by two-dimensional echocardiography have been known for some time. In particular, the left ventricular outflow tract shape is assumed to be circular, yet advanced imaging modalities such as three-dimensional echocardiography, CT, and cardiac MRI have shown the true shape to often be elliptical1-3. The current recommended calculation for stroke volume by the American Society of Echocardiography involves multiplying the cross-sectional area of the left ventricular outflow tract by the velocity time integral at that point 4. The area is determined by the square of the radius of the left ventricular outflow tract, thus magnifying small inconsistencies in the measured dimension of this structure that may exist with a non-circular outflow tract. Furthermore, if the angle of the ultrasound probe is not parallel to the predominant flow vector of blood through the left ventricular outflow tract the VTI may be inaccurate and impair stroke volume calculation. With the recent rise of three-dimensional echocardiography, efforts have been made to employ this technology for more accurate stroke volume assessments.

The primary application of 3-D technology has been in a more accurate three dimensional assessment of volumes that in turn allows for more accurate assessment of

both ejection fraction and stroke volume. This approach has been validated using MRI volumetric assessment as a standard over a wide range of ejection fractions 5-7. 3D echo is an anatomic method for determining stroke volume that has its share of challenges including difficulty with visualization of the endocardial border, respiratory gating for multiple sets of image acquisition, large sets of data required for complete and accurate reconstruction, and time and resource intensive computations for accurate stroke volume assessment8.

A simpler approach combining the essence of the clinically recommended 2D stroke volume assessment with the technological advancement of 3D echocardiography is to perform planimetry of the left ventricular outflow tract area with multiplication by the velocity time index. Only one group to date has published results using this technique in a feasibility study of thirty relatively healthy patients with normal ejection fraction 9. The group compared stroke volume as assessed by the standard 2D VTI method, stroke volume as calculated by 2D biplane Simpson's method, 3D volumetric assessment of stroke volume, and the novel method of multiplying the VTI times the area of the LVOT determined by planimetry. The conclusion of the study was that stroke volume calculated by both 3D volumetric assessment and stroke volume by direct planimetry of the LVOT multiplied by the VTI correlated well with each other and that the planimetry method may be more feasible in routine clinical practice.

413.

QRS Shortening after Cardiac Resynchronization Therapy is Associated with Increased Left Ventricular Ejection Fraction in Patients with Non-Ischemic Cardiomyopathy

William H. Sauer, MD, R. Todd Drexel, MD, Diego F. Belardi, MD, Royce L. Bargas, DO, Christopher S. Stees, DO,
Joseph L. Schuller, MD, Christopher M. Lowery, MD and Michelle SC. Khoo, MBChB.
University of Colorado Denver (2009)

Background
Cardiac resynchronization therapy (CRT) reduces interventricular activation time and improves congestive heart failure (CHF) symptoms.

However, the relationship between reduction in QRS duration and improvement in left ventricular ejection fraction (LVEF) has not been well characterized.

We sought to evaluate the relationship between shortening of QRS duration following CRT and subsequent LVEF.

Methods
A cohort of 127 consecutive patients with QRS duration > 120 msec, LVEF < 35%, and HF undergoing CRT was analyzed to assess the potential relationship between QRS duration reduction and LVEF.

Pre and post implant QRS duration was recorded using standard 12-lead ECG (Figure).

Pre and post implant LVEF was measured by echocardiography.
Conclusions
Compared to the pre-implant QRS complex, a narrower biventricular paced QRS complex with CRT is associated with significant improvement in LVEF in patients with non-ischemic cardiomyopathy.
In addition, there is a direct correlation between LVEF improvement and the amount of QRS shortening. This phenomenon was not seen in patients with prior MI.

414.

Lung to Finger Circulation Time is Prolonged in Patients with Obstructive Sleep Apnea and Underlying Heart Failure

Younghoon Kwon, MD 1 2 3 ; Talha Khan, MD 1 2 ; Conrad Iber, MD 1 2
1 Minnesota Regional Sleep Disorder Center, Hennepin County Medical Center 2 Division of Pulmonary Critical Care &Sleep, University of Minnesota 3 Division of Cardiology, University of Minnesota, Minneapolis, MN

Introduction
Lung to finger circulation time (LFCT) can be estimated from polysomnography (PSG) in the presence of an apneic event by using oxygen as an indicator and finger as a site of detection. The purpose of this study was to determine factors associated with prolonged LFCT in patients with obstructive sleep apnea (OSA).

Research questions:
1. What is the mean and distribution of LFCT in patients with OSA in our cohort?
2. What factors are associated with LFCT?
3. Is LFCT more prolonged in patients with OSA with coexisting CHF?

Gender and age were significantly associated with LFCT in patients with OSA
Underlying Cheyne Stokes respiration and age were significantly associated with prolonged LFCT in patients with OSA and CHF
In entire cohort, CHF, Beta blocker, gender, age were associated with LFCT
Overall, CHF was the most significant predictor of prolonged LFCT
interaction was present between heart failure and beta-blocker use.

Conclusion
LFCT is prolonged in patient with OSA and underlying CHF
LFCT based on PSG may be a useful marker for detection of coexisting CHF in patients with OSA

415.

Baroreceptors gone awry: Exaggerated Impact of Cough on Cardiovascular Dynamics

Oana Dickinson, MD, Prabhjot S. Nijjar, MD, David G. Benditt, MD
Cardiovascular Division, Department of Medicine, University of Minnesota, Minneapolis MN

Introduction:
Cough induced hypotension and syncope is a well known phenomenon, but the pathophysiological mechanism remains incompletely understood. This report presents an interesting case of cough induced syncope, with a marked vasodepressant effect demonstrated on autonomic tilt-table testing.

Case:
A 44 year old obese male presented with a 3 week history of syncopal events preceded by bouts of prolonged coughing. There were no other prodromal symptoms, and he regained consciousness quickly without any confusion or focal neurological signs. 24 hour Holter monitor revealed 5 periods of asystole during sleep for which he underwent cardiac pacemaker placement, but his syncopal episodes persisted. Autonomic evaluation with a tilt-table study was undertaken, the results of which are described below.

Autonomic Maneuvers	Base Line BP(mmHg)	BPat 1minute(mmHg)	BP at 2-5minutes(mmHg)
Sitting	140/80	140/80	135/75
Rapid Standing	135/75	109/67	133/82
Brief Cough	131/85	200/95	117/70
Sustained Cough	139/85	210/100	100/68
Valsalva Maneuver	F1:130/98	F2:100/71	F3:156/90 F4:125/80
Carotid Sinus Massage	R:136/85 L:136/87	R:120/79 L:117/75	R:130/82 L:123/82
Nitroglycerine (NTG)	135/85	129/85	118/75
NTG and Brief Cough	118/80	188/72	87/66
NTG and Sustained Cough	118/75	200/97	85/60

Autonomic Maneuvers	Base Line HR(bpm)	HR at 1minute(bpm)	HR at 2-5minutes(bpm)
Sitting	82	79	79
Rapid Standing	79	86	85
Brief Cough	87	100	79
Sustained Cough	95	125	100
Valsalva Maneuver	F1:90	F2:105 F3:60	F4:80
Carotid Sinus Massage	R:83 L:85	R:88 L:92	R:72 L:85
Nitroglycerine	94	83	89
NTG and Brief Cough	108	114	120
NTG and Sustained Cough	89	100	118

With patient at 700 on head-up tilt table, 1-2 brief coughs caused a fall in systolic BP by 40mmHg followed by pre-syncopal symptoms. No brady-arrhythmias were recorded. To summarize, the autonomic evaluation revealed an aggressive BR response to abrupt increase in BP caused by cough.

Discussion:
Cough-induced syncope is considered a form of neurally mediated reflex syncope in which systemic baroreceptor (BR) responses play a key role.
On immediate standing and Valsalva maneuver, an initial decrease in BP leads to a normal systemic baroreceptor response. An initial, abrupt increase in BP caused by cough causes the systemic BR to respond normally but aggressively, with marked vasodilatation and hypotension. The patient was advised to increase salt and fluid intake, and abstain from smoking and alcohol. The periods of asystole during sleep were likely due to underlying sleep apnea.

416.
High Renal Morbidity with Slow Continuous Ultrafiltration in Advanced Decompensated Heart Failure Despite Hemodynamic Improvement

Background: Several studies have demonstrated the clinical utility of early slow continuous ultrafiltration (SCUF) in patients with acute decompensated heart failure (ADHF) to improve fluid overload, hemodynamics, and readmissions. However, there is limited data supporting the use of SCUF in advanced patients with ADHF refractory to standard medical therapy.

Methods: We reviewed clinical data of all adult patients admitted from 2004 to 2009 to the Heart Failure Intensive Care Unit with ADHF for hemodynamically-guided therapy and SCUF

Results: From our cohort of 61 patients with average age of 59±11 years, 77% were male; 65% had ischemic cardiomyopathy, 21% baseline □Stage Ⅲchroni disease, and mean LV ejection fraction of 25 at the time of admis□5%. Mean admis 1.9 □0.8mg/dL, a admission. After 48 hours of SCUF, there were significant improvement in hemodynamic variables (mean arterial pressure 75±10 vs 71±10mmHg, p=0.01, mean pulmonary arterial pressure 40±12vs33±8mmHg, p=0.002, central venous pressure 20±6 vs 16±8 mmHg, p=0.007, mean pulmonary wedge pressure 27±8 vs 19±7 mmHg, p=0.02, Fick Cardiac index 2.2±0.5 vs 2.6±0.5 L/min/m², p=0.0005) and weight loss (104±23 vs 99±23kg, p=0.0001).However, there were not significant improvement in serum creatinine (2.2±0.9 vs 2.4±1, p=0.12) and BUN (60±30vs 60±28, p=0.97). Fifty-six patients (92%) were switched to continuous hemodialysis, and 7 were dialysis dependent at hospital discharge. Hospital mortality was 31% (19/61), and 6 patients were discharged to hospice.

Conclusion: In our single center experience, the use of SCUF in patients with advanced ADHF refractory to standard medical therapy was associated with high incidence of renal failure requiring temporary renal replacement therapy, and in-hospital mortality despite significant improvement in hemodynamics.

417.

Low Systolic Blood Pressure At Admission Identifies Patients with Decompensated Heart Failure Who are Undergoing Slow Continuous Ultrafiltration At High Risk of Short Term Mortality

Patarroyo M, Wehbe E, Hanna M, Demirjian S, Tang W.H.

Introduction
Slow continuous ultrafiltration (SCUF) has emerged as a new therapeutic modality to improve volume overload and potentially reduce re-hospitalizations in decompensated heart failure patients (ADHF).

We recently reported our experience with high morbidity and mortality rates associated with SCUF in patients with ADHF. We sought to examine factors that predict mortality in this patients.

Methods
Study design
Retrospective cohort study of 61 consecutive patients admitted to the heart failure intensive care unit from January 2004 to June 2009.

Inclusion criteria
-Adult patients (older than 18 years old) that required admission to the intensive care unit for decompensated heart failure

-Requirement of SCUF for at least 24 hours for fluid overload not responsive to medical therapy with maximal dose of diuretics.

Exclusion criteria
- GFR ≤15 ml/min/1.73 m²
- History of cardiac or renal transplant
- Patients on dialysis at the time of admission.

Ultrafiltration protocol:
Ultrafiltration was performed using 2 systems: Gambro's Prisma systems with their M60 and M100 sets, and the NxStage System 1 using the Express dialyser set. Vascular access was gained with central catheter in the femoral or jugular vein. Blood flow rate ranged from 100-180 ml/min and ultrafiltration rate from 100 to 400 ml/h.

Conclusion
Low systolic blood pressure at admission identifies patients with decompensated heart failure that undergo SCUF at high risk of short-term mortality. These findings highlight the importance of contractile reserve to maintain adequate perfusion in the setting of mechanical salt and water removal.

418.
Discordance between Aortic Augmentation Index and Hemodynamic Measurements in Patients with Acute Decompensated Heart Failure Receiving Intensive Medical Therapy
Maria Patarroyo, MD, Yi Lu, RN, Mohammad Rafey, MD, W. H. Wilson Tang, MD.

Introduction
AIx is the ratio of augmentation pressure (difference between the second and first systolic peak caused by early wave reflection) to central pulse pressure. A higher AIx implies increased arterial stiffness and has been reported to be strongly associated with an increased risk of CVD.(Liew Y et al. J Clin Hypertens 2009;11(4):201-206.
Arterial stiffness may contribute to progressive systolic and diastolic dysfunction. There is not a well describe relationship between central hemodynamics measure by invasive monitoring and aortic index specially in decompensated heart failure patients and in response to intensive medical therapy.

Methods
Study design
Prospective cohort study of consecutive adult patients admitted to Heart Failure Intensive Care Unit (ICU), with clinical, laboratory and hemodynamic data were documented at admission and 24 hrs after treatment initiation.
Study population:
-Admitted to the ICU for acute decompensated Heart Failure (ADHF)
-Required hemodinamically-guided intensive medical therapy
Exclusion criteria:
- Patients unable to provide written consent or that refused to participate in the study
- History of obstructive, restrictive or hypertrophic cardiomyopathy, cirrhosis
- Heart transplant patient or left ventricular assisted device (LVAD) surgery
- Severe aortic valve disease.

Blood pressure studies

-Brachial blood pressure: measured using and electronic manometer in the supine position, the mean blood pressure was calculated automatically

- Aortic index calculation was done with a SphygmoCor® device following the manufacture's recommendations using the waveform obtained from radial artery . The Aix was defined as the ratio between the local PP and the augmentation pressure of the reflected wave, and was expressed as a percentage (calculated directly by Pulse wave analysis software).

Statistical analysis:
- Continuous variables are expressed as mean ± standard deviation if normally distributed and median and inter-quartile range for those non-normally distributed. Categorical variables are expressed as proportion and frequencies. All p-values reported were from two-sided tests and a p-value <0.05 is considered statistically significant. All statistical analyses were performed by using JMP 8.0 (SAS Institute, Cary, NC). The authors had full access to the data and take responsibility for its integrity.

Conclusion
In our cohort of patients with acute decompensated heart failure, changes in AIx response does not change in concordance with hemodynamic response to intensive medical therapy. Our data suggested that determinants and modulation of AIx may be independent of strategies to restore optimal hemodynamic balance in the failing heart.

419.
Multiple Systemic Emboli Originating from the Aorta and Left Atrium in a Patient with Reduced Left Ventricular Ejection Fraction

Ann Coumbe MD, Emil Missov MD, PhD
Cardiovascular Division, University of Minnesota, Minneapolis, Minnesota

65-year-old female admitted with acute altered mental status and left lower extremity pain
Past medical history includes hypothyroidism and psoriasis
Admission one week prior for angioedema that improved with steroids
Six months of diarrhea and unintentional weight loss
Former significant other with hepatitis C

CT head obtained and negative for acute changes
Lower extremity ultrasound demonstrated left iliac and popliteal artery occlusions
Underwent emergent thrombectomy
Microscopic evaluation confirmed thrombus

Postoperative course complicated by hypotension requiring norepinephrine, respiratory failure and anuric renal failure requiring dialysis
Empiric antibiotics for possible sepsis
Stress-dose steroids for possible underlying vasculitis

Laboratory evaluation with anemia, thrombocytopenia and elevated inflammatory markers
Cardiac troponin elevated with peak level 1.84 mcg/L (normal < 0.03 mcg/L)
Electrocardiogram with normal sinus rhythm and no acute changes

Due to hypotension, elevated cardiac troponin an arterial occlusions a transthoracic echocardiogram (TTE) was performed

TTE demonstrated a left atrial mass measuring 3.2 cm by 2.1 cm (Image 1), ejection fraction of 35% with anterior, septal and apical wall akinesis

Transesophageal echocardiogram (TEE) obtained and demonstrated two echodensities in the left atrium measuring 0.8 cm by 0.7 cm and 2.7 cm by 1.6 cm (Image 2) and a third echodensity 1.5 cm above the non-coronary cusp of the aortic valve measuring 1.7 cm by 1 cm (Images 3 and 4)

Given that pathology from arterial thrombectomy demonstrated thrombus, thought that left atrial and aortic root masses were also thrombi

MRI/MRA of her brain and neck revealed multiple punctate infarctions throughout both cerebral hemispheres

Patient had gradual symptomatic improvement and able to participate in treatment decisions

Cardiothoracic surgery consulted and thought that surgical removal of the the atrial and aortic thrombi possible but high risk

Patient developed acute dysarthria, expressive aphagia, right hemiplegia and right-sided clonus
Patient made comfort cares and discharged to hospice

Evaluation for autoimmune disease and hypercoagulable state returned negative

420.

Long-term Follow-up of Elderly Patients with Mobitz Type I, Second Degree Atrioventricular Block

Ann Coumbe, MD, Niyada Naksuk, MD, Marc Newell, MD, Porur Somasundaram, MD, Jian-Ming Li, MD, PhD, David Benditt, MD, Selcuk Adabag, MD, MS
Division of Cardiology, Veterans Administration Medical Center, Minneapolis, MN and the Cardiovascular Division, University of Minnesota, Minneapolis, MN

Background

Mobitz I, second degree atrioventricular (AV) block is a benign finding in young healthy individuals
Little is known about the long-term outcome of older patients with Mobitz I AV block
In the 2008 AHA/ACC/HRS guidelines, implanting a permanent pacemaker (PPM) in asymptomatic patients with Mobitz I AV block is not indicated
However, Devon heart survey, conducted 30 years ago, suggested that patients with Mobitz I AV block who were older than 45 years lived longer if they had a PPM vs those without a PPM (five-year survival 78% vs. 42; $p < 0.01$)

Objective: To asses the outcome of older patients with Mobitz I AV block on ECG

Two hypotheses:
Elderly patients with Mobitz I AV block have shorter survival than a matched control group of patients with no AV block on ECG
Elderly patients with Mobitz I AV block who have a cardiac implantable electronic device (CIED) have longer survival than those who do not

Methods
299 Consecutive patients with Mobitz I AV block were identified from the electrocardiogram (ECG) laboratory of the Minneapolis Veterans Administration (VA) Medical Center from 1992 to 2010
Exclusion criteria: 1) age < 45 years, 2) digitalis, beta blocker or calcium channel blocker overdose, 3) ECG performed in the intensive care unit, 4) ECG performed while inpatient after cardiac surgery, 5) ECG demonstrating acute myocardial infarction 6) atrial rate >120 bpm, 7) 2:1 AV block
Control group of patients with no AV block on ECG matched to Mobitz I cases (1:1 ratio) by age, ECG and ECG location
Clinical information was abstracted from electronic medical records and the cardiac implantable device database at the Minneapolis VA Medical Center
Survival was assessed by the social security death index and the VA Beneficiary Identification Records Locator Subsystem
In patients who died, cause of death ascertained from death certificates

Primary outcome: All-cause mortality

Propensity scores were generated to adjust for the baseline differences of the CIED and non-CIED groups
Kaplan-Meier survival curves and Log-Rank test Cox proportional hazards model were used to compare survival of patients with and without CIED and controls.
Cox proportional hazards model used to examine survival of patients with and without CIED

Conclusions
In this retrospective cohort study of 299 older patients with Mobitz I AV block

Older pts with Mobitz I and CIED had a higher incidence of CHD and HF than those without CIED
Despite greater CV co-morbidity, patients with CIED had almost 50% reduction in adjusted mortality compared to those without CIED
The survival benefit persisted after adjusting for baseline differences and propensity score for having a CIED and after excluding patients with ICD
Trend for increased survival with CIED in a subgroup of relatively healthy Mobitz I pts without CHD, HF or LV dysfunction
Mortality rate of older pts Mobitz I significantly greater than matched controls with no AV block on ECG
Mobitz I is not a benign finding in the elderly and the outcome of these pts might be improved by a PPM`

421.
Lack of Association between Operative Technique and Early Atrial Arrhythmias after Orthotopic Heart Transplantation

Srinivasan Sattiraju MD, David Benditt MD, Kenneth Liao MD PhD, Ilknur Can MD, Balaji Krishnan MD MS, Venkatakrishna Tholakanahalli MD, Mariana Canoniero MD, Lauren Benditt MA, Philippe Gaillard PhD, Wayne Adkisson MD, Lin Y Chen MD
Department of Medicine, Cardiovascular Division, University of Minnesota

Introduction
The risk of atrial arrhythmias after orthotopic heart transplantation (OHT) may be associated with operative technique. We hypothesized that the biatrial (BA) operative technique is associated with a higher risk of early post-operative atrial arrhythmias than the bicaval (BC) technique.

Methods
Study Participants: Patients who underwent OHT between 1997 and 2007 at the University of Minnesota
Early post-operative arrhythmias within 30 days after surgery
Atrial fibrillation (AF)
Atrial flutter (AFL)
Atrial tachycardia (AT)
Statistical Analysis: Multivariate logistic regression was used to model early post-operative arrhythmia in relation to operative technique, adjusting for the following
Comobidities: Age Hypertension
Diabetes Smoking
pre-transplant AF AFL

Conclusion
In contrast to certain prior reports, we did not find an association between operative technique and the risk of early post-operative atrial arrhythmias.

We observed a strong association between pre-transplant smoking and a higher risk of early post-operative atrial arrhythmias, particularly AF.

422.
Hospital Readmissions Are A Common Occurrence in the Current Era with Continuous Flow (CF) LVADs

Forum Kamdar, MD1, Jason Rasmussen, MD1, Peter Eckman, MD1, Kenneth Liao, MD1, Brian Milavitz2, Monica Colvin-Adams, MD1 and Ranjit John, MD1.

1University of Minnesota, Minneapolis, MN, United States and 2Fairview Health, Minneapolis, MN, United States.

CF LVADs are an accepted option for patients with end-stage heart failure. However, morbidity and the resulting hospital admission may limit the application of CF LVADs to less sick patients. The objective was to study hospital readmissions and associated costs in patients with the HeartMate II LVAD.

We reviewed all patients who received HM II at a single center from 10/05-1/11, excluding patients who died prior to discharge. Total cost of readmissions was obtained from a retrospective review of claims data.

Of 129 discharged patients, 108 were BTT. 45 (35%) patients had no readmissions and 84 (65%) had at least 1 readmission. There were a total of 312 readmissions in this patient group. The median readmission per patient was 1 (range:1-29) and the mean number of readmission per patient was 2.6 3.8. The mean time to readmission after LVAD implant was 139± 16 days. The mean length of stay for readmission was 7 ± 9 days. The main reasons for readmission included heart failure exacerbation (38, 12.2%), gastrointestinal bleeding (29, 9.3%), driveline infections (26, 8.3%), and elective procedures (22, 7.1%). Freedom from first readmission was 61% and 39% at 3 and 6 months. There was no significant difference between patients who were readmitted and those who were not in regards to age, gender, etiology, or duration of support (p = NS). The mean total cost per first readmission was $25,713 (interquartile range $5,935 - 23,793).

Readmission following LVAD implantation is a common and costly event. Further research focused at decreasing GI bleeding and driveline infections as well as identifying risk factors for readmission will improve the quality of life and costs associated with CF VADs.

423.
COPD as a Predictor of Adverse Outcomes in Heart Failure with Preserved Ejection Fraction: Data from IPRESERVE Trial.
Ashenafi Tamene, MD; Sithu Win, MD, MPH; Inder S. Anand, MD, FRCP, D Phil (Oxon.)

Introduction:
Heart failure and chronic obstructive pulmonary disease (COPD) are major contributors of morbidity and mortality in the developed world. Patients with heart failure, particularly those with preserved ejection fraction (HFPEF) are known to have multiple non-cardiac comorbidities the presence of which has been associated with adverse outcomes. COPD is considered to be such comorbidity; however, there is limited data specifically addressing the prognostic value COPD in HFPEF.

Methods:
Using the IPRESERVE trial database of 4128 patients, various clinical, laboratory, ECG and echocardiographic variables were compared between COPD vs. non-COPD groups. A multivariate Cox proportional hazard model was used to test the prognostic value of COPD.

Results:
Patients with COPD were more likely to be male and smoker. They also have important comorbidities such as diabetes, chronic kidney disease, atrial fibrillation and coronary artery disease. There were no clinically significant differences in the echocardiographic parameters studied. Occurrence of left ventricular hypertrophy based on ECG criteria was less common in patients with COPD. After adjustment, COPD was found to be a significant predictor of the primary composite end point of death from any cause or hospitalization (HR 1.25; 95% CI: 1.05-1.49; P=0.012) but not a predictor of all-cause mortality (HR: 1.15; 95% CI: 0.92-1.44; P=0.214). The treatment effect (of Irbesartan) was found to be significant in the COPD group for the primary composite end point (HR: 0.69; 95% CI: 0.50-0.97; P=0.03).

Conclusion:
COPD was found to be an independent predictor of risk of death from any cause or hospitalization but not a predictor of all-cause mortality. Most of the risk associated with the primary outcome seems to be attributed to increased risk of hospitalization for worsening heart failure. A potential beneficial role of angiotensin-II receptor blockers has been described in pulmonary disease which might explain the treatment effect of Irbesartan. However, caution should be taken in interpreting the results of post-hoc analysis.

424.
COPD as a Predictor of Adverse Outcomes in Heart Failure with Preserved Ejection Fraction: Data from IPRESERVE Trial.

Ashenafi Tamene, MD; Sithu Win, MD, MPH; Inder S. Anand, MD, FRCP, D Phil (Oxon.)

Introduction:

Heart failure and chronic obstructive pulmonary disease (COPD) are major contributors of morbidity and mortality in the developed world. Patients with heart failure, particularly those with preserved ejection fraction (HFPEF) are known to have multiple non-cardiac comorbidities the presence of which has been associated with adverse outcomes. COPD is considered to be such comorbidity; however, there is limited data specifically addressing the prognostic value COPD in HFPEF.

Methods:
Using the IPRESERVE trial database of 4128 patients, various clinical, laboratory, ECG and echocardiographic variables were compared between COPD vs. non-COPD groups. A multivariate Cox proportional hazard model was used to test the prognostic value of COPD.

Results:
Patients with COPD were more likely to be male and smoker. They also have important comorbidities such as diabetes, chronic kidney disease, atrial fibrillation and coronary artery disease. There were no clinically significant differences in the echocardiographic parameters studied. Occurrence of left ventricular hypertrophy based on ECG criteria was less common in patients with COPD. After adjustment, COPD was found to be a significant predictor of the primary composite end point of death from any cause or hospitalization (HR 1.25; 95% CI: 1.05-1.49; P=0.012) but not a predictor of all-cause mortality (HR: 1.15; 95% CI: 0.92-1.44; P=0.214). The treatment effect (of Irbesartan) was found to be significant in the COPD group for the primary composite end point (HR: 0.69; 95% CI: 0.50-0.97; P=0.03).

Conclusion:
COPD was found to be an independent predictor of risk of death from any cause or hospitalization but not a predictor of all-cause mortality. Most of the risk associated with the primary outcome seems to be attributed to increased risk of hospitalization for worsening heart failure. A potential beneficial role of angiotensin-II receptor blockers has been described in pulmonary disease which might explain the treatment effect of Irbesartan. However, caution should be taken in interpreting the results of post-hoc analysis.

425.
Survival of Kidney Transplantation Patients in the United States After Cardiac Valve Replacement

Alok Sharma, MD; David T. Gilbertson, PhD; Charles A. Herzog, MD

Background— Few published studies address the survival of kidney transplantation patients after valve surgery, and none address relative outcomes related to tissue versus nontissue prosthesis. This study aimed to assess survival of US kidney transplantation patients after cardiac valve replacement and to compare associations of valve selection.

Methods and Results— Of 1 698 706 patients in the US Renal Data System database, we identified 1335 kidney transplantation patients hospitalized in 1991 to 2004 for cardiac valve replacement. Survival was estimated by the Kaplan-Meier method; independent predictors of death were examined in a comorbidity-adjusted (by Charlson and propensity score) Cox model. Of the cohort, 17% were 0 to 44 years of age, 50% were 45 to 64 years of age, 28% were 65 to 74 years of age, and 5% were ≥75 years of age; 78% were white; 63% were men; and 20% had kidney failure caused by diabetes mellitus. Of 369 patients (28%) who received tissue valves, 75% had aortic valve replacement, 20% had mitral valve replacement, and 5% had both. Use of tissue valves increased from 13% in 1991 to 1995 to 38% in 2000 to 2004. Age, diabetes mellitus, and combined aortic and mitral valve replacement were the strongest predictors of all-cause mortality. In-hospital mortality was 14.0% overall, 11.4% for tissue-valve patients, and 15.0% for nontissue-valve patients (P=0.09). Two-year survival estimates were 61.5% for tissue-valve and 59.5% for nontissue-valve patients (P=0.30). The adjusted hazard ratio of death for tissue- versus nontissue-valve patients was 0.83 (95% confidence interval, 0.70 to 0.99).
Conclusions— Renal transplantation patients requiring valve replacement have high mortality rates (≈20%/y). These data suggest minimally reduced mortality risk for patients receiving tissue versus nontissue valves.

426.

Beneficial Effects of Carvedilol in Dilated Cardiomyopathy in Dialysis Patients.

Alok Sharma, Charles Herzog.
University of Minnesota Medical School, Hennepin County Medical Center.

Dilated cardiomyopathy in chronic dialysis patients is an independent risk factor for cardiac mortality. Carvedilol has been shown to improve mortality and ejection fraction in heart failure pts. But data looking at similar effect in dialysis pts is lacking. We sought to evaluate the effects of carvedilol on dilated cardiomyopathy in chronic dialysis patients.
Methods: We retrospectively identified 33 patients on chronic dialysis with low ejection fraction (< 45%) who were initiated on carvedilol or switched to carvedilol if they were previously on a different beta blocker. Patients were followed for 2 years and changes in EF, HR, BP, LV end systolic and diastolic dimensions, left atrial size, aortic root diameter and LV Mass were noted. Of cohort, 55% were 40-60 years of age, 52% were male, 61% were African American, 70% were on ACE/ARB, 61% were previously on a different beta blocker, 45% were on calcium channel blocker, 49% were on both ACE/ARB and beta blocker, 58% had HTN as cause of renal failure, 67% were on dialysis for > 2 years, 52% had non-ischemic cardiomyopathy. Mean duration of follow up in 1st year was 7.4 months; in 2nd year 22 months.
Results: Treatment with carvedilol resulted in a significant improvement in Ejection fraction along with significant reduction in heart rate, systolic and diastolic blood pressure.
Conclusion: This study validates the use of carvedilol in all dialysis patients with dilated cardiomyopathy.

TABLE 2: Blood pressure, Heart Rate and Echocardiographic Parameters (mean ± SEM)

	Baseline	Within 1 year #	Within 2 years #
Heart Rate	83.60 ± 2.18	73.00 ± 2.15 **	74.56 ± 2.99 *
Systolic Blood Pressure	135.8 ± 4.45	118.6 ± 3.95 **	119.7 ± 6.52 *
Diastolic Blood Pressure	81.00 ± 3.07	69.04 ± 3.07 **	68.47 ± 3.70 *
LVEF (%)	31.76 ± 1.64	37.62 ± 2.80 *	43.42 ± 2.80 ***
LVEF (%) prior BB	33.90 ± 2.09	36.63 ± 3.52	40.10 ± 4.45
LVEF (%) BB Naïve	28.46 ± 2.52	39.20 ± 4.82 *	47.11 ± 3.03 ***
LVEF (%) Pts w HTN	31.25 ± 1.81	40.47 ± 3.11*	44.70 ± 3.42***
LVEF (%) Pts w/o HTN	32.54 ± 3.16	32.22 ± 5.39	42.00 ± 4.70
LVEDD (mm)	59 ± 1.37	56.12 ± 1.75	55.86 ±1.70
LVEDD (mm) prior BB	59.07 ± 1.70	56.08 ± 2.32	58.43 ± 2.38
LVEDDD (mm) BB Naïve	58.89 ± 2.44	56.20 ± 2.55	53.29 ± 2.24
LVESD (mm)	45.88 ± 1.60	40.82 ± 1.97 *	41.29 ± 2.35
LVESD (mm) prior BB	46.20 ± 1.74	40.75 ± 2.46	43.86 ± 3.87
LVESD (mm) BB Naïve	45.33 ± 3.30	41.00 ± 3.55	38.71 ± 2.62
LV mass (gm)	402 ± 26.75	389.1 ± 40.34	377.8 ± 31.17
Left Atrium (mm)	43.83 ± 1.73	44.35 ± 1.66	43.00 ± 1.78
Aortic Root (mm)	33.5 ± 1.46	33.65 ± 1.75	32.38 ± 0.85
Interventricular Septum	13.22 ± 0.60	13.44 ± 0.516	12.77 ± 0.54
LV Posterior Wall	13.07 ± 0.52	12.88 ± 0.58	12.62 ± 0.41

#Mean time interval between baseline and follow up echocardiogram within 1 year: 7.4 months
#Mean time interval between baseline and follow up echocardiogram within 2 year: 22 months

427.

Comparative Long-Term Survival of Dialysis Patients in the US after Mitral Valve Replacement and Mitral Annuloplasty.

Alok Sharma, Eric Weinhandl, Charles Herzog

ABSTRACT: There are no published data comparing the long-term outcome of dialysis patients after mitral valve replacement (MVR) surgery and mitral annuloplasty (MA). We searched the records of 1,698,706 pts in the United States Renal Data System database and identified 4413 dialysis patients hospitalized from 1991–2004 for MVR or MA only (other valve sites excluded). Long-term survival was estimated by Kaplan-

Meier method and independent predictors of death were examined in a comorbidity-adjusted Cox model.
RESULTS: The study cohort was 55% female, 58% white, 37% black, 36% DM as primary cause of ESRD, and 26% age 65+. MVR occurred in 3122 pts (71%) and MA in 1291pts (29%). Concomitant CAB occurred in 33.2% of MVR and 49.7% of MA. In-hospital death was 25.0% for MVR and 15.9% for MA. Median survival after MVR was 1.05 years (95% CI: 0.91-1.16), while median survival after MA was 2.01 years (95% CI: 1.78-2.33). In a multivariate analysis, MA was associated with a 35% decrease in mortality risk (95% CI: 29-40%), as compared with MVR.
Conclusion: Mitral valve surgery is associated with high short and long-term mortality in dialysis patients. The survival of dialysis pts undergoing mitral valve surgery is better after mitral annuloplasty compared to mitral valve replacement.